"Biocatalysis of fumarate derivatives by flavocytochrome c_3"

Caroline Wardrope

Thesis presented for the degree of Doctor of Philosophy

April 2007

Declaration

The work presented in this thesis is the original work of the author, except where specific reference is made to other sources. It has not been submitted in part, or in whole, for any other degree. Some of the results have already been published.

Acknowledgements

I would like to thank my supervisor Professor Steve Chapman for giving me the opportunity to do this project and for all of his guidance throughout. I would also like to thank Dr. Caroline Miles for all of her help in molecular biology and Dr. Chris Mowat for crystallographic data. Many thanks to everyone in the lab for making the whole experience enjoyable and to the BBSRC for funding.

Biocatalysis of Fumarate derivatives by Flavocytochrome c_3

Abstract

Flavocytochrome c_3 (Fcc_3) is a 63.8 kDa soluble fumarate reductase produced by the bacterium *Shewanella frigidimarina* when grown under anaerobic conditions with fumarate present. It is composed of a single polypeptide chain that incorporates four *c*-type haems and a non-covalently bound flavin adenine dinucleotide molecule as redox co-factors. Electrons are transferred to the active site where they are used for the catalytic reduction of fumarate to succinate. As the kinetics of fumarate reduction have previously been established (k_{cat} = 509 ± 15 s^{-1}, K_m = 25 ± 2 μM at pH 7.2), the aim of this project was to investigate the ability of Fcc_3 to reduce alternative substrates, particularly those that may result in the production of chiral molecules. Fcc_3 is able to reduce 2-methylfumarate to 2-methylsuccinate *in vitro*, with a k_{cat} of 8.97 ± 0.43 s^{-1}, and a K_m of 31.7 ± 8.5 μM at pH 7.2. Circular dichroism spectroscopy revealed that reduction of 2-methylfumarate by wild-type Fcc_3 is stereospecific, producing S-methylsuccinate. The crystal structure of wild-type Fcc_3 with 2-methylfumarate bound was solved to 1.5 Å and showed that the mode of 2-methylfumarate binding to the active site always results in the production of S-methylsuccinate. A range of fumarate derivatives were tested as potential substrates but wild-type Fcc_3 did not catalyse the reduction of anything other than fumarate and 2-methylfumarate. In order to find out if the substrate specificity of Fcc_3 could be altered, active site residues involved in Hydrogen-bonding with substrate were substituted by site-directed mutagenesis. Subsequent kinetic studies demonstrated that most of the mutant enzymes were still able to reduce fumarate and 2-

methylfumarate, although at rates differing from that measured for wild-type Fcc_3. Crystal structures were obtained for the mutants T377A and H365G at 2.0 Å and 1.9 Å respectively. When T377 is replaced with alanine, it can be seen from the crystal structure that the substrate is held by two less hydrogen-bonds than when bound to wild-type and is no longer held in the characteristic "twisted" conformation, an important aspect of the catalytic mechanism. All crystal structures obtained for Fcc_3 so far have shown the protein in the "closed" conformation. Other studies have demonstrated that the clamp domain of Fcc_3 is capable of movement and can exist in an "open" form where substrate is not bound. The crystal structure of H365G was obtained in the "open" conformation and is the only structure of Fcc_3 without substrate bound. Previous theoretical modelling studies had predicted that some mutants (especially H365G) may be able to catalyse the reduction of some mono-acids. However, it appears that this is not the case as none of the engineered forms of Fcc_3 were able to reduce any substrates other than fumarate and 2-methylfumarate. Fcc_3 is therefore a highly substrate-specific fumarate reductase.

Abbreviations

Amino acids

Alanine	Ala	A	Leucine	Leu	L
Arginine	Arg	R	Lysine	Lys	K
Asparagine	Asn	N	Methionine	Met	M
Aspartic acid	Asp	D	Phenylalanine	Phe	F
Cysteine	Cys	C	Proline	Pro	P
Glutamic acid	Glu	E	Serine	Ser	S
Glutamine	Gln	Q	Threonine	Thr	T
Glycine	Gly	G	Tryptophan	Trp	W
Histidine	His	H	Tyrosine	Tyr	Y
Isoleucine	Ile	I	Valine	Val	V

Textual abbreviations

Abs	Absorbance
Da	Daltons
ε	Extinction coefficient
Fcc_3	Flavocytochrome c_3
FPLC	Fast protein liquid chromatography
ΔG°	Standard free energy change
IFcc_3	Iron-induced Flavocytochrome c_3
LB	Luria Bertani
ox	oxidised
PDB	Protein Data Bank (http://www.rcsb.org/pdb)
red	reduced
QFR	Quinol: Fumarate Reductase
SQR	Succinate: Quinone Oxidoreductase

Chemicals

ADP	Adenosine Di-phosphate
ATP	Adenosine Tri-phosphate
DTT	Dithiothreitol
DMSO	Dimethyl Sulphoxide
FAD	Flavin Adenine Dinucleotide
FMN	Flavin Mononucleotide
IPTG	Isopropyl-β-D-thiogalactopyranoside
MK	Menaquinone
MV	Methyl Viologen
NADH	β-Nicotinamide Adenine Dinucleotide
NADPH	β-Nicotinamide Adenine Dinucleotide
SDS	Sodium Dodecylsulphate
UQ	Ubiquinone

Buffers

CHES	2-[N-Cyclohexylamino]ethanesulfonic acid
HEPES	N-[2-Hydroxyethyl]piperazine-N'-[2-ethanesulfonic acid]
KPi	Potassium Phosphate: K_2HPO_4/KH_2PO_4
MES	2-[N-Morpholino]ethanesulfonic acid
MOPS	3-[N-Morpholino]propanesulfphonic acid
TRIS	Tris[hydroxymethyl]aminoethane

Standard units

m	metre	M	molar
g	gram	^oC	degree Celcius
l	litre	V	volt
s	second	Å	Angstrom

Contents

List of figures

List of tables

Chapter 1

Introduction

1.0 Redox co-factors

Redox reactions in biology are catalysed by oxidoreductase enzymes and many biochemical processes depend on efficient electron transfer. Broadly, there are two types of electron transfers; intermolecular electron transfer in which mobile electron carriers donate or accept electrons to and from other carriers or oxidoreductase enzymes, and intra-molecular transfer in which electrons are passed between different redox centres within the same protein. A wide variety of redox-active centres are used in biology. Some proteins incorporate centres that contain bound metal ions, examples of which include iron, copper, nickel and molybdenum. Non-metallic redox cofactors such as flavins may also be bound within proteins but others, like NADH and quinones, exist freely within the cell. Some examples will be discussed in the following pages.

1.0.1 Haem co-factors

Haems are redox-active centres that contain an iron atom which is ligated by four nitrogen atoms from surrounding pyrole groups. In its simplest form, this system is termed protoporphyrin IX and constitutes the b-type haem (figure 1.1 *b*). This is the most common type of haem and is incorporated by proteins such as cytochrome b_5 [Durley and Mathews, 1996] and the cytochrome bc_1 complex (discussed later in this thesis) [Iwata *et al*, 1998]. Variations of the protoporphyrin IX give rise to four major types of haem, classed as haems a, b, c and d. The a-type haems have a hydroxyethylfarnesyl chain attached via the C3B carbon and a formyl group on the C3A carbon (figure 1.1 *a*). This type of haem is incorporated by the cytochrome c oxidase complex which forms part of the aerobic electron transport chain [Yoshikawa *et al*, 1998]. The c-type haems (figure 1.1 *c*) bind covalently to cysteine residues

Figure 1.1 Haem co-factors

a)

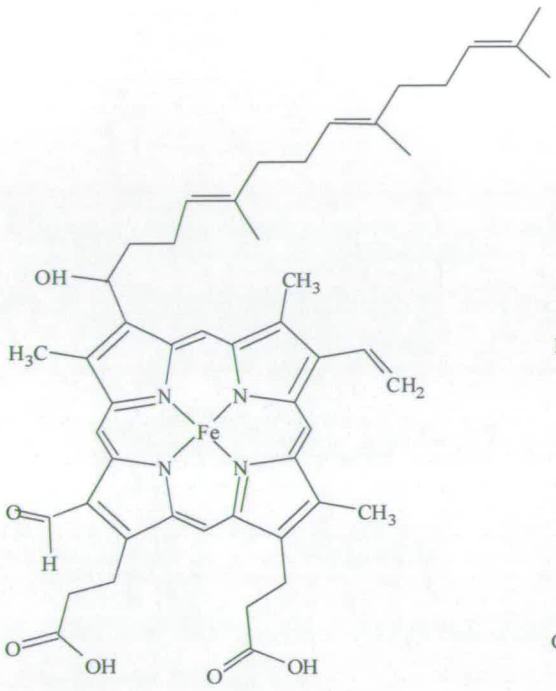

Haem a

b)

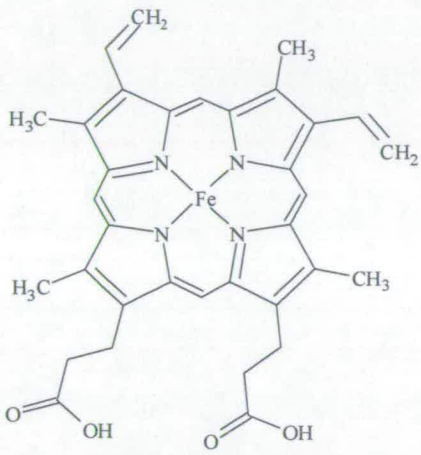

Haem b

c)

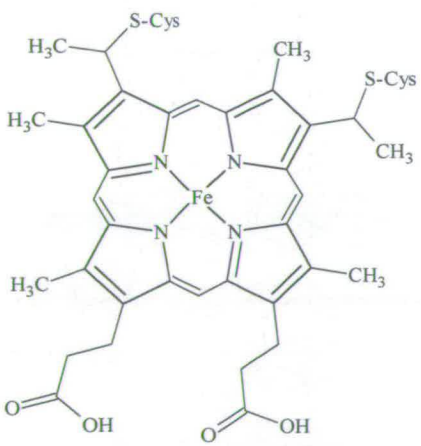

Haem c

Types of haem co-factors incorporated by proteins. a) Haem a has a hydroxyethylfarnesyl chain attached via the C3B carbon and a formyl group on the C3A carbon b) protoporphyrin IX, the most commonly found type of haem c) haem c which attatches to the protein backbone via covalent thioether linkages with cysteine residues

within proteins by means of a condensation reaction with the two vinyl groups of the porphyrin ring to form thioether linkages. An example of this is found in the soluble electron transporter cytochrome c. The d-type haems have fewer double bonds and contain additional carboxylic acid groups on the periphery of the ring system. In most cases, iron atoms within haems exist in either the ferric (Fe^{3+}) or ferrous (Fe^{2+}) oxidation states and transfer one electron at a time.

1.0.2 Iron-sulpur redox centres

Iron can also be incorporated within proteins in the form of iron-sulphur clusters. There are five different types that vary according to the number of iron and sulphur atoms present and in the way in which they are ligated. Examples are shown in figure 1.2. The simplest type contains only one iron atom which is coordinated by four sulphur atoms provided by cysteine residues. There are two types of [2Fe2S] clusters: one is the "Rieske" cluster which is ligated by two S atoms fom cysteines and two N atoms from histidines (figure 1.2 *a*). The other type of [2Fe2S] is coordinated by four cysteines. The fourth type of cluster is the [3Fe4S] cluster (figure 1.2 *b)*) coordinated by three cysteines, and the fifth is the [4Fe4S] cluster (figure 1.2 *c)*), coordinated by four cysteines. Like haem co-factors, iron-sulphur clusters participate in one-electron transfers.

1.0.3 Flavin

Flavins are incorporated into proteins as either flavin mononucleotide (FMN) or flavin adenine dinucleotide (FAD) molecules. They may be covalently attached to proteins via cysteine, tyrosine or histidine residues, or bound non-covalently through hydrogen-bonding and van der Waals interactions. The redox active part of flavin is

Figure 1. 2 Iron-sulphur clusters

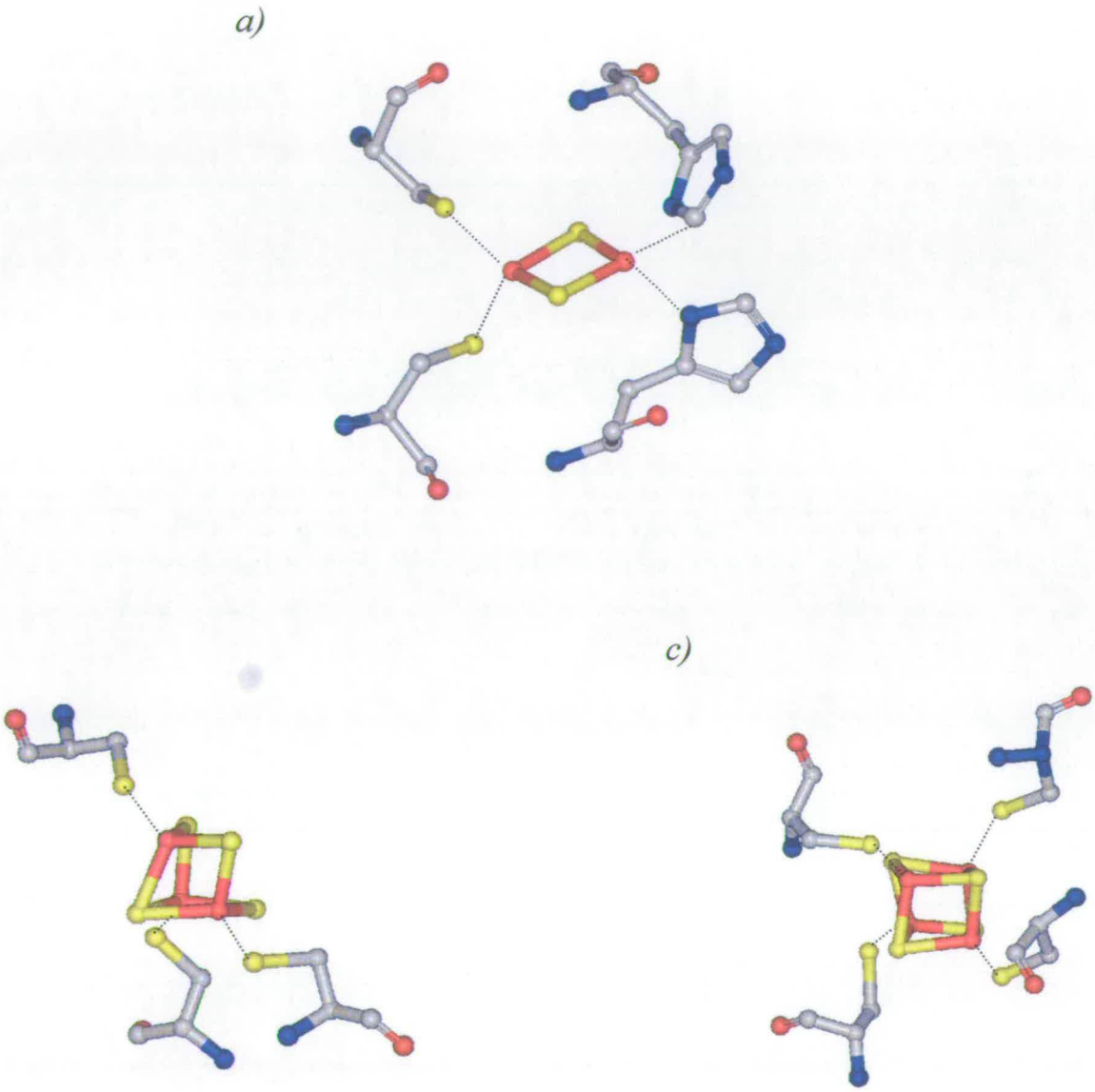

Stick representations of different types of iron-sulphur clusters incorporated within proteins. Sulpur atoms are shown in yellow, iron atoms are whown in red and amino acid residues that ligate the clusters are shown in grey. a) [2Fe2S] cluster also called the "Rieske cluster" to differentiate it from other [2Fe2S] clusters. They are ligated by two S atoms from cysteine residues and two N atoms from histidine residues. b) [3Fe4S] cluster which is ligated by 3 cysteine residues. c) [4Fe4S] cluster which is ligated by four cysteine residues.

Figure 1.3 Flavin Adenine Dinucleotide co-factor

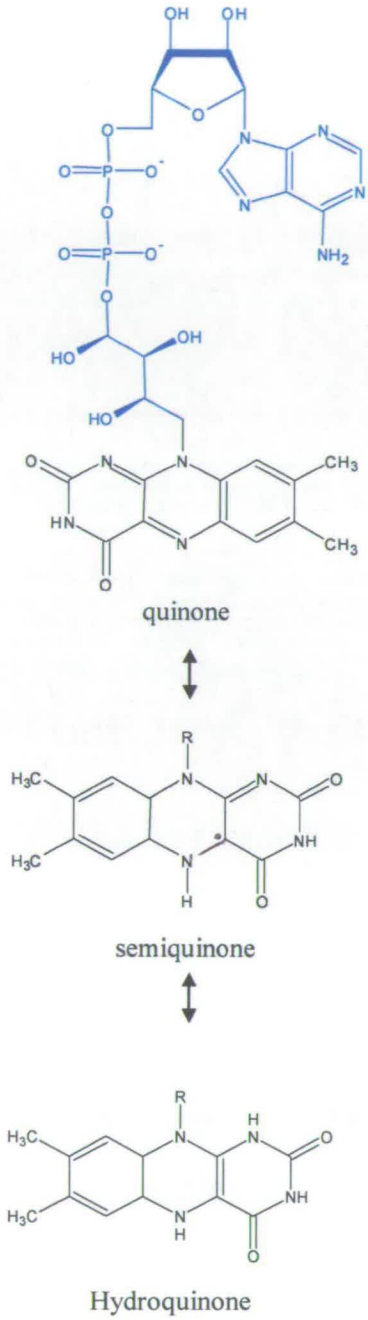

Flavin adenine dinucleotide. FAD can exist in three different oxidation states: the oxidised quinone, semiquinone and the fully reduced hydroquinone. They can accept or transfer either one or two electrons at a time and in this way they often act as tranceivers.

the isoalloxazine ring which can exist in three different oxidation states: the fully oxidised quinone state, the semiquinone (one-electron reduced) and the fully reduced hydroquinone state (figure 1.3). This means that flavin can accept one electron at a time but transfer two electrons simultaneously (or the reverse – accept two electrons and then transfer them one at a time). In this way flavin acts as a transceiver, a property that is often exploited by proteins that catalyse two-electron oxidations or reductions, including Flavocytochrome c_3.

1.0.4 Quinones

Quinones are mobile hydrophobic molecules that are constrained within cell membranes and like flavins, are able to exist in three oxidation states. As will be discussed later, they are essential components of respiratory electron transport chains. Two examples of quinone are shown in figure 1.4. Ubiquinone is shown in 1.4 *a)* and is generally utilised by cells that respire aerobically. Menaquinone (shown in 1.4 *b)*) has a lower reduction potential than ubiquinone and is found in cells that respire anaerobically. The figure shows both types in the fully oxidised and fully reduced states.

1.0.5 NADH/NADPH

Nicotinamide Adenosine Dinucleotide (NADH) and Nicotinamide Adenosine Dinucleotide Phosphate (NADPH) are mobile electron carriers which are soluble and exist freely outwith cell membranes. Apart from the additional phosphate attached to

Figure 1.4 – Mobile electron carriers

a)

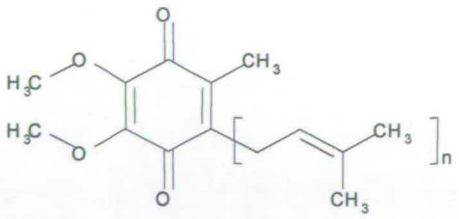

Ubiquinone

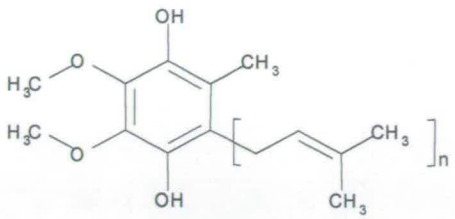

Ubiquinol

b)

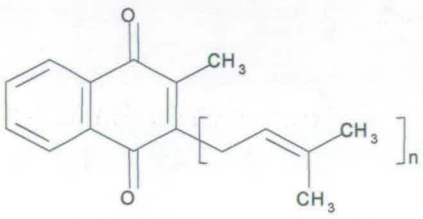

Menaquinone

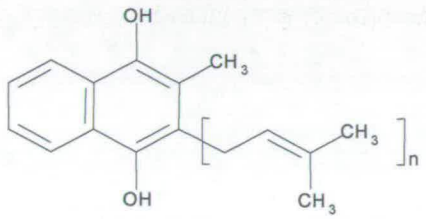

Menaquinol

c)

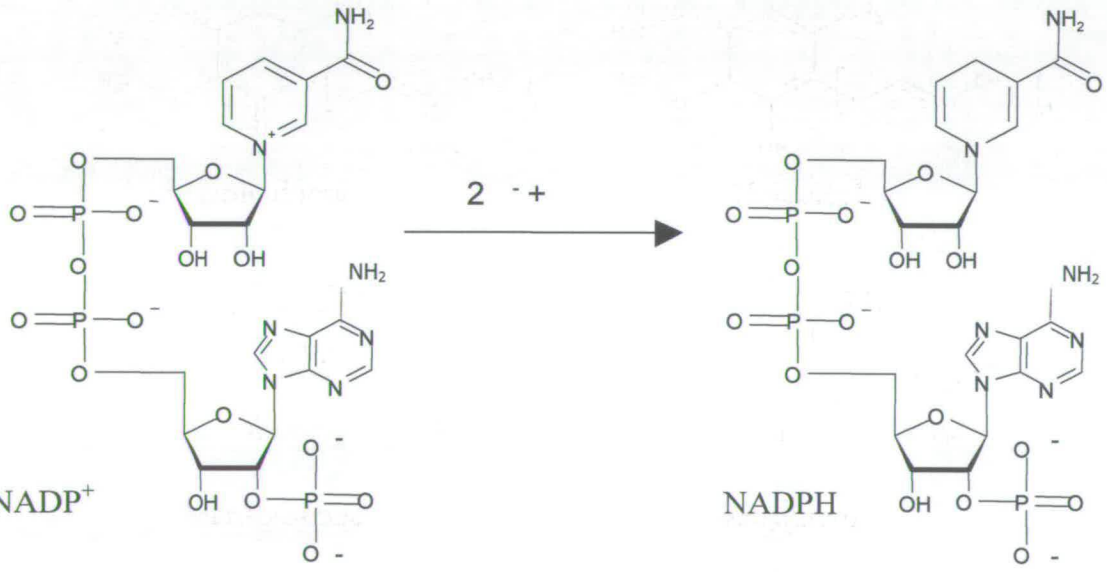

a) Ubiquinone (oxidised form) and ubiqunol (reduced) which diffuse freely through the plasma membrane where they transfer electrons between protein complexes during anaerobic respiration. b) Menaquinone (oxidised) and menaquinol (reduced) which perform the same function, but are used preferentially during anaerobic respiration. c) $NADP^+$ (oxidised) and NADPH (reduced) which are identical to NAD^+/H apart from the additional phosphate group. Both molecules are soluble and act as electron carriers in the cytoplasm.

NADPH, the two molecules are identical, although NADH is generally involved in catabolic processes while NADPH is utilised in anabolic processes. Both always transfer two electrons in the form of a hydride (H^-) and share the same reduction potential. Figure 1.4 c shows a molecule of NADPH in the oxidised and reduced form.

1.1 Overview of Aerobic Metabolism

All organisms on earth require energy, which can be utilised by cells in the readily accessible form of Adenosine tri-phosphate (ATP). ATP is continually generated during the catabolic breakdown of lipids, proteins and carbohydrates in a process called respiration. The most common form of respiration is Aerobic respiration, which couples the breakdown of food molecules to the reduction of molecular oxygen to water. The complete oxidation of glucose can be represented as the equation:

$$C_6H_{12}O_6 + 6O_2 \longrightarrow 6CO_2 + 6H_2O + 38ATP \quad \Delta G^{\circ\prime} = -2823 kJ.mol^{-1}$$

It can be seen that oxidation of glucose is a highly exergonic process but this energy is not released all at once. Instead it is released gradually via many enzymatically controlled reactions. Figure 1.5 shows an overview of the different stages of aerobic respiration (breakdown products from proteins and lipids also enter either glycolysis or the citric acid cycle but have been omitted for simplicity). Electrons are captured at various steps of glycolysis and the citric acid cycle by the electron carriers NAD^+ and FAD, where they are reduced to NADH and $FADH_2$. These reducing equivalents then enter the electron transport chain where they are oxidised. The energy released by the stepwise transfer of electrons between a series of protein complexes before being transferred to the terminal electron acceptor oxygen, powers the production of

Figure 1.5 Overview of Aerobic respiration

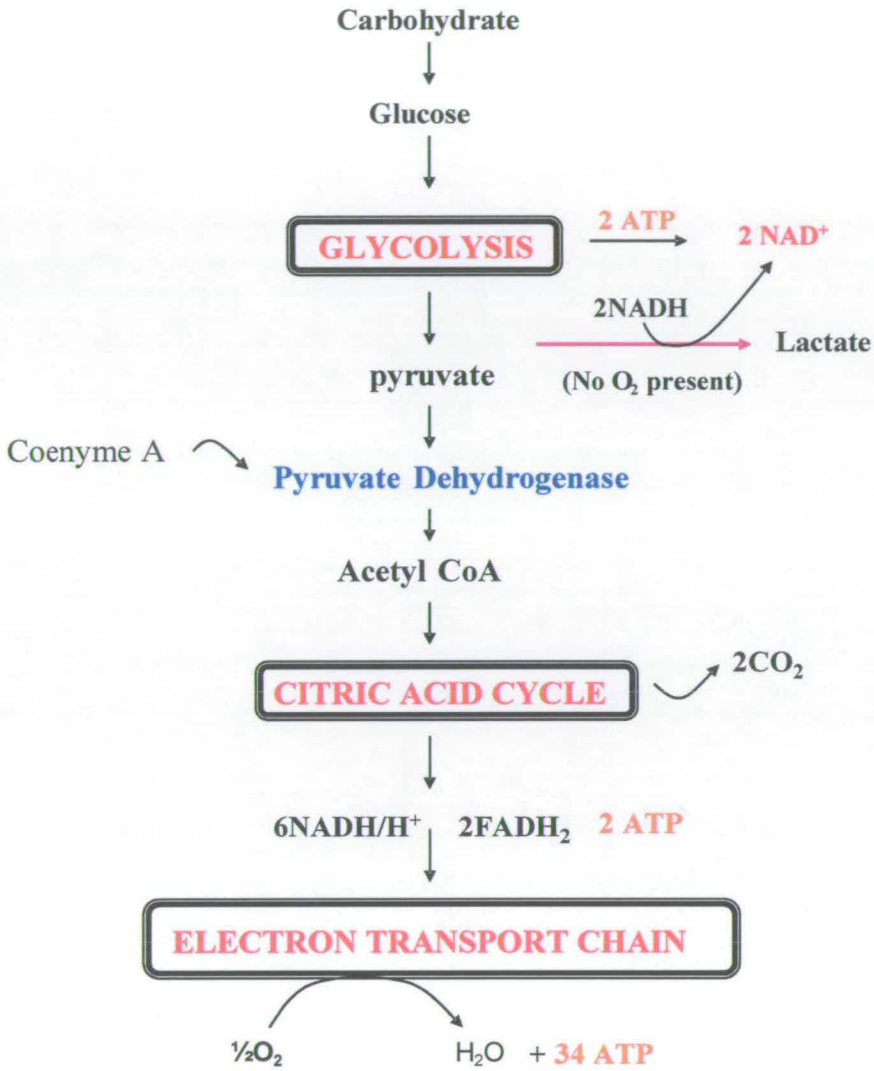

Overview of the catabolic breakdown of carbohydrates that generates cell energy in the form of Adenosine tri-phosphate (ATP). Carbohydrates are enzymatically broken down to glucose which then enters the first major stage of respiration – Glycolysis. Glycolysis results in production of two molecules of pyruvate which, after conversion to acetylCoA, then enter the citric acid cycle. The citric acid cycle consists of a series of reactions which harvest electrons from the complete oxidation of pyruvate, in the form of $NADH/H^+$ and $FADH_2$. These reducing equivalents then enter the electron transport chain. Energy released as electrons move along the chain and ultimately to oxygen, powers production of ATP. When no oxygen is present, the citric acid cycle shuts down and only the glycolytic pathway can proceed. This leads to the net production of only 2ATP (compared to the 38 ATP produced by the complete oxidation of glucose.

ATP. NAD^+ and FAD can then re-enter glycolysis and the citric acid cycle to ensure the whole respiratory process continues. In the absence of oxygen, simple life-forms such as fungi and bacteria are able to respire anaerobically using alternative terminal electron acceptors to oxygen, or by the process of fermentation.

1.1.1 Glycolysis

Glycolysis takes place in the cell cytosol or the cytoplasm of bacteria. It is the process by which glucose is broken down to two molecules of pyruvate involving ten reactions, each catalysed by different enzymes. Pyruvate is then transported to the matrix of the mitochondrion where it is converted to AcetylCoenzymeA by the pyruvate dehydrogenase complex before entering the citric acid cycle. In addition to pyruvate, glycolysis results in the net formation of two ATP molecules plus two NADH. The formation of ATP occurs by the direct transfer of a phosphate from substrate (in this case a product of glucose catabolism) to ADP (Adenosine di-phosphate) and is an example of substrate level phosphorylation which differs from oxidative phosphorylation discussed later. When no oxygen is present, the citric acid cycle and electron transport chains do not function because reducing equivalents cannot be oxidised due to the lack of a terminal electron acceptor. As glycolysis still results in the production of ATP, simple organisms can survive if they are able to regenerate NAD^+. They do this by converting pyruvate to waste products such as lactate or ethanol, a process called fermentation. Lactic acid fermentation involves the direct reduction of pyruvate to lactate by NADH and is catalysed by lactate dehydrogenase (figure 1.5). This regenerates NAD^+ which can then be used to sustain the glycolytic process. This also occurs temporarily in muscle tissue in humans under

Figure 1.6 Fermentation of pyruvate

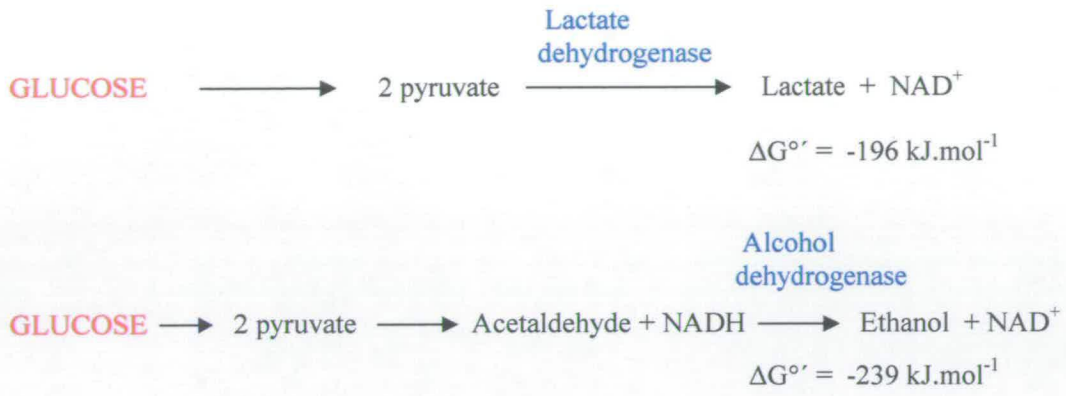

When oxygen is absent, NAD^+ can be regenerated by either reduction to Lactate, or by a two-step reduction to ethanol. Fermentation releases less energy (kJ) than aerobic respiration per mole of glucose but it is enough to sustain single celled organisms.

conditions when oxygen supply cannot keep up with energy demands, such as during strenuous exercise. In yeast, pyruvate can be converted to alcohol in a two-step process that involves decarboxylation of pyruvate to acetaldehyde by pyruvate decarboxylase, before reduction to ethanol by NADH catalysed by alcohol dehydrogenase. It can be seen from figure 1.6 that both of these fermentation processes do not harness as much energy as the complete oxidation of glucose, but enough to enable single-celled organisms to survive.

1.1.2 Citric acid cycle

The citric acid cycle takes place in the mitochondrial matrix of eukaryotic cells or the cytoplasm of bacterial cells. Its purpose is to produce reducing equivalents that enter the electron transport chain. It consists of a continuous cycle of eight reactions that begins with the addition of AcetylCoA to oxaloacetate, which is always regenerated at

Figure 1.7 - The citric acid cycle

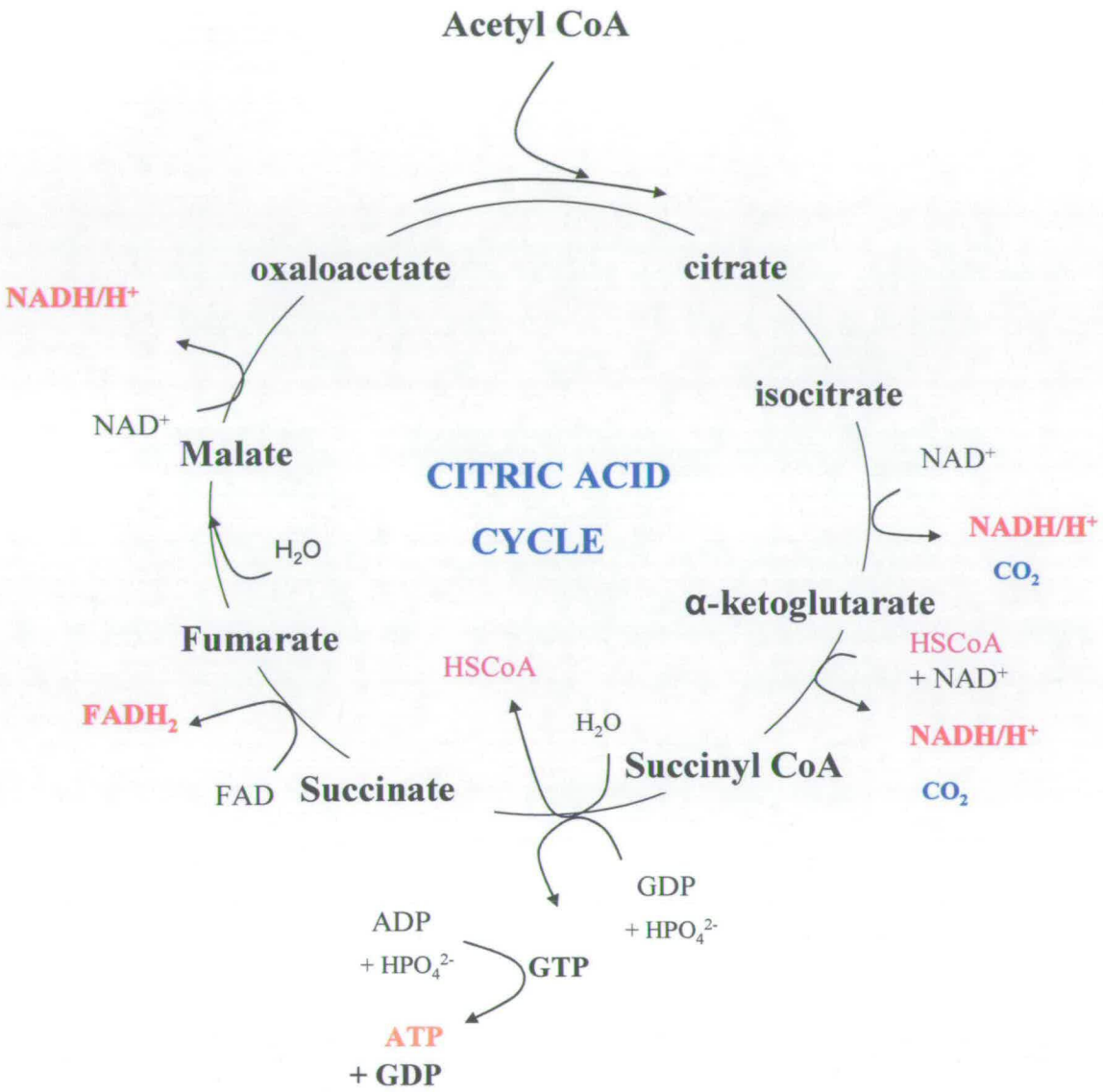

Schematic of the citric acid cycle showing the various steps at which $NADH/H^+$ and $FADH_2$ are produced. The cycle always regenerates oxaloacetate and Co-enyme A so that it can run continuously, provided that oxygen is present in order to regenerate NAD^+ and FAD via electron transport.

the end of the cycle (figure 1.7). At various stages energy from the oxidation of organic molecules is harvested by coupling it to the reduction of NAD^+ and FAD. In addition to this, ATP is generated by the substrate phosphorylation of GDP (guanosine diphosphate) to GTP during the conversion of succinylCoA to succinate catalysed by succinylCoA synthetase. GTP is subsequently converted to ATP by nucleoside diphosphate kinase. In many organisms ATP is produced directly at this step by phosphorylation of ADP instead of GDP. The oxidation of succinate to fumarate is carried out by succinate quinone oxidoreductase (SQR), which as well as contributing to the citric acid cycle, also functions as part of the electron transport chain where it is often referred to as complex II. This multi-subunit enzyme contains an FAD molecule at its active site which is reduced to $FADH_2$ during the oxidation of succinate. Unlike the other enzymes involved in the citric acid cycle, the SQR complex is embedded in the inner mitochondrial membrane (or the periplasmic membrane in bacteria). Electrons from $FADH_2$ are fed into the electron transport chain by SQR via quinones that diffuse freely within the membrane, where they interact with the other complexes of the chain. The complete oxidation of two molecules of pyruvate (from one molecule of glucose) during the citric acid cycle results in production of 6NADH, $2FADH_2$ and 2 molecules of ATP.

1.1.3 Aerobic electron transport chain.

The aerobic electron transport chain is composed of five multi-subunit protein complexes including the ATP synthase which is responsible for generation of cell energy in the form of ATP (figure 1.8). When the inner surface of the inner mitochondrial membrane is viewed under the electron microscope it appears to have a rough surface, which is due to peripheral regions of these complexes which exist in

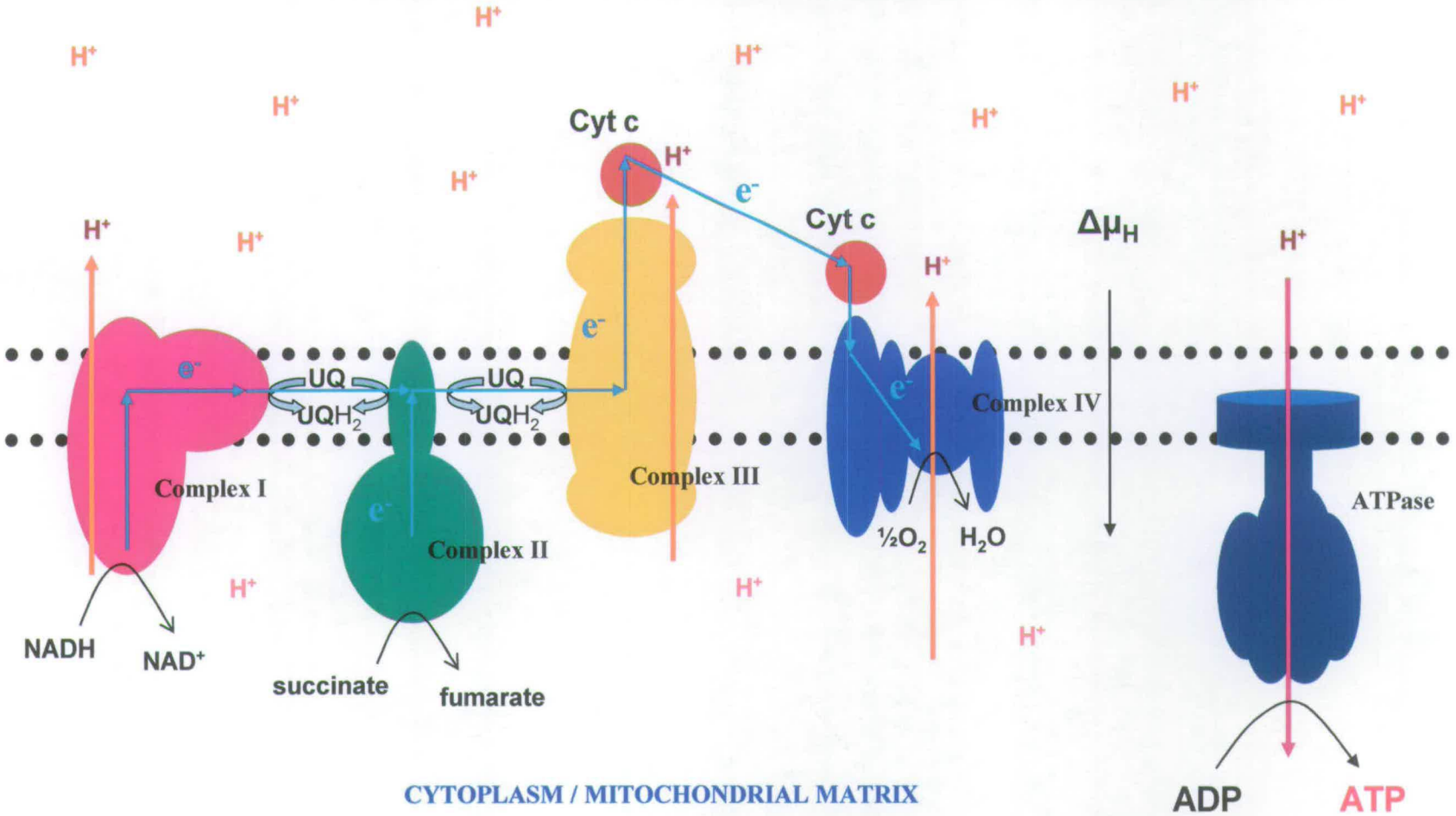

Figure 1.8 Aerobic electron transport chain

Schematic of the Aerobic electron transport chain. NADH transfers electrons to ubiquinol through complex1 regenerating NAD^+. Oxidation of succinate during the citric acid cycle by complex II reduces bound FAD to $FADH_2$. $FADH_2$ then transfers electrons to ubiquinol molecules in the plasma membrane. Ubiquinones can then transfer electrons to complex III which then transfers them to cytochrome c – a soluble electron carrier). Cytochrome c docks with complex IV, transferring electrons one at a time which are then transferred to the terminal electron acceptor oxygen. Electron transfer along the chain is exergonic and this energy is utilised by complexes I, III and IV to drive the translocation of protons from the cytoplasm to the periplasm. Consequently an electrochemical gradient builds up across the membrane. The ATP synthase complexes are the only point of proton entry back into the cytoplasm. As they rush through channels down the gradient in the centre of these complexes, the energy released drives the catalytic production of ATP. The purpose of electron transport is to ensure that this electrochemical gradient (sometimes called the "proton motive force") is maintained.

numerous copies and are densely packed together. Complexes I – IV are oxidoreductases which transfer electrons in an exergonic manner from redox centres that have more negative reduction potentials to centres that have more positive reduction potentials. Complexes I, III and IV utilise the energy released by these electron transfers to drive the pumping of protons into the intermembrane space of mitochondria or the periplasm in bacterial cells. The inner membrane is not very permeable to H^+ ions so consequentially an electrochemical gradient of protons ($\Delta\mu H^+$) is created between the intermembrane space and the matrix of mitochondria. This results in a potential difference (ΔV) across the membrane (due to the difference in charge) and also a concentration gradient (ΔpH) which combined, constitute the proton motive force (Δp). Protons can only re-enter the matrix via channels enclosed by the ATP synthases (also called complex V). The potential energy of the proton motive force is harnessed by ATP synthase as protons move down the gradient to the negative side of the membrane, driving conformational changes that enable the catalytic phosphorylation of ADP to ATP. This process is termed "oxidative phosphorylation" because it is coupled to the reduction of molecular oxygen by the electron transport chain. It is also called "chemiosmosis" as the diffusion of H^+ ions from a region of high concentration to a region of low concentration is analogous to the movement of water molecules across cell membranes. A more detailed description of each complex that constitutes the aerobic electron transport chain now follows.

1.1.4 Complex I

Complex I of the electron transport chain is the NADH:Ubiquinone oxidoreductase. This complex oxidises NADH, utilising ubiquinone as an electron acceptor. This

reaction is highly exergonic and is coupled to the translocation of protons into the intramembrane space of mitochondria or the periplasm in bacteria. Complex I is one of three proton pumps that contribute to the proton motive force (Δp). The transfer of protons and electrons by this complex can be represented by the following equation:

$$NADH/H^+ + Q + 4H_n^+ \longrightarrow NAD^+ + QH_2 + 4H_p^+$$

Where Q = ubiquinone, H_n^+ = protons taken up from the negative matrix side (or cytoplasmic side) of the membrane and H_p^+ = protons released into the intermembrane space (or periplasm). The composition of complex I varies between species but all contain a non-covalently bound flavin mononuleotide molecule plus up to nine iron-sulphur clusters [Friedrich and Böttcher, 2004]. Electrons from NADH are first transferred to FMN before being transduced through the iron-sulphur clusters to ubiquinone. The large size and complicated nature of complex I has meant that so far, no high resolution structure of the entire assembly has been obtained. However, the structure of the hydrophilic domain of complex I from *Thermus thermophilus* has recently been solved at 3.3 Å [Sazanov and Hinchliffe, 2006]. Low resolution structures (17- 34 Å) have revealed that overall it forms an L-shaped structure that spans the inner mitochondrial membrane with peripheral regions projecting out on both sides (figure 1.8). The simplest type of complex I is expressed by bacteria and is composed of 14 subunits, homologues of which have been found in all other organisms studied to date (in eukaryotes, complex I contains at least 32 extra subunits). Seven of these "core" subunits project into the matrix and contain the redox co-factors and the NADH binding site. The other seven form 54 helices that span the inner membrane and include the site of interaction with quinones that freely diffuse through the membrane. This transmembrane section is also thought to play a

part in proton translocation, which is suspected to be driven by conformational changes.

1.1.5 Complex II

Succinate-ubiquinone oxidoreductase (SQR) is often referred to as succinate dehydrogenase or complex II of the aerobic electron transport chain [Lancaster, 2002]. It couples the oxidation of succinate to fumarate to the reduction of ubiquinone to ubiquinol. SQR is structurally and functionally related to the Menaquinol-fumarate reductase (QFR) which catalyses the reverse reaction (fumarate-succinate) *in vivo*, although both complexes can catalyse both reactions. Depending on whether the organism is respiring aerobically or anaerobically, either SQR or QFR will be expressed accordingly [Hägerhäll, 1997]. The crystal structure of *Escherichia coli* SQR was resolved to 2.6 Å [Yankovskaya, 2003] . It is composed of four subunits; two of which are hydrophilic in nature (a flavoprotein subunit and iron-sulphur subunit) and project into the cytoplasm, and two hydrophobic membrane spanning subunits that serve to anchor the protein into the membrane and are the site of interaction with ubiquinones.

The flavoprotein subunit SdhA, has a mass of 65kDa and can be divided into two domains: an Flavin adenine dinucleotide-binding domain, which exhibits a Rossman-like fold and covalently binds the FAD molecule via an Nε atom of a histidyl residue side chain and the flavin C8α methyl group [Mewies *et al*, 1998], and also a capping domain. This capping domain is connected via a hinge that is able to move at least 30° relative to the flavin domain and the active site is located at the interface between the two domains. The iron-sulphur subunit SdhB, consists of a [2Fe-2S] iron-sulphur cluster at the N-terminal domain resembling that found in plant ferrodoxins, and a C-

terminal domain that incorporates a [4Fe-4S] cluster and a [3Fe-4S] cluster. Together the FAD and iron-sulphur cofactors form a chain approximately 40 Å in length, along which electrons are transferred from succinate to ubiquinone. The ubiquinone binding site (Q site) consists of residues from the SdhA, SdhB and SdhC subunits and is located 7.6 Å from the terminal [3Fe-4S] cluster [Yanovskaya *et al*, 2003]. Ubiquinone is ligated by a tyrosine residue and a tryptophan residue, the latter of which has been proposed to play a dual role in reduction to ubiquinol. Because electrons are transferred to ubiquinone one at a time, it is thought that the semiquinone is stabilised by hydrogen bonding to the tryptophan sidechain. This tryptophan also donates protons during reduction. There is a b-type haem located 9.8 Å from the Q site and 11.4 Å from the [3Fe-4S] cluster but its role is unclear. It is further away and has a lower reduction potential than ubiquinone so electron transfer via this haem would be less favourable and much less likely to occur than direct transfer from the [3Fe-4S]. Also it is not found in the *E. coli* QFR enzyme and mutagenesis experiments suggest that it is not essential for quinone reduction [Maklashina *et al*, 2001]. After reduction by complex II, ubiquinol then diffuses through the plasma membrane where it can donate electrons to other components of the electron transport chain.

1.1.6 Complex III

Complex III is the Cytochrome bc_1 complex which like complex I, also doubles as a proton pump. It couples the transfer of electrons from ubiquinone (reduced by complex I and complex II) to mobile cytochrome c to the translocation of protons across the mitochondrial membrane [Wikstrom et al, 1981]. Again composition of the complex varies between organisms but all possess three subunits containing two

Figure1.9 - The "Q cycle"

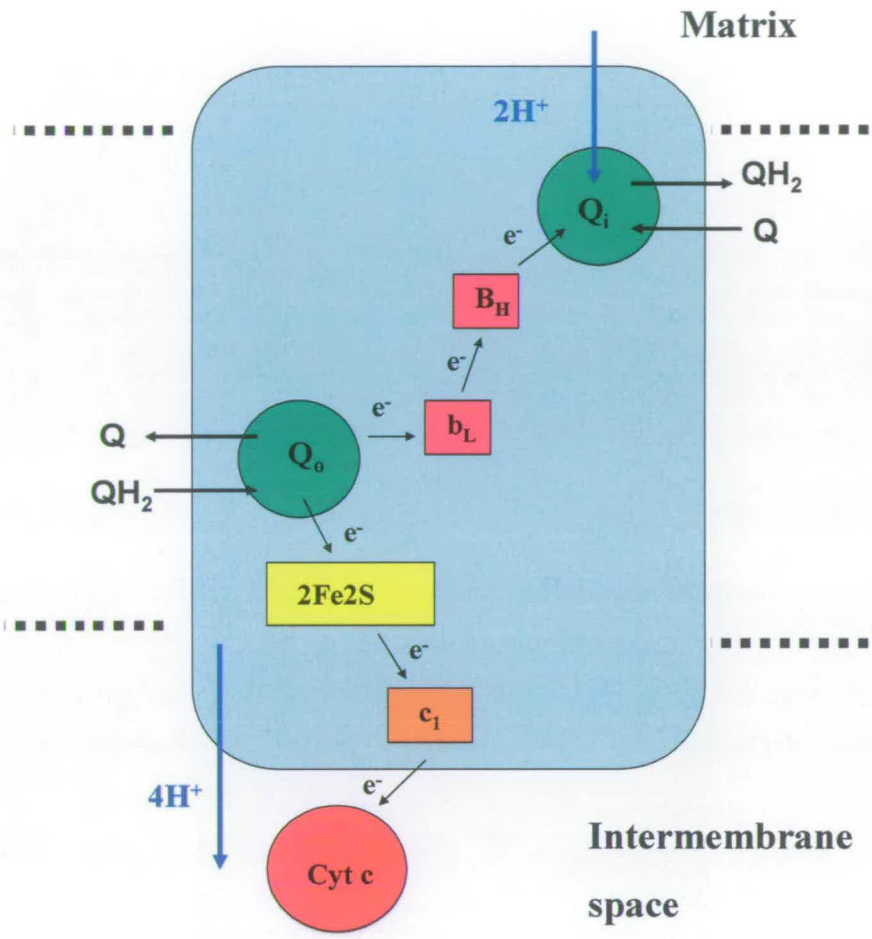

"Q- cycle" – Schematic of complexIII redox centres and binding sites. There are two quinol binding sites; Q_o which is the site of quinol oxidation, and Q_i which is the site of quinine reduction. One electron from ubiquinol (QH_2) is transferred to cytochrome c (red) via an iron-sulphur cluster (yellow and a c-type haem (orange), while the other is transferred to the Q_i site via two b-type haems (pink), where it is used in the reduction of ubiquinone (Q). To complete reduction of ubiquinone, two molecules of Ubiquinol (QH_2) are consumed. Therefore each complete cycle uses two QH_2, and results in production of one reduced ubiquinone, two reduced cytochrome c and translocation of four protons across the membrane.

b-type haems, cytochrome c_1 and a "Rieske" [2Fe-2S] iron-sulphur cluster [Iwata *et al*, 1998]. The crystal structure of the 11-subunit bovine heart mitochondrial bc_1 was resolved to 2.8 Å. The complex spans the width of the inner mitochondrial membrane and contains peripheral subunits that project out on both sides. The intermembrane

peripheral region contains the iron-sulphur cluster and cytochrome c_1, and is also the site of interaction with soluble cytochrome c. The coupling of exergonic electron transfer to the translocation of protons has been proposed to occur by the "Q cycle" mechanism (figure 1.9) [Trumpower and Gennis, 1994]. There are two separate quinol binding sites; one for the oxidation of ubiquinol (Q_o site) and one for the reduction of ubiquinone (Q_i site). Ubiquinol undergoes a two-electron oxidation at Q_o in a bifuricated manner. One electron is transferred to the [2Fe-2S] cluster, then to the c_1 haem before being accepted by soluble cytochrome c. This electron transfer is accompanied by the release of 2 protons to the intermembrane space. The other electron is transferred to the Q_i site via the two b-type haems (b_L and b_H) where it reduces ubiquinone. A second molecule of ubiquinol has to enter the Q cycle in order complete reduction along with the uptake of 2 protons from the matrix. Therefore, the complete Q-cycle oxidises two ubiquinol molecules and consumes two protons. This results in the production of two reduced cytochrome c and one reduced ubiquinol while also translocating 4 protons into the intermembrane space . This can be summed up as:

$$2QH_2 + 2Cytc_{ox} + 2H_n^+ \longrightarrow QH_2 + 2Cytc_{red} + 4H_p^+$$

Reduced cytochrome c then goes on to donate electrons to complex IV.

1.1.7 Complex IV

Complex IV is the Cytochrome c oxidase complex and like I and III it is a proton pump contributing to the proton motive force. It catalyses the reduction of the terminal electron acceptor oxygen, converting it to water. Crystal structures of both prokaryotic and eukaryotic forms of complex have been obtained and although they differ in size and composition, all contain two catalytic subunits [Iwata *et al*, 1995]

[Yoshikawa *et al*, 1998]. Subunit I contains haem a plus a binuclear centre containing haem a_3 and a copper ligated by three histidine residues (Cu_B) which is the site of oxygen reduction. Subunit II projects out into the intermembrane space/periplasm and contains another copper centre (Cu_A) which is the site at which cytochrome c docks and donates electrons to the complex. Electrons are transferred between centres in the following way:

$$\text{Cytochrome c} \rightarrow Cu_A \rightarrow \text{haem a} \rightarrow \text{haem } a_3\text{: CuB} \rightarrow O_2$$

When the binuclear centre is in the reduced state it binds oxygen which then exists briefly as a ferrousoxy species before forming a bridging peroxoide between haem a_3 and Cu_B. A series of electron transfers breaks the O–O bond and results in the production of two water molecules, accompanied by the translocation of four protons [Michel, 1998]. It is thought that these protons are pumped into the intermebrane space through the "D-channel" which is so called due to its being lined by negatively charged aspartate residues.

1.1.8 Complex V: ATP synthase

The ATP synthase complex couples the movement of protons down the electrochemical gradient ($\Delta\mu H^+$) with the production of the cell's energy currency ATP [C. Gibbons *et al*, 2000]. The complex can be divided into two regions – a globular catalytic region (F_1) that projects out into the mitochondrial matrix and a proton-translocating intermembrane region (F_0). These two regions are connected by a "stalk" which is composed of three subunits. One of these subunits (the γ subunit) projects into the catalytic region and is surrounded by six alternating α and β subunits. The β subunits contain the catalytic nucleotide binding sites, making three in total per ATPase. The production of ATP is thought to occur by the "binding change

mechanism" [Boyer, 1993]. This postulates that the three nucleotide binding sites have different affinities for the ADP substrate. The "open" site has the lowest affinity, the "loose" site is able to bind ADP reversibly and the "tight" site binds ADP in such a way that ATP is formed spontaneously from bound ADP and an inorganic phosphate. The only way protons can pass through the inner membrane is through the central channels of the ATPases. The energy released as protons rush through to the more negative matrix powers rotation of the catalytic region of the ATPase. Rotation occurs in 120° steps and every complete 360° turn takes each of the three ADP binding sites through all of the aforementioned binding states [Yasuda *et al*, 1998]. Therefore, each rotation step results in the production of one ATP molecule.

1.2 Anaerobic electron transport chains

In environments where there is no oxygen present many organisms are able to respire utilising alternative electron acceptors. These include inorganic species such as nitrate (NO_3^-), sulphate (SO_4^{2-}), ferric iron (Fe^{3+}) and manganese (Mn^{4+}) as well as organic compounds such as fumarate and trimethylamine oxide (TMAO). Certain eukaryotes such as ciliates and fungi even possess anaerobically functioning mitochondria that contain the same complexes found in aerobic mitochondria, although electron transfer is coupled to the reduction of NO_3^- to nitrous oxide [van Hellemond *et al*, 2003]. Amongst bacteria, anaerobic electron transport chains vary depending on the terminal electron acceptor used. Figure 1.10 shows an example of a bacterial anaerobic electron transport chain where fumarate is the terminal electron acceptor. Fumarate is commonly used, which is not surprising as it is an intermediate formed during the citric acid cycle so the organism does not have to depend on its availability in the immediate environment. Instead of coupling the oxidation of NADH and $FADH_2$ to the generation of the electrochemical gradient ($\mu\Delta H^+$), this chain involves complexes that catalyse oxidation of formate and molecular hydrogen. Instead of ubiquinones, lower potential menaquinones act as electron acceptors/donors during anaerobic electron transport [Wistance and Terelfall, 1968]. The reason for this may be that most alternative terminal electron acceptors have lower potentials than oxygen, so the lower potential menaquinones ensure that electron transfers between redox centres are exergoninc. Electrons from the oxidation of formate and H_2 are transported by menaquinols to the Quinol fumarate reductase complex (QFR), where they are used in the catalytic reduction of fumarate to succinate. Oxidation by formate dehydrogenase and hydrogenase generates protons which are released into the periplasm, contributing to generation of

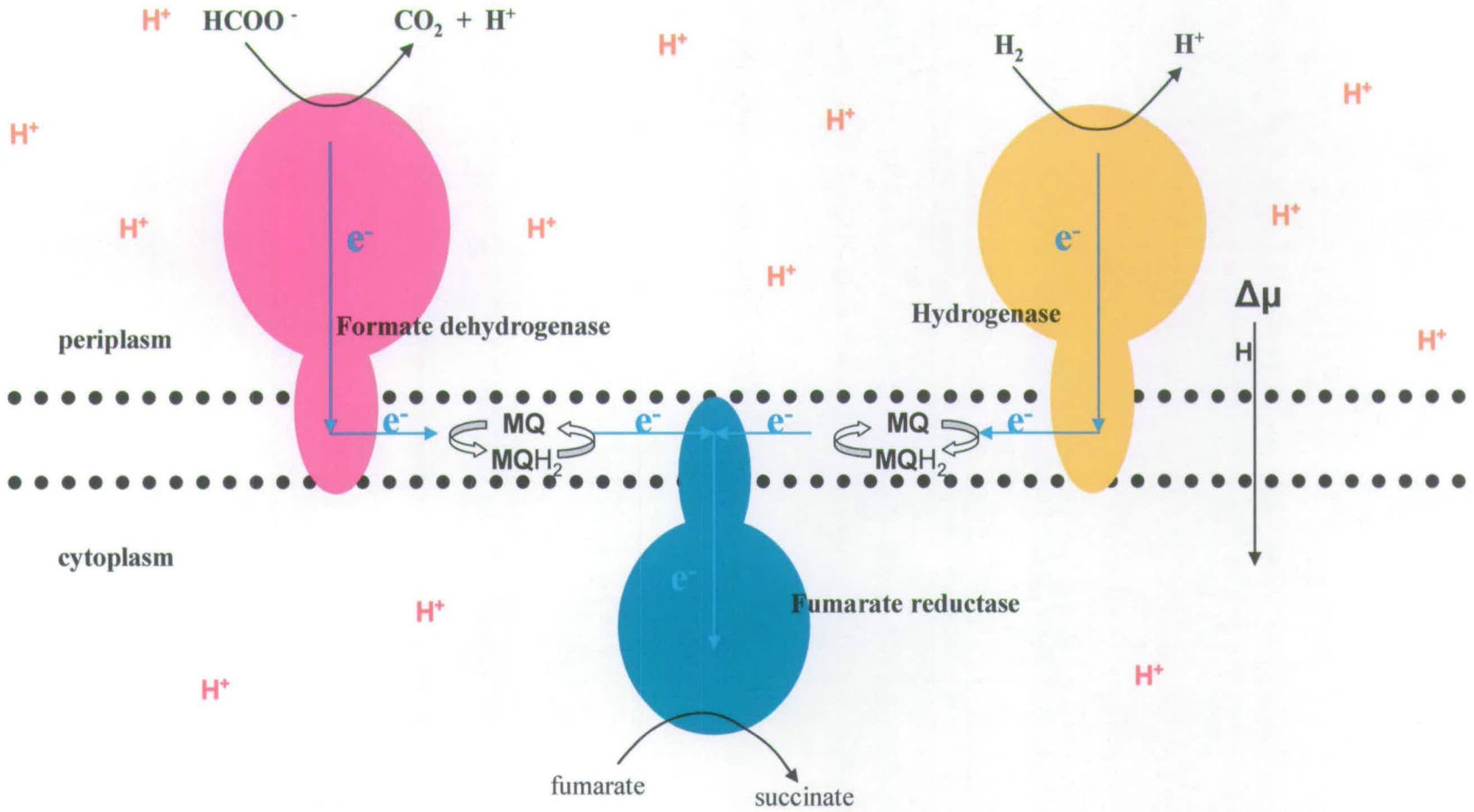

Figure 1.10 – Example of part of an anaerobic electron transport chain

Schematic of part of an anaerobic electron transport chain . Oxidation of formate by the formate dehydrogenase complex and also H_2 by hydrogenases, produce electrons which are then transferred to fumarate, (the terminal electron acceptor) via the quinol/fumarate reductase complex (QFR). The hydrogenases release protons into the periplasm thus maintaining the proton motive force (p.m.f.) . ATP is generated by the harnessing of the p.m.f. by ATP synthases as in aerobic electron transport.

a proton motive force. As in aerobic electron transport chains, this drives synthesis of ATP by ATPases.

1.2.1 Formate dehydrogenase

Formate dehydrogenase isolated from *Escherichia coli* is synthesised from a single polypeptide that can be divided into four domains. It has a mass of 79kDa and contains three redox co-factors; a selenocysteine, a molybdenum atom ligated by two molydopterin guanadine dinucleotide (MGD) molecules, and a Fe_4S_4 cluster [Bonnington *et al*, 1997]. This enzyme catalyses the oxidation of formate to CO_2 while releasing a proton into the periplasm, thus maintaining the proton gradient across the membrane. The active site molybdenum:MGD cofactor is tightly bound to the protein via hydrogen bonding, salt bridges and van der Waals interactions with domains II, III, and IV. Of the 35 H-bonding interactions, 23 are conserved in other formate dehydrogenases of the same type. In both the oxidised and the reduced forms of the enzyme, Mo is ligated to four S atoms of the two MGD's plus the selenocysteine. Prior to catalysis, the oxidised Mo centre displays trigonal prismatic geometry. However when it becomes reduced by the oxidation of formate, the coordination geometry is square pyramidal and Mo sits ~0.4Å above the equatorial plane. The oxidation of the Mo centre as electrons are transferred from the active site, results in the breakage of an H-bond between SeCys and a histadine residue causing a proton to be released into solvent. Electrons are transferred to the iron sulphur cluster one at a time and shuttled to an acceptor, perhaps menaquinone, although the physiological acceptor is not at this moment known. It is possible that it does not reduce menaquinone directly but instead donates electrons to an intermediate carrier.

However, for the purpose of assaying enzymatic activity, the artificial electron mediator benzyl viologen can play this role *in vitro*.

1.2.2 H_2 Hydrogenase

Hydrogenases couple the oxidation of molecular Hydrogen to the reduction of fumarate or other terminal electron acceptors.

$$H_2 \rightleftharpoons 2H^+ + 2e^-$$

They are also able to catalyse the reverse reaction and are thought to play a role in the clearing of excess electrons produced during fermentative processes [Rousset *et al*, 1998]. The structure of the NiFe hydrogenase from *Desulfovibrio vulgaris* was resolved to 1.8Å [Higuchi *et al*, 1997]. It has a molecular weight of 91kDa and possesses two $[Fe_4S_4]$ clusters, one $[Fe_3S_4]$ cluster and a Ni atom closely associated with an iron atom forming a heterobinuclear active site. The Ni atom is coordinated by four S atoms from cysteine residues, two of which also coordinate Fe, forming bridges between the two atoms. The Ni atom is coordinated with square pyramidal geometry whereas the coordination geometry around the Fe atom centre displays distorted octahedral geometry. This enzyme also incorporates a Mg atom but at present its role in enzyme function is not known.

1.2.3 Quninol fumarate reductase

As previously mentioned, quinol:fumarate reductase (QFR) is very similar to succinate:quinol reductase (SQR) or complex II of the aerobic electron transport chain. It contains four subunits designated FrdA, FrdB, FrdC and FrdD. These two enzymes only really differ from each other in their membrane-spanning regions, probably due to the fact that they interact with different types of quinone [Lancaster, 2001]. Under aerobic conditions SQR donates electrons from the oxidation of

succinate to ubiquinone, reducing it to ubiquinol. Under anaerobic conditions, menaquinol donates electrons to QFR which are then used in the reduction of fumarate to succinate. In addition, SQR contains a b-type haem cofactor and QFR does not. These factors along with differences in the measured potentials for the redox centres (including FAD) determine whether the enzyme is biased towards succinate oxidation or fumarate reduction. Despite the differences, the active site and residues surrounding the iron-sulphur clusters are conserved in sequence across SQR's and QFR's of different species. The crystal structure of *Escherichia coli* fumarate reductase with two molecules of menaquinone bound was resolved to 3.3 Å in 1999 [Iverson *et al*, 1999]. In addition to the covalently bound FAD and three iron-sulphur clusters, it contains two quinol binding sites in the membrane-spanning region, designated Q_P and Q_D. The Q_P site is distanced 8.2 Å from the [3Fe4S] cluster and in a reversal of the electron transfer pathway in SQR, electrons are transferred from bound menaquinone at Q_P to FAD at the active site via the iron-sulphur clusters where they are used in the catalytic reduction of fumarate to succinate. All edge to edge distances between redox centres are under 14 Å, facilitating fast electron transfer. The function of the Q_D site is unclear. It is over 25 Å away from the Q_P site making it unlikely that it participates in any electron transfer pathway. It was proposed to have a structural role but mutagenesis studies do not appear to support this [Iverson *et al*, 2002].

1.3 Shewanella frigidimarina

The genus *Shewanella* contains diverse species of Gram-negative bacteria that are found mostly in marine environments. The genus includes a bioluminescent species *Shewanella hanedai* [Jensen *et al*, 1980] a tetrodotoxin producing species *Shewanella alga* [Khashe and Janda, 1998] and *Shewanella benthica* which inhabits the gut of marine crustaceans [Bowman *et al*, 1997].

The first species to be discovered was originally obtained from rancid butter by Derby and Hammer in 1931 who called it *Achromobacter putrefaciens*. Over the years since, it has been re-classified several times, until 1997 (prior to which it was known as *S. putrefaciens*) when it was designated *Shewanella frigidimarina* [Bowman *et* al, 1997]. There have been cases when *S. frigidimarina* has been known to be pathogenic to humans in the form of soft tissue infections, cellulitis and septicaemia. Cases are relatively few however and have occurred almost exclusively in patients that were immunocompromised by existing illness especially liver disease.

Shewanella frigidimarina are rod-shaped and may be curved or straight. The bacteria are psychrotrophic and grow between <0-27° centigrade but optimally at 23°. They are able to ferment D-glucose under anaerobic conditions and can utilise inorganic as well as organic sources of nitrogen [Bowman *et* al, 1997].

They respire aerobically but are facultative anaerobes known to be capable of utilising many different electron acceptors during anaerobic respiration. These include ferric compounds [Loveley and Philips, 1986], manganese oxide, molybdenum oxide, nitrate and elemental sulphur [Moser and Nealson, 1996].

1.3.1 Flavocytochrome c_3

When growing under anaerobic conditions with fumarate present, *Shewanella frigidimarina* abundantly produces a unique soluble fumarate reductase, Flavocytochrome c_3 [Gordon *et al*, 1998]. The fact that Fcc_3 is soluble enables easy extraction and purification of the active enzyme, making it ideal for the study of electron transfer mechanisms in redox proteins. Like QFR, Fcc_3 catalyses the 2-electron reduction of fumarate to succinate during anaerobic respiration. Fcc_3 is 571 amino acids in length with a mass of 63.8kDa and is synthesised as a single polypeptide encoded by the *fccA* gene [Pealing *et al*, 1992]. Its synthesis is induced by anaerobiosis and thought to be regulated by the *EtrA* gene (electron transport regulator A). This protein is homologous to the DNA-binding protein Fnr from *E.coli* [Guest, 1992], which is a member of the CRP family of transcriptional regulators. *S. frigidimarina* strains deficient in this gene do not grow on fumarate [Saffarini and Nealson, 1993]. Expression of the fccA gene appears to be regulated at the transcriptional level in response to the redox potential of terminal electron acceptors present [Gordon *et al*, 1998]. It is down-regulated when oxygen is present and also if TMAO or nitrate is present, although in the case of the latter two to a lesser extent. This is presumably because components of alternative electron transport chains are synthesised instead when these substrates are present. The signal sequence immediately upstream from the N-terminus of the protein enables transportation of Fcc_3 to the periplasm. When this sequence is disrupted or removed Fcc_3 is still expressed, but located in the cytoplasm and cells are unable to utilise fumarate as a terminal electron acceptor [Gordon *et al,* 1998].

1.3.2 Electron transport in *Shewanella*

In order for *S. frigidimarina* to respire on fumarate, Fcc_3 has to be constantly supplied with electrons. It has been proposed that it may receive electrons from the periplasmic tetrahaem cytochrome *c*, CymA. This 21 kDa protein is anchored to the periplasmic membrane and is a member of the NapC/NirT family of proteins that are known to transfer electrons from quinols in the membrane to periplasmic reductases. Experiments carried out previously in this laboratory have shown that CymA is able to directly transfer electrons to Fcc_3 *in vitro* [Schwalb *et al*, 2002], although it is possible that *in vivo*, electrons are transferred indirectly by way of an as yet unidentified electron carrier. Figure 1.11 shows a possible electron transport chain that includes CymA and Fcc_3 and utilises fumarate as a terminal electron acceptor. It has been hypothesised that CymA is able to interact with different terminal reductases that are expressed depending on which terminal electron acceptors are present. This has been supported by experiments that demonstrated that strains of *S. oneidensis* MR-1 deficient in CymA were no longer able to respire using nitrate, fumarate, Mn^{4+}, Fe^{3+} and DMSO [Myers and Myers, 1997] [Schwalb *et al*, 2003].

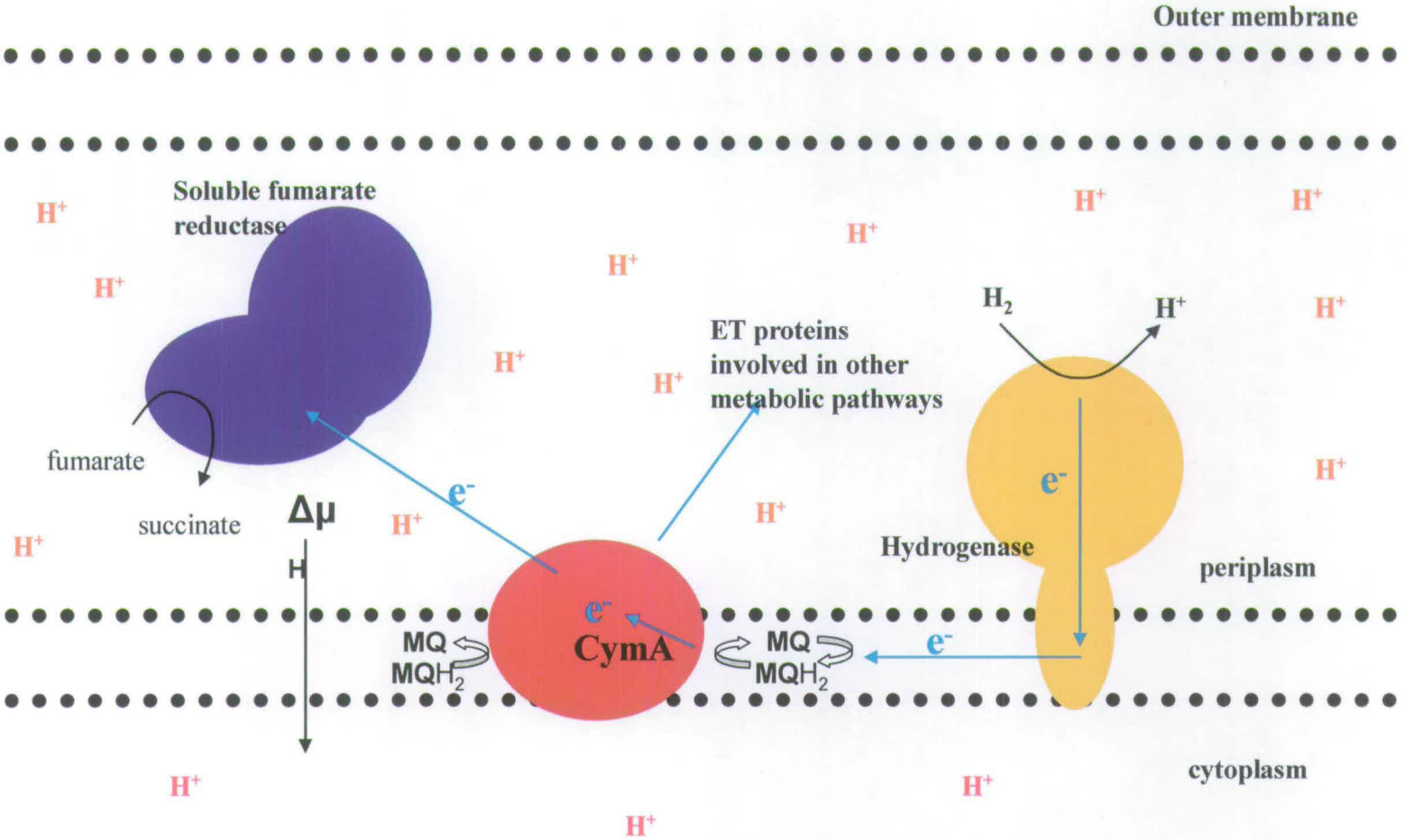

Figure 1.11 Possible electron transport chain involving Fcc_3 and CymA

Hypothetical anaerobic electron transport chain that might be employed during respiration upon fumarate by Shewanella. Electrons from hydrogenases are transferred to ubiquinol which then transfers them to a membrane-bound tetraheme cymA, before they are transferred to the soluble fumarate reductase and used in the catalytic reduction of fumarate to succinate. It is thought that CymA partakes in more than one anaerobic electron transport chain as it is able to donate electrons to a variety of different terminal reductases.

Figure 1.12 Global structure of Flavocytochrome c_3

Global structure of Flavocytochrome c_3. The cytochrome domain which incorporates four c-type haems is shown in red, the Flavin domain is shown in yellow and the mobile clamp domain is shown in blue

1.4 Crystal structure of Fcc$_3$

The crystal structure of *S. frigidimarina* Fcc$_3$ was solved in 1999 to 1.8Å (see Fig 1.12) [Taylor *et al*, 1999]. Structures were also obtained for Fcc$_3$ from *S. putrefaciens* MR-1 (which shares 59% sequence similarity with *S. frigidimarina* Fcc$_3$) and for iron-induced Fcc$_3$, an isoform of Fcc$_3$ [Leys *et al*, 1999] [Bamford *et al*, 1999]. Fcc$_3$ is functionally and structurally related to L-aspartate oxidase which catalyses the oxidation of L-aspartate to iminoaspartate but is also able to reduce fumarate to succinate [Mattevil *et al*, 1999]. It can be divided into three functionally distinct domains; a tetrahaem cytochrome domain, flavin domain and clamp domain. Unlike

QFR, Fcc_3 is not bound to the cytoplasmic membrane and exists freely in the periplasm. Also, it uses c-type haems to transfer electrons to the active site instead of iron-sulphur clusters. Previous studies of fumarate reduction kinetics have shown that Fcc_3 is generally a unidirectional fumarate reductase [Turner *et al*, 1999] as it catalyses the oxidation of succinate at a slow rate compared to QFR, which catalyses succinate oxidation and fumarate reduction with similar efficiencies.

1.4.1 Cytochrome domain

The cytochrome domain is composed of the first 100 residues from the N-terminus (after removal of the signal peptide) and incorporates four *c*-type haem groups (figure 1.13 a) that are bis-His axially ligated and form a molecular "wire" 40 Å in length along which electrons are transferred [Taylor *et al*, 1999]. Studies have indicated that Fcc_3 most likely receives electrons from the small membrane-bound tetrahaem CymA [Schwalb *et al*, 2002], instead of receiving them from the quinone pool (constrained within the membrane) directly. Electrons are then transferred by the haems to FAD (Flavin adenine dinucleotide) at the active site. The rate of electron transfer decreases with distance and in order for transfer to be fast enough to be of use for biological catalysis, redox centres are generally required to be less than 14 Å apart [Page *et al*, 1999]. The short distances between the haems (figure 1.13) and their orientation relative to each other optimise fast electron transfer to FAD [Smith *et al*, 2006] and experiments have shown that it is not the rate-limiting factor [Jones *et al*, 2000] for fumarate reduction. Reduction potentials (figure 1.13) for each of the four haems have been determined by redox potentiometry [Doherty, 1999] and protein film voltammetry [Turner *et al*, 1999].

Figure 1.13 – Cytochrome Domain

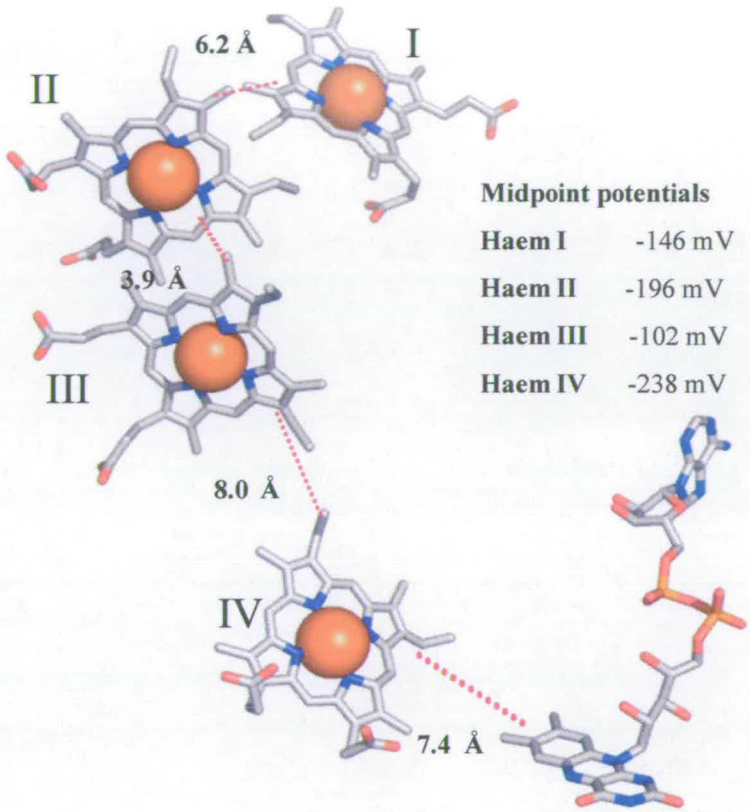

Arrangement of redox cofactors in Fcc_3. Edge to edge distances (pink dashes) are indicated. Haems are numbered I-IV and their midpoint reduction potentials are listed. The short distances between haems facilitate fast electron transfer to the active site FAD.

There is no conclusive evidence that the haems in the cytochrome domain of Fcc_3 are always reduced in a particular order. It has been proposed that the purpose of haems I – III is to maximise electronic coupling between the electron donor to Fcc_3 and FAD at the active site, particularly as all three are located at the surface of the protein and exposed to solvent. Mutation of His 61 (the axial ligand of haem IV) to methionine and alanine resulted in five-fold or 10-fold lower k_{cat} values respectively compared to wild-type [Rothery *et al*, 2003] . Solvent isotope studies of H61M and H61A revealed that electron transfer had become rate-limiting although there is no real

change in the midpoint reduction potential of haem IV. Studies of a closely related flavocytochrome Ifc_3, also expressed by *S. frigidimarina* [Butt *et al*, 2000], [Pessanha *et al*, 2003], have led to the suggestion that two electron transfer pathways each donate an electron to FAD either in parallel, or after first converging, ensuring fast electron delivery to the active site. However, the crystal structure disproves this so it is proposed that haems I - III serve only to maximise electron transfer to haem IV and subsequently FAD at the active site [Rothery *et al*, 2003].

1.4.2 Flavin domain

The flavin domain consists of residues 111-364 and 503-571 [Taylor *et al*, 1999], and forms part of the active site (the rest is composed of residues from the clamp domain) that includes FAD bound via non-covalent interactions. It shares a high level of sequence similarity to the flavin subunits of *Escherichia coli* and *Wolinella succinogenes* fumarate reductases [Iverson *et al*, 1999] [Lancaster *et al*, 1999] and exhibits the typical Rossman-like fold. Despite the differences between Fcc_3 and the membrane-bound fumarate reductases, the architecture of the active site is highly conserved across all fumarate reductases suggesting a common catalytic mechanism. Electron transfer from FAD to fumarate is particularly favoured in Fcc_3 because FAD has a much lower reduction potential (-152mV) than the fumarate-succinate couple (30mV at pH 7.0) [Turner *et al*, 1999]. However, this lower potential does not favour efficient catalysis of succinate oxidation (reverse direction) which only occurs at a low rate with a k_{cat} of ~ $1.s^{-1}$ [Moysey, 2001]. The reason for this low potential is the non-covalent nature of FAD binding. As previously mentioned during discussion of *E. coli* QFR, FAD is bound covalently via a histidyl residue. Substitution of His 44 from the flavin subunit of QFR results in the loss of covalent linkage to the FAD

molecule, although it still remains tightly bound through non-covalent interactions with the protein matrix. This has the effect of knocking out succinate oxidation activity yet the enzyme retains significant fumarate reductase activity. Therefore the way in which the FAD molecule is attatched to the protein appears to determine the directionality of catalysis. [Blaut *et al*, 1989].

1.4.3 Clamp domain

The clamp domain is made up of residues 365-502. In addition to forming one side of the active site (figure 1.14 *a*), the clamp domain is capable of movement, which has been postulated to allow substrate access/product release to and from the active site [Taylor *et al*, 1999]. Comparison of the crystal structure of Fcc_3 in the "closed" conformation (shown previously in figure 1.12) with the crystal structure of an isozyme of Fcc_3 – iron-induced flavocytochrome c_3 (iFcc_3) – obtained in the open conformation [Bamford *et al*, 1999], revealed that the clamp domain moves 14° towards the cytochrome domain, opening a gap at the active site. When the clamp is closed, steric constraints cause fumarate to be held in a twisted conformation at the active site, an important aspect of the catalytic mechanism which will be discussed in section 1.4.4. In order to ascertain the importance of clamp domain mobility to enzyme activity, Fcc_3 was engineered so that the clamp domain was immobilised in the closed conformation [Rothery *et al*, 2004]. This was done by substituting two amino acid residues with cysteines (alanine 251 from the cytochrome domain and serine 430 from the clamp domain) which under oxidising conditions formed a disulphide bridge, locking the two domains together in a fixed position. This bridge could be broken by the addition of dithiothreitol allowing comparison of fumarate reduction rates between "mobile" and "fixed" Fcc_3. It was found that the unbridged

double mutant retained approximately 63% of the activity of wild-type Fcc_3. When the disulphide was formed, activity dropped to about 25% of that observed in wild-type. It was concluded that although clamp domain movement may optimise enzymatic activity, it does not appear to be essential for catalysis of fumarate reduction [Rothery *et al*, 2004].

1.4.4 Catalytic mechanism of fumarate reduction

Figure shows the crystal structure of the active site of Fcc_3 with a malate-like molecule bound [Taylor *et al*, 1999]. The four carbon atoms of the substrate have been labelled 1 – 4 to illustrate their relative orientation to active site residues. Hydrogen bonding interactions and steric constraints imposed by two nearby methionine residues (Met 236 and Met 375) cause the C1 carboxylate to be twisted out of plane. This combined with the positive environment (His 504, Arg 544) surrounding the C4 carboxylate, polarises the C2 - C3 double bond (figure 1.14 *b*). As a result, significant positive charge is conferred on C2, facilitating nucleophilic attack by N5 of the flavin alloxazine ring and hydride transfer (figure 1.14 *b*). To complete formation of succinate, a proton is abstracted from arginine 402 [Doherty *et al*, 2000]. Arg 402 is reprotonated after each reduction by Glu 378, a residue that takes part in the proposed "proton pathway" [Pankhurst, 2002], thought to be the rate-limiting factor in fumarate reduction. Fcc_3 follows Michaelis-Menten kinetics and converts fumarate to succinate with a k_{cat} of 509 ± 15 s^{-1} and a K_m of 25 ± 2 μM [Doherty, 1999]. The k_{cat} represents the number of molecules of fumarate reduced to succinate by a single enzyme molecule per second. The K_m is the Michaelis constant, which is the concentration of substrate when activity is 50 % of the maximum and is

Figure 1.14 Mechanism of fumarate reduction by Fcc_3

a)

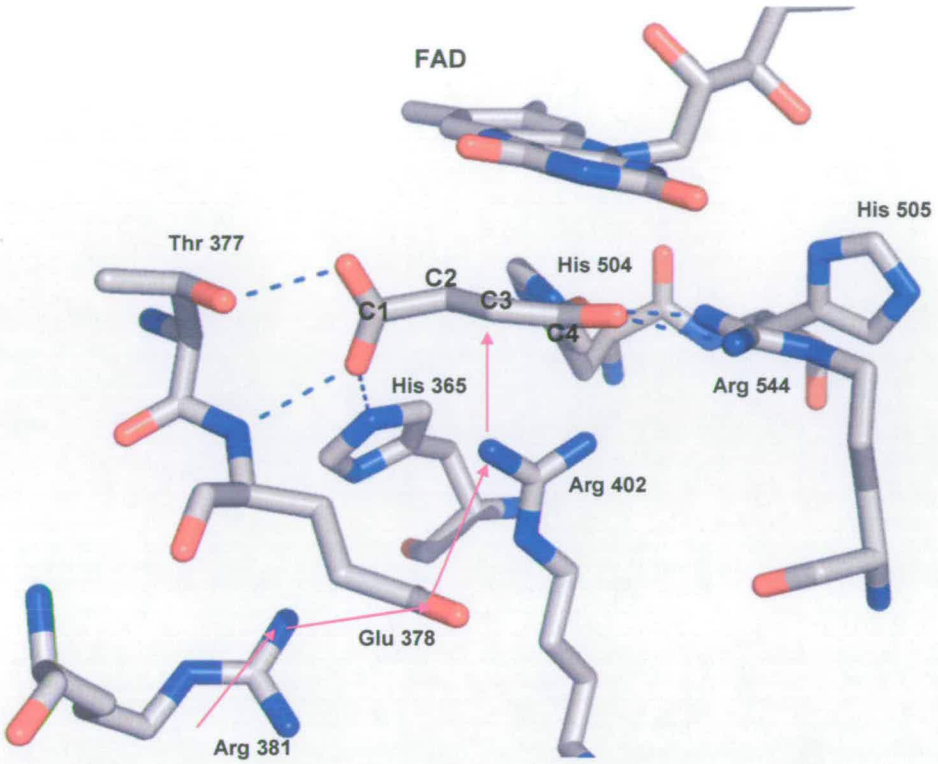

b)

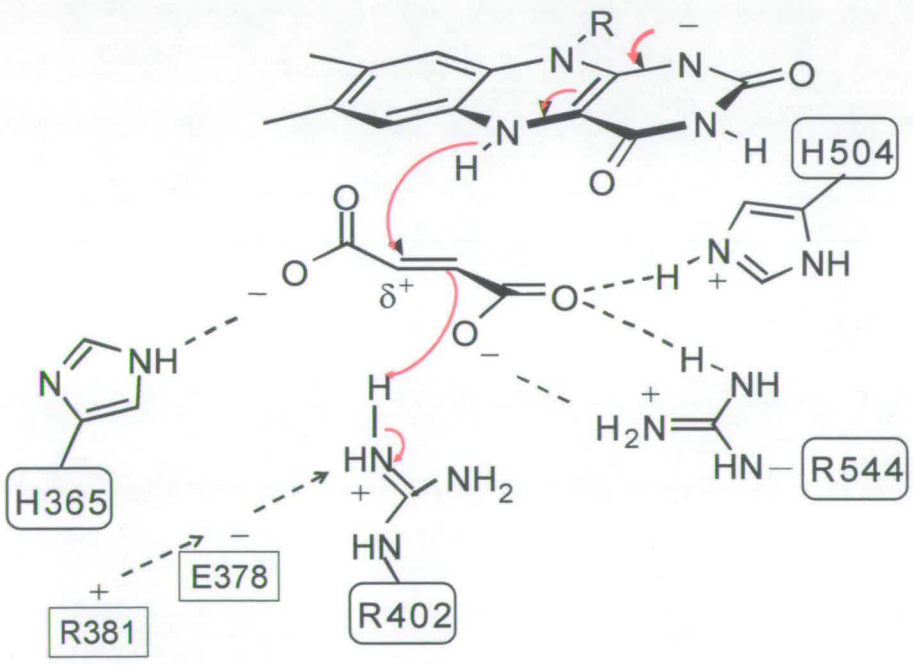

a) Crystal structure of active site of Fcc_3 complexed with fumarate. The carbons of the substrate are numbered 1-4 to indicate their relative orientation to the active site residues. The pink arrows indicate the proton pathway, which continually reprotonates R402 and is the rate-determining step of catalysis H-bonds are shown as blue dashes. b)Polarisation of the double bond in fumarate is aided by twisting of the C1 carboxylate and the influence of positive residues around C4 (His 504 Arg 544). The two electron reduction of fumarate is achieved by hydride transfer from flavin N5 to fumarate C2 followed by proton transfer from Arginine 402 to fumarate C3.

a measurement of how readily the enzyme-substrate complex forms. It is thought that hydride transfer occurs before proton transfer. The malate-like molecule is a hydroxylated intermediate which arises from nucleophilic attack by a water molecule under oxidising cyrstallisation conditions (hydride transfer cannot occur). The geometry of this intermediate suggests it has not yet been protonated suggesting that fumarate reduction occurs in two steps.

1.4.5 Arginine 402

Often the role of an active site acid/base is carried out by a histidine. However, when either His 365 or His 504 were substituted with alanine, the enzyme retained significant activity, approximately 10% of that observed for the wild-type enzyme. This suggests that while these histidines play a role during catalysis of fumarate reduction, they are not essential for it to occur. Mutagenesis experiments that replaced arginine 402 suggested that this residue was the active site acid. Subsequent kinetic assays of these engineered forms of Fcc_3 showed that activity was completely knocked out when Arg 402 was substituted with alanine, but that residual activity was observed for substutions with lysine or tyrosine albeit at levels $10^3 - 10^4$ times lower than wild-type [Mowat *et al*, 2002]. This implies that these residues are also capable of acting as the active site acid. The two positions that each NH_2 of the guanidinium group from arginine 402 occupies are denoted A and B in figure 1.15 and reflect the dual role that arginine has in catalysis. The NH_2 at position A is part of the proton delivery system that transfers protons to the buried active site via residues from the surface exposed to solvent. It is distanced 3Å from C3 of the substrate - ideally placed to donate a proton during catalysis. The NH_2 in position B forms H-bonding interactions with a sidechain amide of Glu 363 and an O atom from the C4 carboxyl

Figure 1.15 Position of arginine 402 relative to substrate

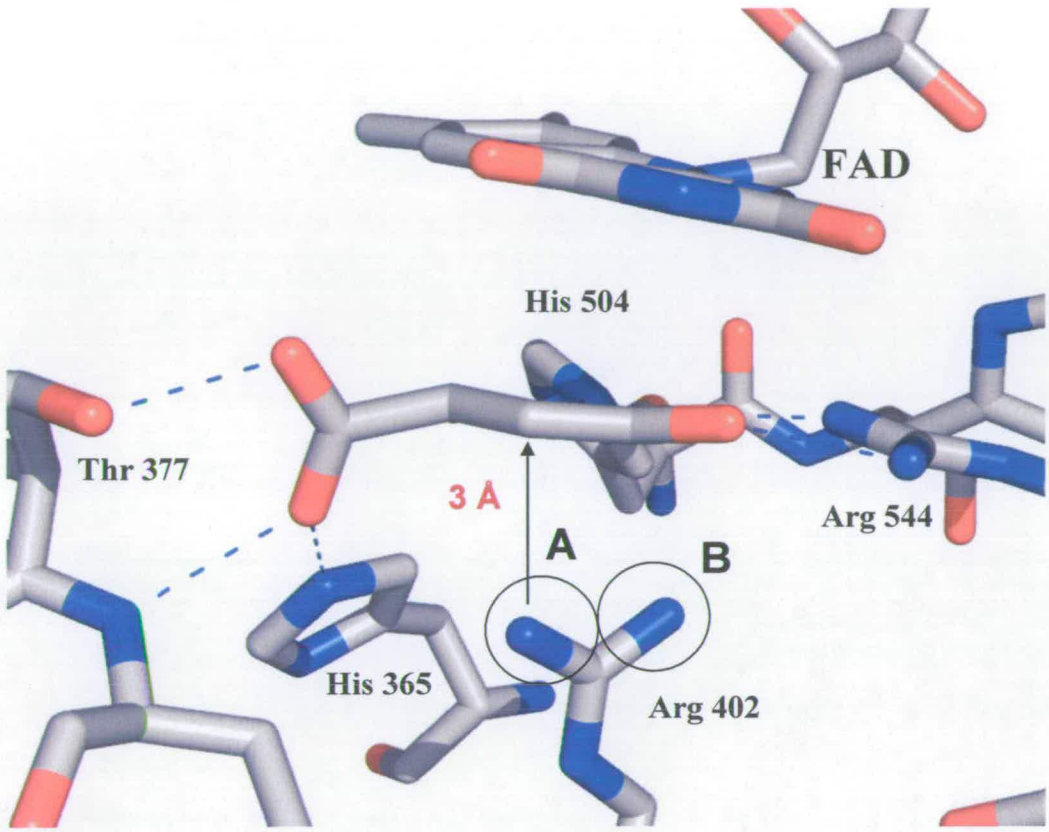

Crystal structure showing positioning of the guanidinium group of Arginine 402 relative to bound fumarate. The NH_2 group at position A donates a proton to C3 of fumarate to complete reduction to succinate. The NH_2 at position B stabilises the build-up of negative charge during the transition state. Arginine 402 thus acts as both a Brønsted and a Lewis acid during catalysis.

of fumarate, stabilising the build-up of negative charge that occurs during the transition state thus acting as a Lewis acid and increasing the rate of the reaction. The tyrosine and lysine residues occupy a similar position in the active site as that of arginine in the WT enzyme. They are distanced 3.2Å and 3.7Å from C3 of fumarate respectively and so are able to transfer a proton and function as a Brønsted acid though less efficiently than arginine. The structures for R402A and R402K show a water molecule at position B, but this is not seen in R402Y. As the water molecule is

unable to stabilise the transition state, the arginine mutants cannot act as a Lewis acid, another reason that reduction rates are so low compared to the wild-type enzyme.

1.5 Project aims

1.5.0 Determination of substrate range

The kinetics of fumarate reduction by Fcc_3 have previously been thoroughly investigated [Doherty, 1999], [Pankhurst, 2002]. The purpose of this project is to determine whether Fcc_3 is able to catalyse the reduction of similar compounds (fumarate derivatives) with any degree of efficiency. The ability of Fcc_3 to reduce or bind to particular chemicals could provide a great deal of information about the chemistry and morphology of the active site as well as explore its catalytic potential. Prior work demonstrated that 2-methylfumarate could bind to Fcc_3 and act as an inhibitor of fumarate reduction [Moysey, 2001]. However, at the time these studies were done, 2-methylfumarate was not thought to act as a substrate.

1.5.1 Engineering of Fcc_3

An obvious question is whether the alteration of the Fcc_3 active site would alter the enzyme's substrate specificity. Previous studies of *Shewanella oneidensis* MR-1 (closely related to *Shewanella frigidimarina*) revealed that it expresses four novel proteins that share high sequence similarity to Fcc_3 [Bilsland, 2004]. These enzymes were denoted Fcc54, Fcc56, Fcc63 and Fcc342. Unlike Fcc_3, these flavocytochromes consist of two subunits instead of a single polypeptide. They are encoded by two separate genes adjacent to each other in the genome for example; *fccA54,* which encodes the flavin domain and *fccB54* which encodes the tetrahaem cytochrome domain for Fcc54. Molecular modelling and sequence alignment studies predicted

that these flavocytochromes may function as monocarboxylate reductases. However, so far no assays of the enzyme's activity in this capacity have yet been carried out. This is due to the fact that so far no intact enzyme containing both subunits has yet been purified. Many of the residues predicted to make up the active site of these putative enzymes appear to be conserved in Fcc_3 and in other monocarboxylate reducing enzymes from other organisms. Examples include a 50 kDa periplasmic flavoprotein purified from *Geobacter sulfurreducens AM-1* [Galouchko *et al*, 1996], and a 52 kDa periplasmic flavoprotein which is the product of the *fccA* gene from *Wolinella succinogenes* [Gross *et al*, 2001]. The *Geobacter* flavoprotein was also found to be able to reduce acrylate, crotonate and pentenoate [Mikoulinskaia *et al*, 1999]. For this reason, mutagenesis experiments that substituted active site residues were carried out in order to determine if Fcc_3 could be engineered to act upon substrates not reduced by the wild-type enzyme.

Chapter 2

Materials and Methods

2.0 Molecular biolgy

Recombinant Flavocytochrome c_3 was prepared using the $pEGX_1$/EG301 expression vector system ($pEGX_1$ plasmid - pMMB503EH fcc_3 with signal sequence, EG301 – *Shewanella frigidimarina* NCIMB400 Str^R, Δfcc:ahp Km^R) [Overbye *et al*, 1995] [Gordon *et al*, 1998]. Bacterial strains were stored long term as DMSO stocks (-80 °C).

2.0.1 Site-directed mutagenesis

Fcc_3 mutants were generated by in-vitro site-directed mutagenesis using the QuikChange® XL system (Stratagene®). Mutagenic primers (shown in appendix 4) were designed by Dr. Caroline Miles and supplied by Invitrogen. The primers were annealed to thermally denatured double stranded plasmid DNA ($pEGX_1$) containing the target gene – fcc_3. *Pfu Turbo*® DNA Polymerase incorporated the mutation as it extended the mutagenic primers and replicated the plasmid, resulting in nicked circular daughter strands. The parental plasmid DNA is methylated so it was digested by the addition of *Dpn* I endonuclease which specifically targets methylated DNA. Because the daughter strands are not methylated, they remained intact and were transformed directly into XL10-Gold ultracompetent cells. Once transformed, cellular enzymes repair the nicks in the DNA to produce the new plasmid containing the mutation.

2.0.2 Cell Transformation

Cell transformations were carried out by the direct addition of the plasmid DNA to chemically competent cells (XL10-Gold - Stratagene®). The mixture was incubated on ice for 45 minutes before being heat-shocked at 45°C for 60 seconds. The cells

were then incubated on ice for five minutes before the addition of 750 µl Luria Broth after which, cells were incubated while shaking at 37°C for One hour. The plasmid contains streptomycin and kanamycin resistance genes so the cells were then plated out on to agar plates containing 25µg/ml streptomycin and 50 µg/ml kanamycin in order to select for transformants. The plates were incubated overnight at 37°C and single colonies were picked and then grown in 5ml LB to an OD of approximately 0.6 before being pelleted in preparation for plasmid purification. Plasmids were purified using the QIAprep® miniprep kit (QIAGEN). Purified plasmids were sequenced (sequencing service at the Institute of Cell and Molecular biology at the University of Edinburgh - ABI 3100 genetic analyser) to ensure that the correct mutation was present. The plasmids were then transformed into competent SM10 *E. coli* cells using the same method as before. The reason for this transformation is that the plasmid has to be transferred finally to *S. frigidmarina* due to the fact that *E. coli* cannot incorporate *c*-type haems into proteins so are no use for expressing Fcc_3. SM10 cells are able to transfer plasmid DNA to *S. frigidimarina* via bacterial conjugation.

2.0.3 Bacterial conjugation

Conjugation and transfer was achieved by mixing cultures of both bacteria (with a ratio of 10:1 *S. frigidimarina*:*E. coli* SM10) before pipetting 50 µl of the mixture on to a nitrocellulose membrane on top of minimal agar. The plates were incubated overnight at 23°C (to favour growth of *S. frigidimarina*) after which the bacteria were removed from the membrane by vortexing in 1 ml LB. The cells were then pelleted by centrifugation and resuspended in fresh LB (1 ml) before a small amount was added to agar plates containing rifampicin (to select for *S. frigidimarina*), streptomycin and kanamycin (to select for plasmid). After incubation at 23°C for

about 48 hours, single colonies of *S. frigidimarina* containing mutant Fcc_3 could be picked for large scale growth of cells and expression of protein.

2.1 Bacterial growth

All cultures were grown in Luria Bertani high salt media containing:

Bacto tryptone	10g/l
Yeast extract	5g/l
NaCl	10g/l

Before use, media was sterilised in autoclave. *Shewanella frigidimarina* cells were inoculated into 75ml starter flasks supplemented with kanamycin (50 μg/ml, sigma) and streptomycin (25 μg/ml, sigma), previously sterilised with a 0.2 μm syringe filter (sartorius). Cells were grown overnight in an Innova 4330 shaker (180 rpm) at 23°C. 5ml of starter culture was inoculated into 1 litre flasks (containing 500ml media plus antibiotic at concentrations stated above) and grown in shaker at 23°C for approximately 8 hours (or optical density of at least 0.6 at 600nm). Overexpression of Fcc_3 was then induced by addition of 500 μl IPTG (isopropyl-β-D-thiogalactopyranoside (Europa bioproducts), 250 mg/ml) and left overnight (remaining in shaker at 23°C).

2.2. Protein Purification

Buffers

TRIS 10mM TRIS (Acros organics)

10mM NaCl (Fisher scientific)

pH adjusted to 8.4 with HCl

Buffer A 10mM MOPS (Sigma)

pH adjusted to 7.8 with NaOH at 25°C

Buffer B 10mM MOPS (Sigma)

0.5M NaCl

pH adjusted to 7.8 with NaOH at 25°C

2.2.1 Harvesting of cells and lysis

Cells were pelleted by centrifugation at 8,000 rpm (Sorvall RC-5B) for 20 minutes. Cells were suspended in buffer (10mM TRIS, pH 8.4) and broken open by sonication (Sanyo soniprep 150) on ice at 10 microns for six 20 second bursts (20 seconds rest in between, left for five minutes after 3rd burst to prevent overheating). The suspension was then centrifuged at 20,000 rpm for one hour to remove cell debris. Fcc_3 was purified from supernatant over a four-step process.

2.2.2. Ammonium sulphate cut

Ammonium sulphate (Fisher Scientific) was added to supernatant to give a final concentration of 243g/l (40%) and left on a magnetic stirrer for 2 hours at 4°C. The mixture was then centrifuged at 20,000 rpm for 20 minutes. Fcc_3 is not precipitated at

this concentration so remains in supernatant which is subsequently dialysed (x3) in 4 litres 10mM TRIS buffer pH 8.4 to remove salt.

2.2.3. Anion exchange, DE-52

A 150ml column of DE-52 (Whatman) was equilibrated with 5 column volumes of 10mM TRIS pH 8.4 before loading protein. Bound Fcc_3 is seen as a dark red band at the top of the column. The column was washed through with 10mM TRIS pH8.4 to remove unbound protein until the flow-through had minimal absorption at 280nm. The column was then washed through with 4 or 5 column volumes of 0.1 M NaCl to remove bound impurities before Fcc_3 was eluted with 0.2 M NaCl in a series of 20 ml fractions. Fractions were retained depending on the ratio of absorbance at 408 nm (haem) to that at 270nm (total protein). For pure protein, Abs_{408}/Abs_{270} is approximately 4 [Kate Pankhurst, 2002], but at this stage, fractions with a ratio >1 were kept. Retained fractions were dialysed (x2) in 4 litres 10mM TRIS pH 8.4.

2.2.4. Anion exchange, Hydroxyapatite

A 60ml Hydroxyapatite column (Bio-Rad) was equilibrated with about 5 column volumes 10mM TRIS before loading protein. The column was washed through with 10mM TRIS to remove unbound protein before eluting Fcc_3 with 0.1 M K_2HPO_4 (fisher scientific). The purity was checked by U.V. spectroscopy as before and fractions with $Abs_{408}/Abs_{270} > 2.5$) were retained, then dialysed against 10mM TRIS pH 8.4.

2.2.5. FPLC - Fast Protein Liquid Chromatography

FPLC (ÄKTA, Amersham Pharmacia Biotech) is an automated step that uses a 60 ml HiLoad 26/10 strong anion exchange Q sepharose column. The column was equilibrated with buffer A prior to loading of protein then washed through with several column volumes of buffer A. Fcc_3 was eluted using a linear salt gradient (0 - 0.5M) achieved by addition of 0 – 100% buffer B.

2.3. Determination of protein concentration and FAD content

2.3.1. Determination of protein concentration

The concentration of purified Fcc_3 was determined by measurement of its absorbance at 419nm using a Shimadzu UV-2101 PC spectrophotometer after its reduction by sodium dithionite (Fisher scientific) (ε = 752800 $M^{-1}.cm^{-1}$ [Pealing *et al*, 1995]).

Protein concentration is calculated using the Beer-Lambert equation;

$$A = \varepsilon.c.l$$

where A = Absorbance, ε = molar absorbance($M^{-1}.cm^{-1}$) and l = pathlength (cm).

2.3.2. FAD determination

FAD is bound non-covalently to Fcc_3. Recombinant Fcc_3 is not expressed with a full complement of FAD and also, some may be lost during purification. To determine the percentage of Fcc_3 that retained bound FAD, 150 µl of 50% Trichloroacetic acid was added to TRIS buffer containing the equivalent of 50µl of 80µM protein, and made up to a total volume of 1250 µl with buffer. The precipitated haem and protein was pelleted by centrifugation in a microcentrifuge (eppendorf) for 2 minutes, leaving FAD in the supernatant. The supernatant was removed and adjusted to pH 7 by

addition of Na_2CO_3 (Fisher Scientific) before measurement of absorbance at 450nm (ε = 11,100). FAD concentration is compared to Fcc_3 concentration and FAD content is taken as a percentage (one Fcc_3 molecule binds one molecule of FAD). All kinetic measurements are adjusted to assume FAD content of 100%.

2.4 Gel electrophoresis

The eluate obtained from each stage of purification was analysed by SDS-polyacrylamide gel electrophoresis followed by Coomassie Blue staining to determine the presence and purity of Fcc_3 .

Figure 2.1 Coomassie stained gel showing purification of Fcc_3

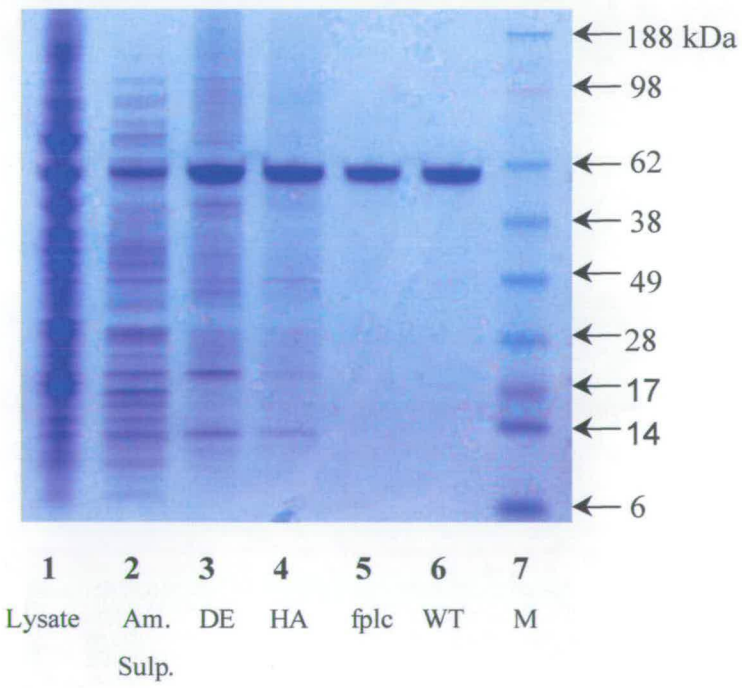

Lane 1 = cell lysate, lane 2 = after 40% Ammonium sulphate precipitation, lane 3 = after anion exchange – DE-52, lane 4 = after anion exchange on Hydroxyapatite, lane 5 = after fast protein liquid chromatography – Q Sepharose, lane 6 = pure wild-type Fcc_3, lane 7 = protein markers.

4X NuPAGE LDS sample buffer (20µl) was added to protein samples (the amount added depends on the concentration of Fcc_3 present determined by UV-Vis spectroscopy) and made up to 50 µl volume with H_2O. Samples were then boiled for two minutes before being loaded on to a prepoured NuPAGE 4-12% Bis Tris gel (Invitrogen) which was immersed in NuPAGE Mes running buffer. The voltage was held at 150 V for approx 45 minutes (or until the gel front reached the bottom). The gel was then stained with a solution containing 1% Commassie Blue, 40% methanol and 10% glacial acetic acid. The gel was then rinsed with destaining solution (40% methanol, 10% glacial acetic acid) to reveal protein bands. A mixture of marker proteins of known molecular weight were also added (figure 2.1, lane 7), in order to check that purified protein was the correct mass. It can be seen from the gel in figure 2.1 (lane 6) that pure protein is obtained using the purification method described in this chapter.

2.5. Steady state Kinetics

Buffers:

pH 6.0, 6.5, 50mM MES (Sigma)
0.45M NaCl
~1 mM Methyl viologen (Sigma)

pH 7.0-8.5, 50mM TRIS.HCl
0.45M NaCl
~1 mM Methyl viologen

pH 9.0-10.0, 50mM CHES (Sigma)
0.45M NaCl
~1 mM Methyl viologen

The activity of Fcc_3 for the reduction of 2-methylfumarate (Fluka) was assayed by monitoring the oxidation of an artificial electron donor, methyl viologen (shown below). The reduced form of methyl viologen readily donates electrons to Fcc_3 *in vitro* because it has a much lower reduction potential (E_m = -430 mV). These electrons are then transferred to substrate by enzymatic reduction. The assay is limited to pH 6 and above as dithionite – which is used to reduce methyl viologen – breaks down under more acidic conditions [Doherty, 1999]).

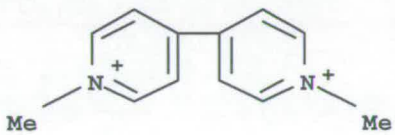

All assays were performed under anaerobic conditions in Belle Technology glovebox (O_2 < 5 ppm) at 25°C. A few milligrams of MV was included in buffer prior to degassing (oxygen in solution replaced with nitrogen). The reduced form of methyl viologen absorbs strongly at 600 nm with a molar absorbance (ε) of 13000 M^{-1} cm^{-1}. The oxidized form has $\varepsilon_{600} = 0$, so as it loses electrons, there is an observable loss in absorbance (colour changes from blue to colourless upon oxidation). An aliquot of sodium dithionite was added to 3ml of buffer in a cuvette to give an Abs_{600} of ~1.0 (approximate concentration of MV_{red} = ~80 μM). Protein was incubated in the buffer and the assay intitated by addition of substrate. The decrease in Abs_{600} was monitored over time using a Shimadzu UV-PC 1501 spectrophotometer. The rate of decrease reflects the rate of reduction by Fcc_3 according to the formula below.

$$k_{obs} = \frac{\Delta Abs}{t \times \varepsilon_{mv} \times [E]}$$

2.6. Bulk reduction

Millimolar concentrations of methylsuccinate product were required for subsequent analysis. This was achieved via a bulk electrochemical reduction using a 3 electrode cell shown in fig 2.2. Current was passed through solution (using platinum electrodes plus an Ag/AgCl reference

Figure 2.2 - Bulk reduction apparatus

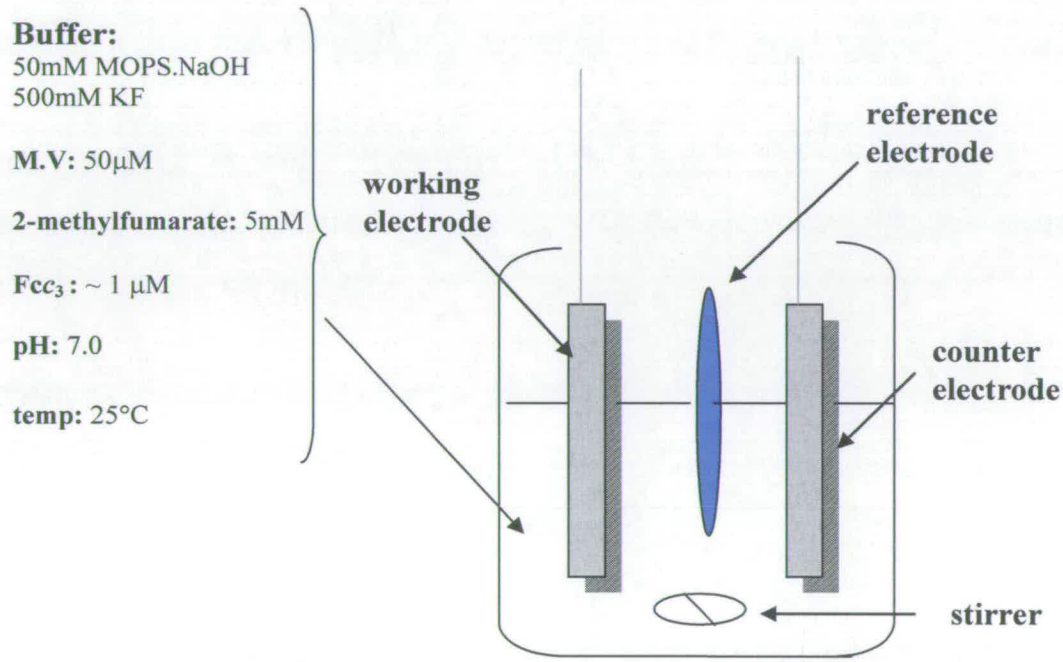

electrode) in order to keep the reaction going until all the substrate was used up (the potential was held at –0.6 V). Although the reduction of 2-methylfumarate proceeds faster at pH 9.0 (see results), the pH was kept neutral. This is because Fcc_3 is less stable at pH 9.0 and would lose activity before the reduction was complete. Protein

was separated from product by centrifugation through a 10 kDa membrane (Centriprep, Millipore)

2.7. Circular Dichroism

Circular Dichroism spectroscopy (Jasco J-810 spectropolarimeter) was used to determine the configuration of the chiral centre in methylsuccinate. R and S-methylsuccinate molecules rotate polarized light in opposite directions and so absorb light differently. CD spectra of the product (generated by electrochemical reduction) were compared with spectra of standard R-methylsuccinate and S-methylsuccinate (Sigma). The concentration of methylsuccinate was ~ 500 μM in quartz cell, pathlength – 1cm.

2.8. Crystallisation and refinement

All crystal structures of wild-type and mutant forms of flavocytochrome c_3 were obtained by Dr Christopher Mowat. Crystallisation was carried out by hanging drop vapour diffusion at 4 °C in Linbro plates. Crystals were obtained with well solutions comprising 100 mM TrisHCl buffer (pH 7.8-8.5)(measured at 25 °C), 80 mM NaCl, 16-19 % PEG 8000. In the case of the wild-type enzyme 1 mM 2-methylfumarate was present in the well solution, for the T377A mutant enzyme 10 mM fumarate was used, and for the H365G enzyme 10 mM trans-2-methyl-2-pentenoate was present. Hanging drops (4 μl volume) were prepared by adding 2 μl of 6 mg/ml protein (in 10 mM TrisHCl pH 8.5) to 2 μl of well solution. After approximately seven days needles of up to 1 mm × 0.2 mm × 0.2 mm and plates of up to 0.5 mm × 0.5 mm × 0.2 mm were formed. Crystals were immersed in a solution of 100 mM sodium acetate buffer (pH 6.5), 20 % PEG 8000, 1 mM 2-methylfumarate/ 10 mM fumarate, 10 mM

trans-2-methyl-2-pentenoate as appropriate, and 80 mM NaCl, containing 23 % glycerol as a cryoprotectant, prior to being mounted in nylon loops and flash cooled in liquid nitrogen. For the wild-type enzyme a data set was collected to 1.5 Å at station 14.1 (λ = 0.975 Å) at SRS Daresbury using an ADSC Quantum 4 CCD detector. Crystals belonged to space group $P\ 2_1$ with cell dimensions a = 45.449 Å, b = 91.687 Å, c = 78.287 Å, and β = 91.13 °. For the T377A mutant enzyme data to a resolution of 2.0 Å were also collected at SRS Daresbury (station 14.1; λ = 0.975 Å) using the same detector. These crystals were found to belong to space group $P\ 2_1$ with cell dimensions a = 45.331 Å, b = 91.415 Å, c = 78.171 Å, and β = 91.12 °. In the case of the H365G mutant enzyme a data set to a resolution of 1.9 Å was collected at ERSF Grenoble (beamline BM14; λ = 0.9785 Å) using a Mar Research Mar225 detector. The crystals belonged to space group $P\ 2_1\ 2_1\ 2_1$ with cell dimensions a = 57.642 Å, b = 83.322 Å, and c = 139.703 Å.

In all cases data processing was carried out using the HKL package [Otwinowski and Minor, 1997]. The wild-type flavocytochrome c_3 structure (PDB ID: 1QJD), stripped of water, was used as the initial model. Electron density fitting was carried out using the program Turbofrodo [Roussel and Cambillau, 1991] and structure refinement was carried out using Refmac [Murshudov *et al*, 1997].

Chapter 3

Crystal structures

3.0 Introduction

Crystal structures were obtained for WT (wild-type) Fcc_3 and two engineered forms of the enzyme (T377A, H365G). Data refinement statistics for all three structures are included in table 3.1. There were already several crystal structures of WT and mutant forms of Fcc_3 available but all were bound to fumarate. The aim was to find out if there were any differences in binding interactions with the enzyme active site when 2-methylfumarate was the substrate. As will be discussed in chapter 5, alterations to the active site were made by substituting amino acid residues that form hydrogen-bonds with the substrate. A crystal structure was obtained for mutant Fcc$_3$ where threonine 377, which forms two hydrogen-bonds with fumarate at the WT active site, was replaced with alanine (T377A). Another mutant (H365G) contained a glycine residue at position 365, which is normally occupied by a histidine that forms a single hydrogen bond with the substrate. Crystals obtained for WT and T377A were in the "closed" form, with substrate bound. The H365G crystals were formed from Fcc_3 without substrate bound, in the "open" conformation. Crystallographic results for each structure are discussed in the following pages.

Table 3.1 – Crystallographic data for WT, T377A and H365G Fcc_3

resolution (Å)	24.0-1.5	50.0- 2.0	50.0- 1.9
total no. of reflections	678137	249461	699812
no. of unique reflections	99564 (9590) (1.55 – 1.50 Å)	42317 (3594) (2.07 – 2.00 Å)	54417 (5208) (1.97 – 1.90 Å)
completeness (%)	97.2 (94.0)	98.2 (83.6)	99.3 (96.2)
$I/[\sigma(I)]$	21.0 (3.1)	11.8 (5.1)	15.1 (2.2)
R_{merge} (%)[a]	4.8	9.0	6.8
R_{merge} in outer shell (%)	37.3	16.7	49.5
R_{cryst} (%)[b]	15.08	16.13	19.45
R_{free} (%)[b]	18.35	19.78	23.98
rmsd from ideal values			
bond lengths (Å)	0.014	0.016	0.019
bond angles (deg)	1.5	1.4	2.1
Ramachandran analysis			
most favoured (%)	88.1	89.1	87.3
additionally allowed (%)	11.7	10.9	12.4

3.1 Crystal Structure of Fumarate Reductase with 2-Methylfumarate Bound

A data set to 1.5 Å resolution was used to refine the structure of wild-type flavocytochrome c_3 with 2-methylfumarate bound to a final *R*-factor of 15.08 % (R_{free} = 18.35 %), and the data collection and refinement statistics are summarised in table 3.1. The final model consists of one protein molecule comprising residues 1-568, four hemes, one FAD, one sodium ion, one 2-methylfumarate molecule, and 1249 water molecules. The atomic coordinates have been deposited in the Protein Data Bank, accession code: 1Y0P.

The quality of the final electron density map around the FAD and 2-methylfumarate is shown in figure 2(a). As found for other FR structures, residues 569-571 at the C-terminus of the enzyme could not be located in the electron density maps. The rmsd fit of all backbone atoms between this model and the earlier wild-type enzyme structure (PDB ID: 1QJD) [Taylor *et al*, 1999] is 0.2 Å, indicating no major differences between the two protein structures. 2-Methylfumarate is found at the active site of the enzyme in the same twisted conformation observed for the malate-like molecule (henceforth referred to as malate for the sake of simplicity) in the original crystal structure (PDB ID: 1QJD) [Taylor *et al*, 1999] and for fumarate in structures of mutant forms of the enzyme (e.g. PDB ID: 1JRX) [Mowat *et al*, 2001]. An overlay of 2-methylfumarate (in purple) and the malate from the structure of Taylor *et al* is shown in figure 2(b), indicating the complete superposition of the two with the exception of the C2-substituent on each. Accordingly, the bound 2-methylfumarate maintains the same interactions with the protein as displayed by malate. These include an electrostatic interaction between the C1-carboxylate group and the positively-charged sidechains of Arg544 and His 504 which serve to polarise and activate the double bond for hydride attack by FAD. The C4-carboxylate end of

Figure 3.1 Crystal structure of wild-type Fcc_3 with 2-methylfumarate bound

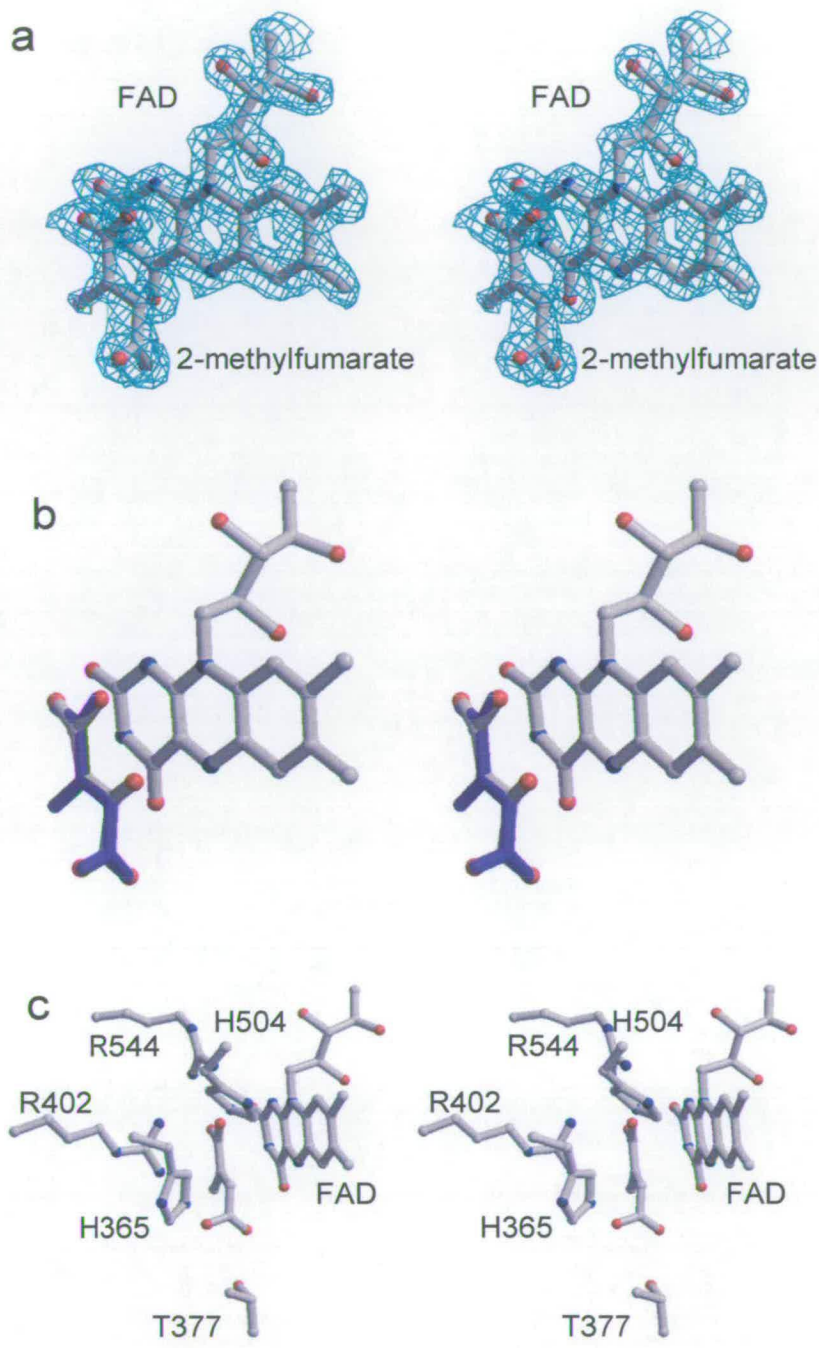

Figure 3.1 (a) Stereoview of the active site of the wild-type enzyme with 2-Me-fumarate bound. The electron density map was calculated using Fourier coefficients $2F_o - F_c$, where F_o and F_c are the observed and calculated structure factors, respectively, the latter based on the final model. The contour level is 1σ, where σ is the rms electron density. (b) Stereoview of the overlay of 2-Me-fumarate (purple) and the malate-like substrate found in the initial wild-type structure (PDB ID 1QJD). (c) Stereoview of the active site of the 2-Me-fumarate bound wild-type enzyme. All of the important substrate interactions with fumarate are maintained in the case of 2-Methylfumarate.

2-methylfumarate is hydrogen bonded to several residues including His635 and Thr377. The interactions of 2-methylfumarate at the active site of FR are shown in figure 2(c). The mechanism of 2-methylfumarate reduction is assumed to be the same as that shown for fumarate in figure 1, and is proposed to involve proton delivery via a pathway comprised of Arg381, Glu378, and Arg402. In the 2-methylfumarate-bound protein all proton transfer distances are identical to those observed in the malate-bound structure, as is the hydride transfer distance from FAD to substrate. These results are discussed in relation to the kinetics of 2-methylfumarate reduction by WT Fcc_3 and the stereochemistry of 2-methylsuccinate in chapter 4.

3.2 Crystal Structure of the T377A Mutant Enzyme

A data set to 2.0 Å resolution was used to refine the structure of Fcc_3 T377A to a final *R*-factor of 16.13 % (R_{free} = 19.78 %), and the data collection and refinement statistics are summarised in table 3.1. The final model consists of one protein molecule comprising residues 1-568, four hemes, one FAD, one sodium ion, one fumarate molecule, and 376 water molecules. The electron density around the active site is shown in figure 3.2 (a). The substitution of threonine 377 by alanine is shown to remove two hydrogen-bonding interactions between the residue and the bound fumarate molecule that is observed in the structure of the wild-type enzyme (figure 3.2 (b)). This results in the fumarate being oriented slightly differently than is observed for the bound malate molecule in the wild-type enzyme. In this mode of binding the fumarate is less twisted than observed in the wild-type enzyme (and therefore less activated toward hydride attack during catalysis), while other important interactions with the protein are maintained. These include electrostatic interactions with Arg544 and His504, a hydrogen-bonding interaction with His365, and

Figure 3.2 Crystal structure of T377A active site

a)

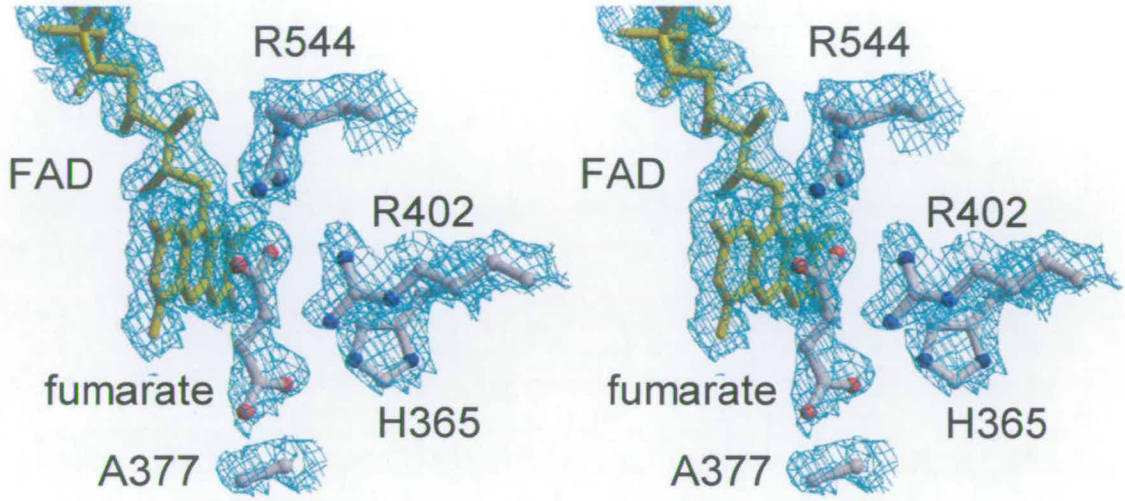

b)

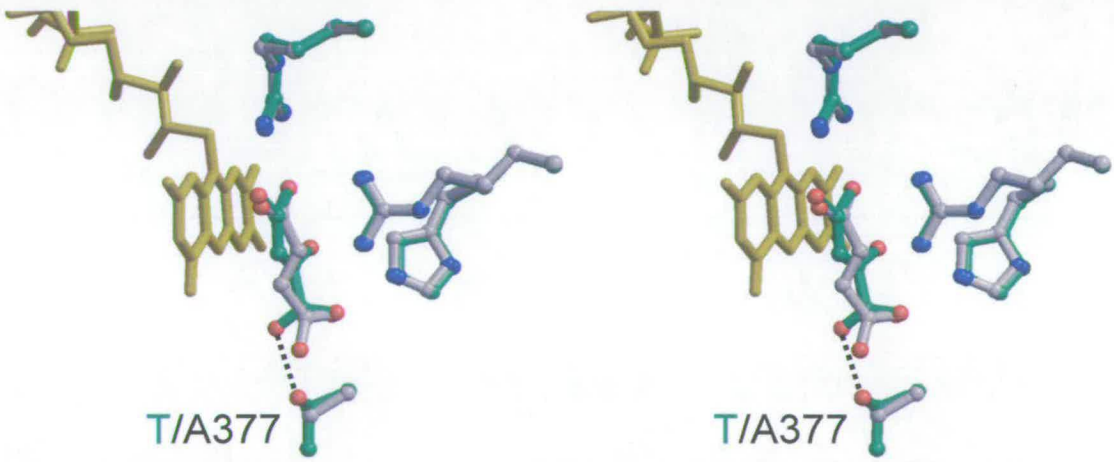

Figure 3.2 (a) Stereoview of the active site of the T377A mutant enzyme. The electron density map was calculated using Fourier coefficients $2F_o - F_c$, where F_o and F_c are the observed and calculated structure factors, respectively, the latter based on the final model. The contour level is 1σ, where σ is the rms electron density. (b) Stereoview of the overlay of the active sites of wild-type (green) and T377A enzymes showing the different orientations of the bound substrate. The hydrogen bond between Thr377 and the substrate carboxylate is shown.

maintenance of the hydride- and proton-transfer distances observed in the wild-type enzyme. Further discussion of T377A structure in context with kinetics of fumarate and 2-methylfumarate reduction is included in Chapter 5.

3.3 Crystallisation of H365G

Enzyme crystallisation conditions were the same as described in chapter 2 (materials and methods) except that prior to crystallisation, Fcc_3 (H365G) was put through a G25 filtration column. The reason for this was to remove fumarate, which in all crystal structures (apart from WT with 2-methylfumarate bound) is always bound to the active site. In addition, Fcc_3 (H365G) was incubated with 10mM trans-2-methyl-2-pentenoate, in order to ascertain if it would bind to the active site (it had not yet been confirmed by enzyme assays that this would not occur). It was thought that fumarate may be bound to the active site of Fcc_3 upon its expression and remains bound throughout purification. It was proposed that the presence of fumarate competitively prevents binding of other substrates, so it was hoped that its removal would promote binding of other substrates. Even if this was not the case, it was hoped that removal of excess fumarate would result in crystals of Fcc_3 that did not have substrate bound. Up to this point crystal structures of "substrate free" Fcc_3 had not yet been obtained.

3.3.1 Crystal Structure of the H365G

A data set to 1.9 Å resolution was used to refine the structure to a final *R*-factor of 19.45 % (R_{free} = 23.98 %). The final model consists of one protein molecule comprising residues 1-568, four hemes, one FAD, one sodium ion and 325 water molecules. The electron density around the FAD is shown in figure 3.3 (a).

Figure 3.3 Crystal structure of H365G

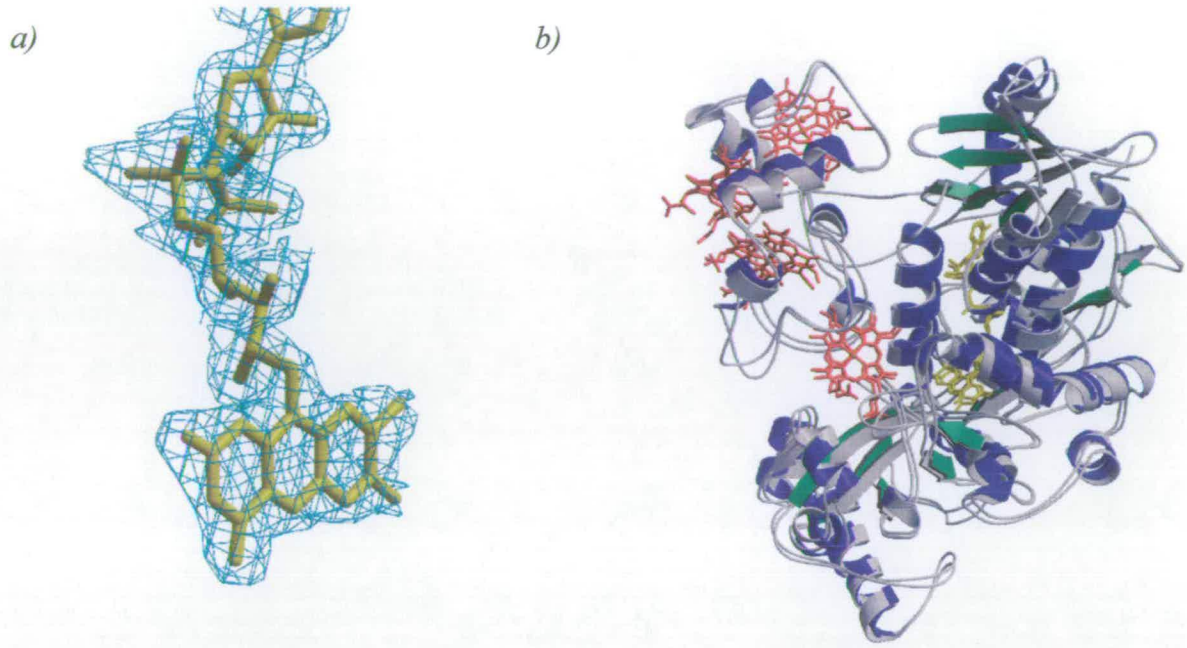

Figure 3.3 (a) The electron density around the FAD in the structure of the H365G mutant enzyme. The electron density map was calculated using Fourier coefficients $2F_o - F_c$, where F_o and F_c are the observed and calculated structure factors, respectively, the latter based on the final model. The contour level is 1σ, where σ is the rms electron density. (b) Overlay of the H365G mutant enzyme (green/ purple) with that of the IFcc_3 (PDB ID 1Q08).

In this case the protein is observed in the open conformation with no substrate bound at the active site (the structures obtained for WT and T377A are all in the closed conformation with substrate bound). This is analogous to the structure of the substrate-free iron-induced iso-fcc_3 (IFcc_3) fumarate reductase from *Shewanella frigidimarina* (Bamford *et al.* 1999: PDB ID 1Q08) which is super-imposable with that of the H365G mutant fcc_3 (figure 3.3 (b)).

Figure 3.4 crystal structures of Fcc_3 in the open and closed conformations

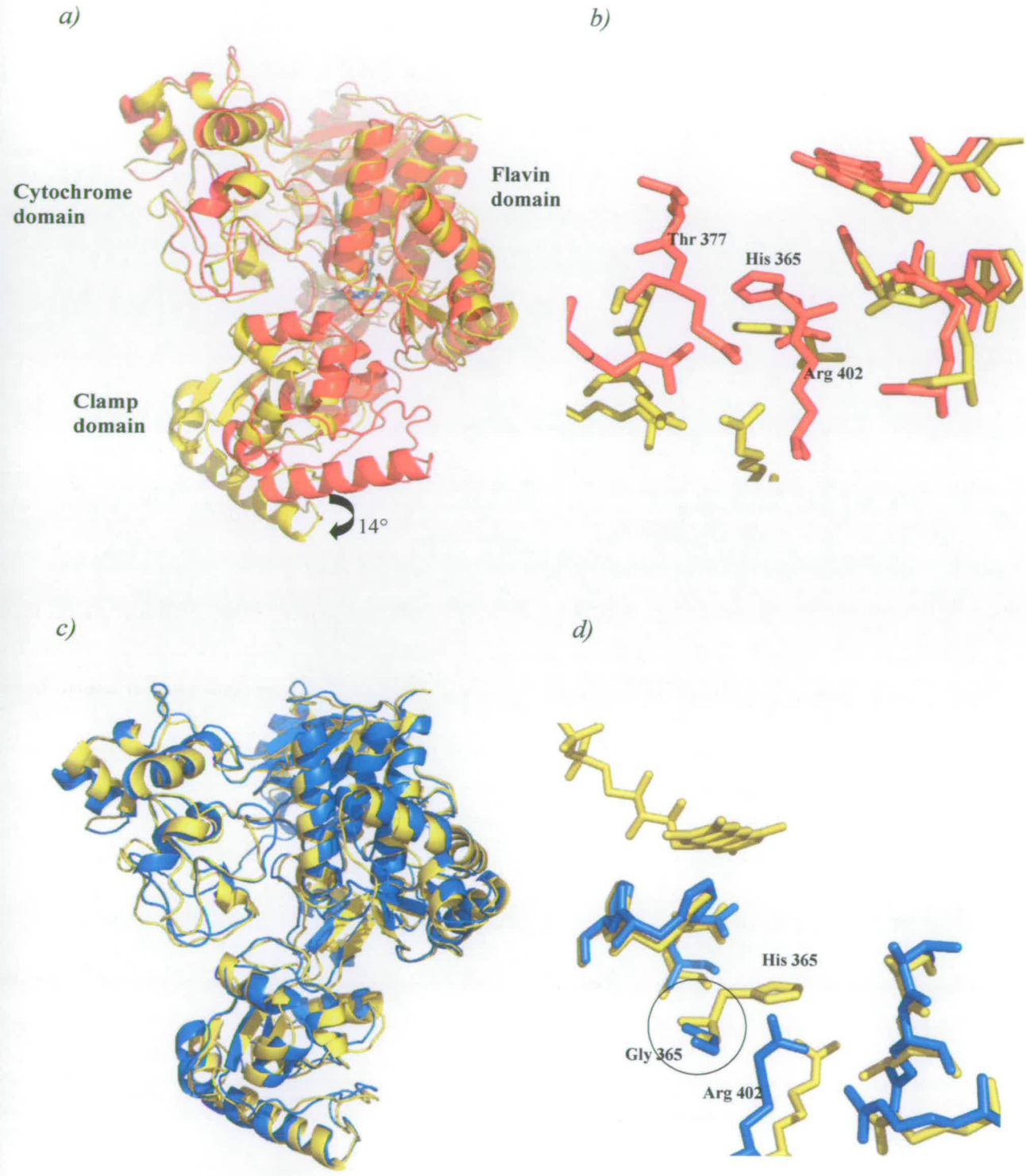

a) Global protein structures of WT Fcc_3 in the closed conformation (red) overlaid on $IFcc_3$ in the open conformation [Bamford et al, 1999]. The clamp domain has moved 14° relative to the flavin domain in the open conformation. The arrow indicates the direction of movement. b) Close-up of active site for the closed (red) and open (yellow) conformations. c) H365G global structure (blue) overlaid on $IFcc_3$ (yellow). d) Close-up of active site. Positioning of residues is similar in H365G (blue) to $IFcc_3$ although substitution with glycine (circled) increases the space available.

3.3.2 Comparison of open and closed Fcc_3

As mentioned in the introduction, the clamp domain is capable of some movement. This is illustrated in figure 3.4 a) by the crystal structures of "closed" WT Fcc_3 (in red) superimposed on to "open" IFcc_3 (iron-induced Fcc_3, an isozyme of Fcc_3 shown in yellow) [Bamford *et al*, 1999]. It would appear that the clamp domain is able to move 14 degrees relative to the flavin domain. It can be seen from figure 3.4 b) that the relative positioning of some of the residues to FAD is different and that there is more space available for product release/entry of substrate in the open conformation. Figures 3.4 c) and d) show H365G (in blue) overlaid on to IFcc_s (yellow) and it can be seen that they are in the same open conformation and that the active site is not much altered with respect to positioning of surrounding active site residues. However, the substitution of histidine 365 with glycine appears to have increased the size of the active site cavity. Without a crystal structure of H365G with substrate bound, it is not possible to say exactly what happens to the active site when the clamp is closed.

Chapter 4

Reduction of 2-methylfumarate by WT Fcc_3

4.0 Introduction

As mentioned briefly in the introduction (chapter 1.5), Fcc_3 is able to bind 2-methylfumarate which acts as a potent inhibitor of fumarate reduction. It has a K_i of 1 μM and it also inhibits the reverse reaction – oxidation of succinate to fumarate – with a K_i of 32.3 μM [Moysey, 2001]. Previous studies had not revealed whether 2-methylfumarate was actually reduced to 2-methylsuccinate by Fcc_3 so it seemed logical to investigate this. Also, because the product of 2-methylsuccinate reduction is chiral, its stereochemistry could be used to determine hydride and proton transfer trajectories, which although they have been predicted, have not yet been confirmed experimentally.

The activity of Fcc_3 was assayed by monitoring the oxidation of an artificial electron donor, methyl viologen (see materials and methods). In order to carry out reduction of the substrate, the active site must be constantly supplied with electrons. The reduction of 2-methylfumarate by WT (wild-type) Fcc_3 proceeds at different rates depending upon environmental pH and concentration of substrate present. Fcc_3 exhibits Michaelis-Menten kinetics and measurement of reduction rates at increasing concentrations of substrate allows the determination of k_{cat} and K_m values. Figure 4.1 shows plots of observed rate constants (k_{obs}) versus 2-methylfumarate concentration at pH 7.2 (*a*) and pH 9.0 (*b*).

Figure 4.1 Reduction of 2-methylfumarate by WT Fcc_3 at pH 7.2

a) pH 7.2

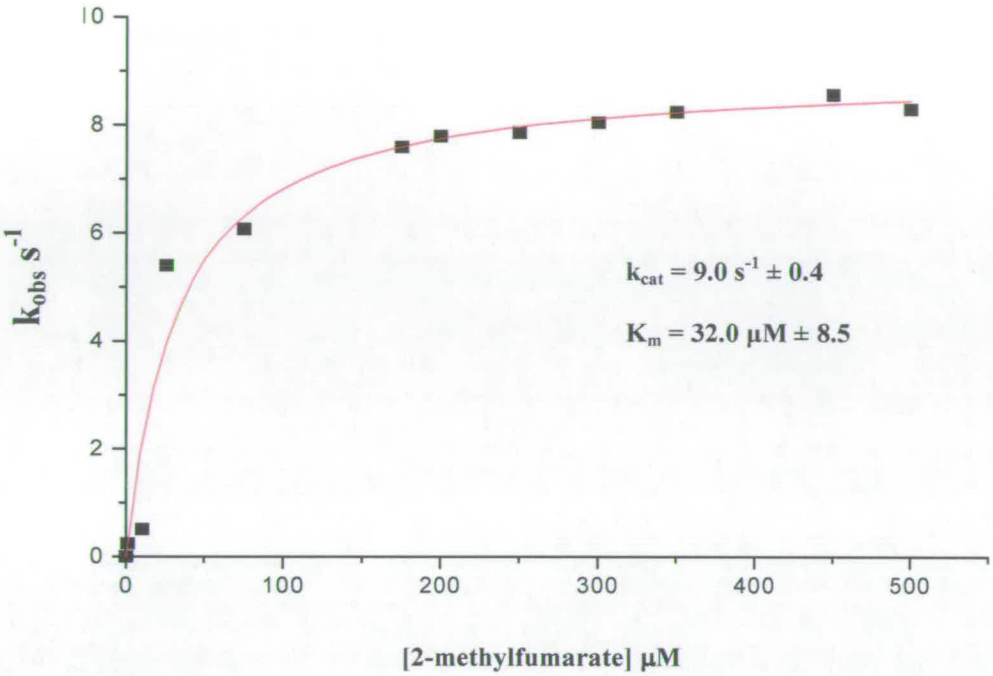

b) pH 9.0

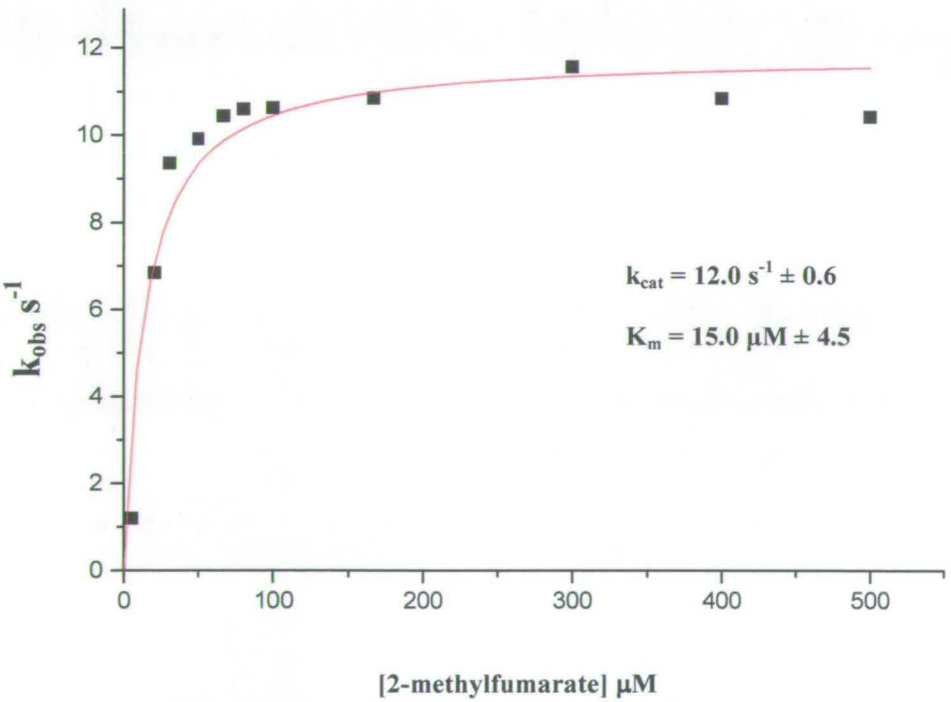

a) Plot of 2-methylfumarate reduction by wild-type Fcc_3 at pH 7.2 b) at pH 9.0. Observed rate constants versus substrate concentration were fitted to the Michaelis-Menten equation by least squares regression using Microcal Origin.

4.1 Kinetic parameters for 2-methylfumarate reduction by WT Fcc_3

Rate constants for fumarate reduction established from previous studies [Turner *et al*, 1999] are listed alongside those obtained for 2-methylfumarate in table 4.1. The activity of Fcc_3 is approximately 50-fold lower with 2-methylfumarate than that observed for fumarate with a k_{cat} (maximum rate) at pH 7.2 of 9.0 $s^{-1} \pm 0.4$. The K_m is only slightly increased relative to fumarate at 32.0 $\mu M \pm 8.5$ which is consistent with data obtained from prior experiments that demonstrated that it is a potent inhibitor of fumarate reduction when both are present [Moysey, 2001].

Table 4.1 – Kinetic parameters for fumarate and 2-methylfumarate reduction by wild-type Fcc_3

Fumarate			
pH	**k_{cat} (s^{-1})**	**K_m (μM)**	**k_{cat}/K_m ($M^{-1}s^{-1}$)**
7.2	509 ± 15	25 ± 2	2×10^7
9.0	210 ± 13	7 ± 2	3×10^7
2-methylfumarate			
pH	**k_{cat} (s^{-1})**	**K_m (μM)**	**k_{cat}/K_m ($M^{-1}s^{-1}$)**
7.2	9 ± 0.4	32 ± 8.5	3×10^5
9.0	12 ± 0.6	15 ± 4.5	8×10^5

Although the Michaelis constant for 2-methylfumarate reduction indicates that it binds to the active site as readily as fumarate does, there is a drop in catalytic efficiency (k_{cat}/K_m) by a factor of 100. When fumarate is the substrate, the rate of reduction at pH 9.0 decreases to less than 50 % of the activity observed at pH 7.2 [Doherty, 1999]. However, when 2-methylfumarate is the substrate, reduction

actually increases at pH 9.0 by about 30% compared to rates observed at pH 7.2, with a k_{cat} of 12 s^{-1} ± 0.6. As with fumarate, the K_m is lowered at pH 9 although to a lesser degree, but the catalytic efficiency (k_{cat}/K_m) actually increases. The pH profiles for 2-methylfumarate and fumarate reduction are shown in figure 4.2. The data for 2-methylfumarate fit a bell-shaped curve with two pKa values (7.09 ± 0.22, and 9.92 ± 0.21) and activity is greatest at approximately pH 9.0. Fumarate reduction has an optimum pH of 6.0 (rate = 658 s^{-1} ±34) [Turner *et al*, 1999] and a single pKa of 7.5 ± 0.1 [Pankhurst, 2003] but at pH 6.0, the rate of 2-methylfumarate reduction is lowest, at 7.0 s^{-1} ± 0.6.

Figure 4.2 Comparison of fumarate and 2-methylfumarate reduction rates at different pH values

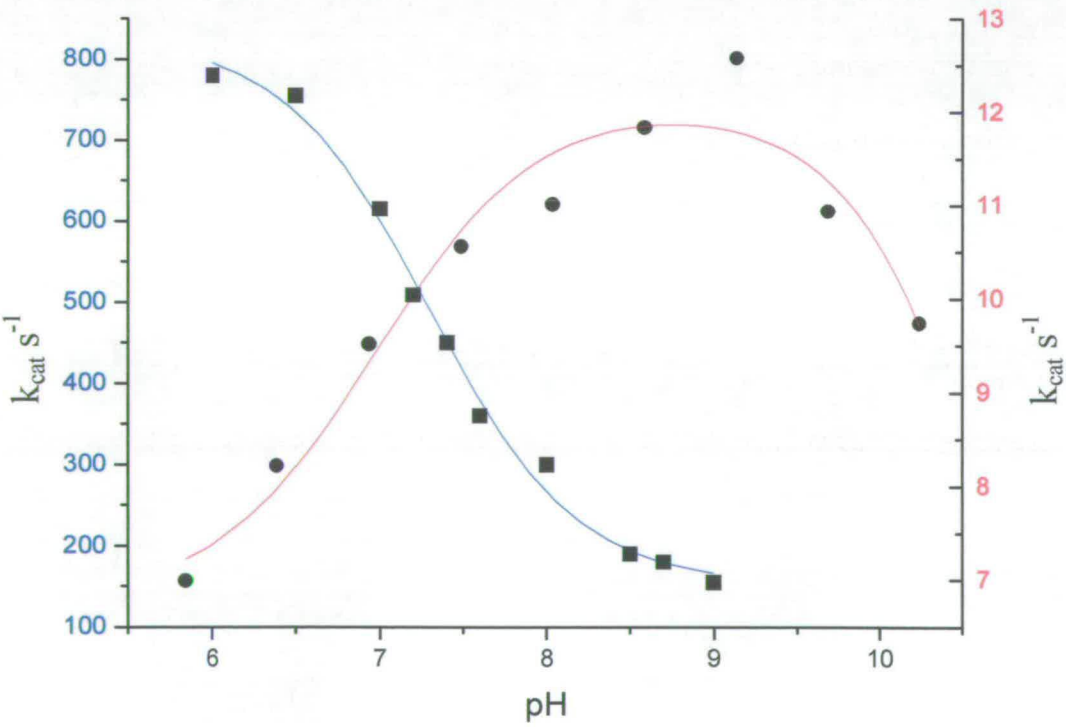

Graph showing pH curves for fumarate (blue) and 2-methylfumarate (red). Data fitted as before using Microcal Origin

4.2 Structure of bound 2-methylfumarate

The crystal structure of Fcc_3 complexed with 2-methylfumarate was recently solved by our laboratory to 1.5 Å (fig. 4.3 a). As in the structure previously published by Taylor *et al* [1999] with malate bound (fig 4.3 b), the enzyme is in the closed conformation and the substrate is bound to the active site by formation of multiple hydrogen bonds with the surrounding residues. The carbon atoms of the substrate in figures 4.3 a) and 4.3 b) are numbered 1 – 4 so that their orientation to the flavin alloxazine ring can be compared. It can be seen that in both structures, the C1 carboxylate of the substrate is twisted out of plane. As previously mentioned in the introduction, this twisted conformation results from hydrogen-bonding and steric constraints imposed by nearby residues when the clamp is in the "closed" position. It was thought that the decrease in rate when 2-methylfumarate is the substrate, may be partly due to slight differences in the positioning of substrate relative to active site residues, due to the presence of the extra methyl group. The crystal structure shows that this is unlikely to be the case because not only does 2-methylfumarate retain the same hydrogen-bonding contacts as fumarate, distances for hydride and proton transfer also remain the same. This is consistent with the similarity in K_m values obtained for fumarate and 2-methylfumarate indicating that both bind as readily to the active site. The mechanism proposed for the two-electron reduction of substrate by hydride transfer is driven by polarisation of the C2 – C3 double bond, aided by twisting of the C1 carboxylate and the positively charged environment around the C4 carboxylate. The crystal structure demonstrates that these two factors are still present when 2-methylfumarate is bound. However, the methyl substituent inductively donates electrons which would interfere with bond polarisation and/or destabilise the localised build-up of negative charge around C3 that occurs upon formation of the

Figure 4.3 Crystal structures of fcc3 with substrate bound at the active site

a) with 2-methylfumarate

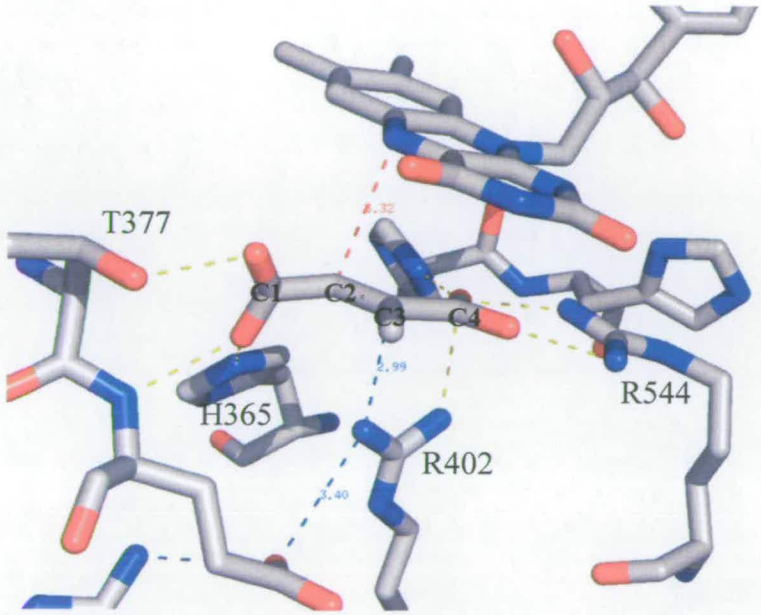

b)with malate-like molecule

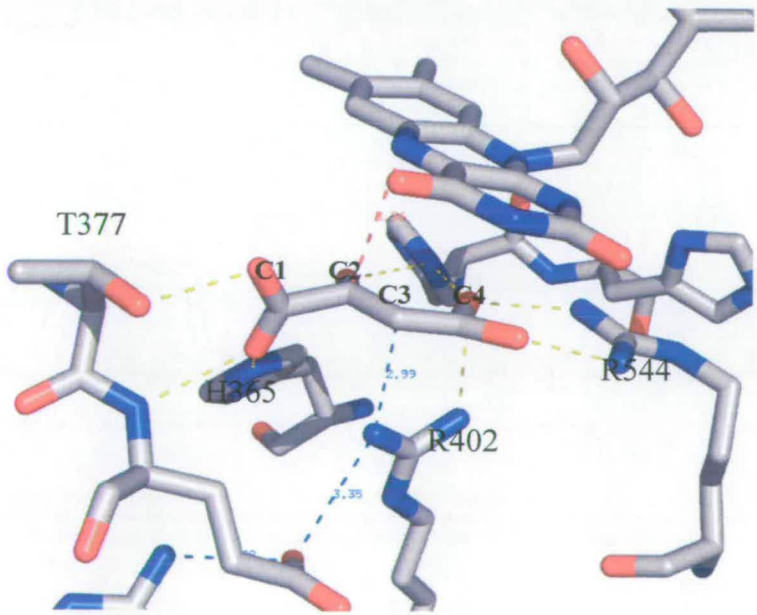

Crystal structures of the active site of Fcc_3 (wild-type) with 2-methylfumarate (a) and a hydrated intermediate derived from fumarate (b). The red dashes represent the path of hydride transfer, the blue dashes show theproton transfer pathway and the yellow dashes indicate hydrogen bonding contacts

transition state. In order to overcome this, a larger amount of free energy would be required for formation of product and it is thought that this may be the reason for the observed decrease in k_{cat}.

4.3 Stereochemistry of 2-methylsuccinate

The reduction of 2-methylfumarate results in the formation of 2-methylsuccinate, which has a chiral (asymmetrical) centre, and could be present as either the R or S enantiomer shown below. (Enantiomers are stereoisomers which are mirror images of each other and are non-superimposable, differing only in the arrangement of atoms around the chiral centre.)

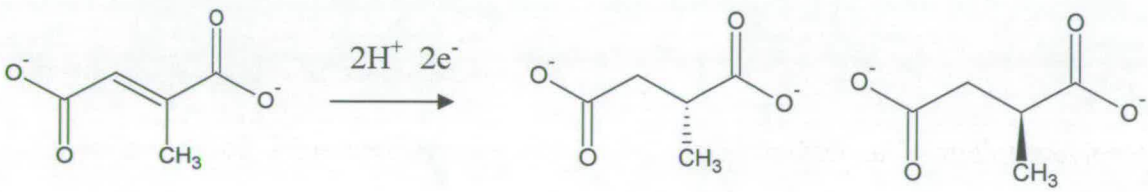

2-methylfumarate **R-methylsuccinate** **S-methylsuccinate**

As mentioned in the introduction, the crystal structure of fcc_3 obtained previously by Taylor *et al* [1999] contained a malate-like molecule (instead of fumarate) bound at the active site with a chiral centre at the C2 position displaying R-stereochemistry (see fig 4.3 b and 4.4 b). When compared with the crystal structure showing 2-methylfumarate (fig4.3a and 4.4 a), it can be seen that the mode of binding to the active site is actually different. The methyl substituent is located at the C3 position (site of proton transfer from Arg 402) and based on the mechanism proposed, hydride transfer followed by protonation would result in S-methylsuccinate being produced

Figure 4.4 Mode of 2-methylfumarate binding at Fcc_3 active site

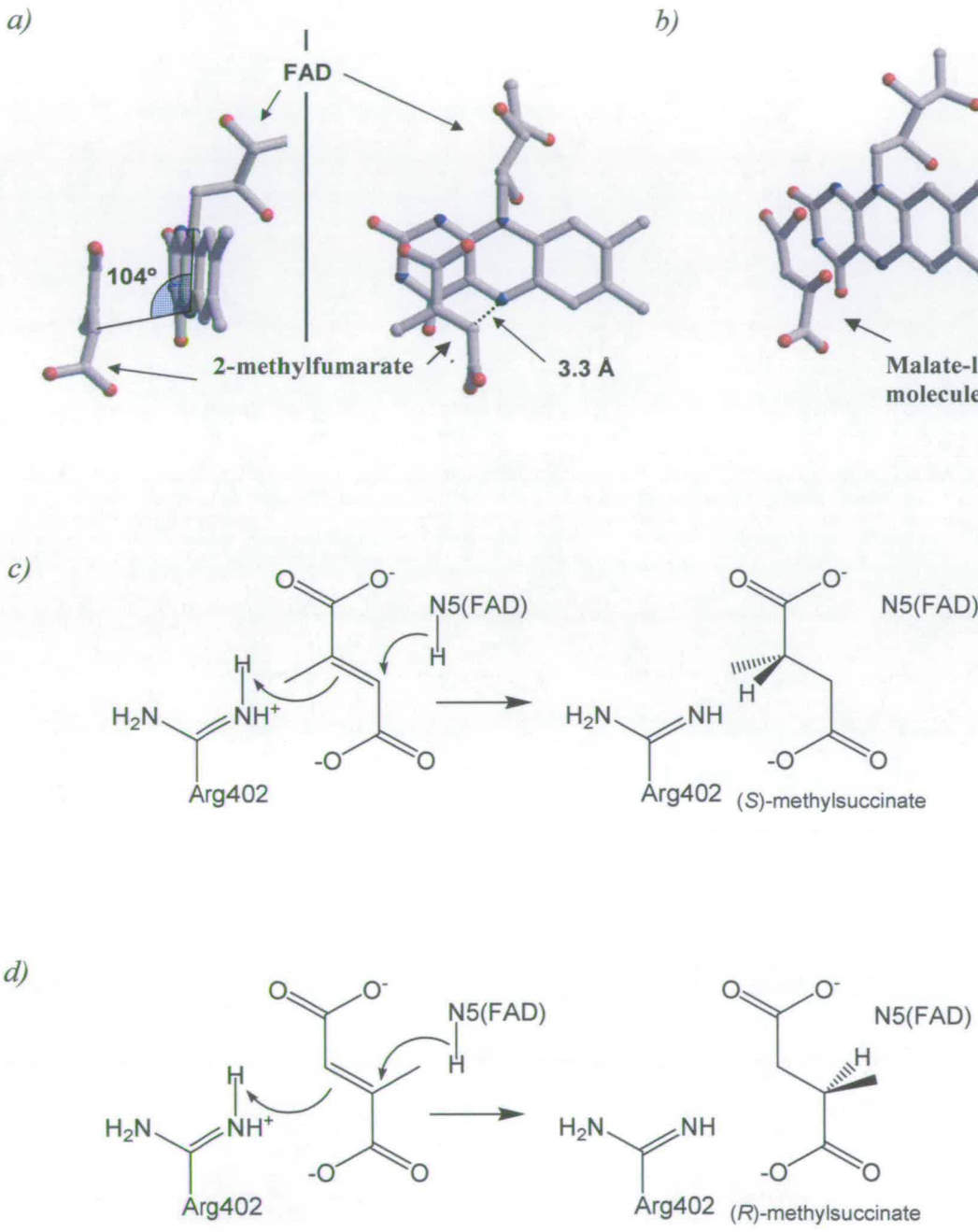

a)Mode of 2-methylfumarate binding relative to the alloxazine ring of FAD from the crystal structure. The angle between the substrate and the alloxazine ring of the flavin is shown, as is the distance for hydride transfer from N5 of the flavin to substrate, on the carbon that does not contain the methyl group b)The malate-like molecule (from crystal structure) binds in exactly the same way with the same angle and distance however the hydride is transferred to the carbon which has a substituent attatched to it c) mechanism of S-methysuccinate formation, d) mechanism of R-methylsuccinate formation if the substrate bound in a manner analogous to that in figure b)

(figure 4.4 c). If it bound in an analogous manner to the malate-like molecule (with the substituent located at the C2 position subject to nucleophilic attack by N5 of the Flavin), then R-methylsuccinate would be produced (figure 4.4 d). In order to determine the stereochemistry of the product, bulk reduction of 2-methylfumarate using coulometry was performed to make enough product for subsequent analysis by circular dichroism spectroscopy.

4.4 Bulk electrocatalytic reduction of 2-methylfumarate

Various electrochemical techniques have been employed in the study of Fcc_3 and it has been shown that catalytic reduction can be effectively driven electrochemically.

A 3-electrode cell was set up with platinum working and counter electrodes and a Ag/AgCl reference electrode. Methyl viologen was added to the buffer (final concentration was 50 μM) and the concentration of fcc_3 present was approximately 1μM. The potential was held at -600mV until 5mM 2-methylfumarate was electrocatalytically reduced. 5mM substrate was chosen as previous tests of standard R and S-methylsuccinate using the CD spectropolarimeter had produced the most reliable traces at this concentration. The end point of the reaction could be detected by a flattening out of the trace as current ceases to flow (no more substrate left to act as an electron acceptor).

Figure 4.5 Bulk electrocatalytic reduction of 2-methylfumarate

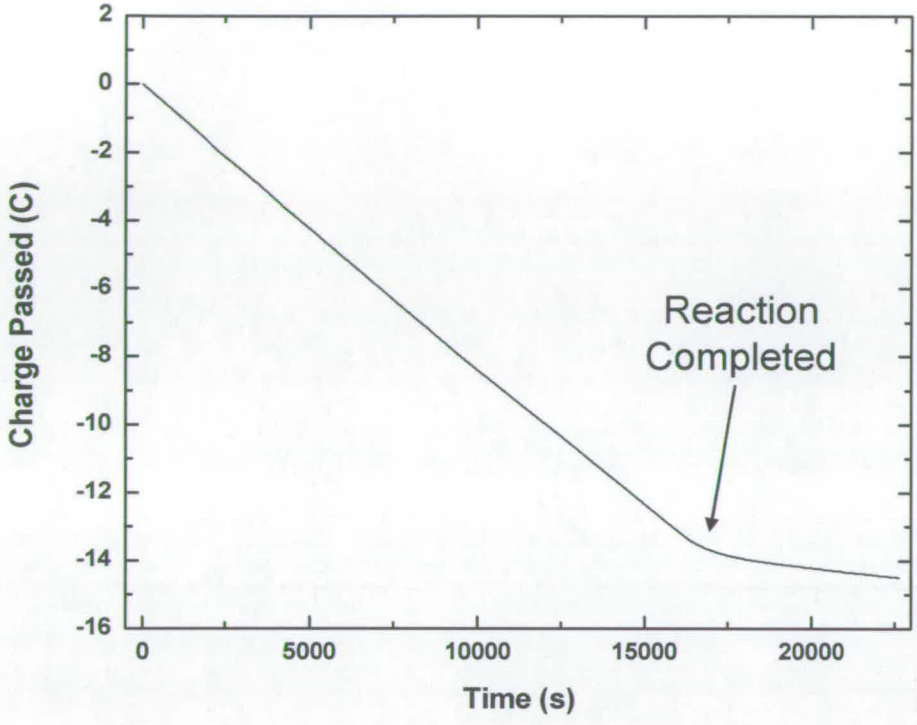

Ttrace showing electrochemically driven reduction of 2-methylfumarate by Fcc$_3$. The reaction stops when all of the substrate has been consumed and transfer of charge ceases

4.5 Circular Dichroism spectroscopy of 2-methylsuccinate

The product was compared with samples of enatomerically pure R and S-methylsuccinate obtained commercially (Sigma). It can be seen from fig. 4.6 that the trace for product is identical to that obtained for S-methylsuccinate suggesting that reduction of 2-methylfumarate by WT Fcc_3 always produces S-methylsuccinate. Therefore, the circular dichroism spectrum of product conclusively showed that reduction is stereospecific with the S-enantiomer being produced.

Figure 4.6 Circular dichroism spectra of product

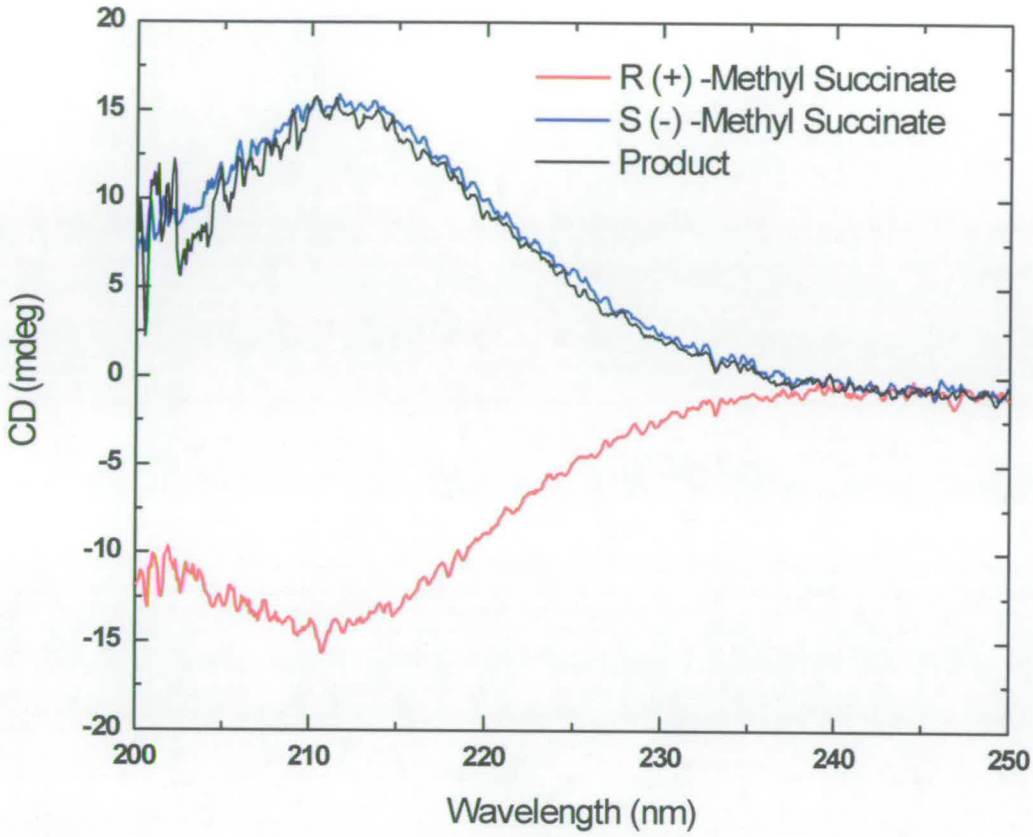

CD traces obtained for R-methylsuccinate (red), S-methylsuccinate (blue) and product of bulk reduction of 2-methylfumarate by WT Fcc$_3$. The ellipticity (which is proportional to the difference in absorbance) is on the y axis and the wavelengths of light utilised by the polarimeter are on the x axis. A racemic mixture of both R and S methylsuccinate (not shown) was also tested and is seen as a flat line at 0 mdeg.

4.6 Conclusions

The CD results along with the crystal structure of WT Fcc$_3$ with 2-methylfumarate bound at the active site, appear to confirm predicted hydride and proton transfer trajectories and the two-step mechanism for fumarate reduction originally proposed when the crystal structure of Fcc$_3$ was obtained in 1999 [Taylor *et al*, 1999]. Theoretical studies recently carried out using density functional theory also support this [Lucas and Ramos, 2006]. Bulk reduction *in vitro* (see materials and methods) seems to be an effective and relatively simple way of obtaining product from Fcc$_3$ at

concentrations useful for further study. These results raised the possibility that Fcc_3 would be able to catalyse the reduction of other derivatives of fumarate (with different groups at C3) that result in chiral products. Chiral synthesis using biocatalysis is currently being researched by many labs, and advances in genomic analysis mean genomes can now be "mined" for potential biocatalysts. Possible applications include drug development [Patel, 2001], industrial synthesis of bulk chemicals [Shoemaker *et al*, 2003] and organic synthesis [Koeller and Wong, 2001]. In light of this, it is of interest to determine whether Fcc_3 could be used to produce other stereospecific chiral compounds.

Chapter 5

Engineering of the active site of Fcc_3

5.0 Introduction

To date there have been two enzymes discovered that are capable of reducing the mono-acid methacrylate (table 5.2). A 50 kDa periplasmic flavoprotein purified from *Geobacter sulfurreducens AM-1* [Galouchko *et al*, 1996], and a 52 kDa periplasmic flavoprotein which is the product of the *fccA* gene from *Wolinella succinogenes* [Gross *et al*, 2001]. The *G. sulfurreducens* flavoprotein is dependent on a 30 kDa cytochrome c for activity and it is able to catalyse the reduction of Methacrylate, acrylate, crotonate and pentenoate [Mikoulinskaia *et al*, 1999]. The gene responsible for expression of this protein has not yet been identified so only the N-terminal sequence has been elucidated. It was found to have 80% similarity to the 52kDa protein from *W. succinogenes* FccA, which shares 31% identity to the C-terminal section of Fcc_3 (figure 5.1). The active site of Fcc_3 contains what has been dubbed the "HPT triad" (highlighted in cyan), which includes histidine 365 and is a conserved feature of all fumarate reductases, but is absent in FccA [Gross, 2001]. Instead there is a glycine at this position and the threonine residue is replaced with tryptophan. Also, instead of T377 (highlighted in cyan) there is a valine. The other active site residues (R402, H504, H505 and R544 highlighted in yellow) are conserved. Activity tests had shown that WT Fcc_3 was not able to bind or reduce any of the potential substrates shown in table 5.2 other than fumarate and 2-methylfumarate. FccA is able to reduce acrylate and methacrylate, so it was thought that substitution of H365 and T377 as well as H504 (another residue that forms hydrogen-bonds with substrate) with other amino acids may enable Fcc_3 to catalyse reduction of these mono-acids. R402 was not substituted as it has been previously shown to be critical for enzymatic activity (see enzymatic mechanism in section 1.4.4).

Figure 5.1 Protein Sequence alignment of Fcc_3 from S. frigidimarina and FccA from W. succinogenes

Alignment comparing Fcc_3 from Shewanella frigidimarina and FccA from Wolinella succinogenes generated using Clustal W. The HPT motif is highlighted in cyan and is conserved in all fumarate reductases. The residues located at the equivalent position at the active site are highlighted in green. R402, H504, H505 and R544 are conserved between the two proteins and are highlighted in yellow.

R544 was also left untouched as it is important for the polarisation of the C2-C3 double bond, an important aspect of the catalytic mechanism. Therefore, the mutants shown in table 5.1 were constructed by site directed mutagenesis. Table 5.2 lists potential substrates for engineered forms of Fcc_3. These particular chemicals were chosen because their size and shape could be expected to be accommodated by the active site cavity and are compounds that are found abundantly in environments that *Shewanella* species inhabit (mono-acids and mono/di-esters) and because some of them would result in chiral compounds if reduced (e.g. tiglic acid). The resulting stereochemistry of these products would give valuable information about hydride and proton transfer trajectories as well as other aspects of the enzymatic reaction

mechanism. The various mutant forms of Fcc_3 will be discussed in this chapter with regard to their properties and their ability to reduce any of the compounds listed in table 5.2.

Table 5.1 – Fcc_3 mutants constructed for activity studies

H365A	**H365L**	**H365G**
H504A	**H365I**	
T377A	**T377V**	
H365A/H504A		
H365A/T377A		

Table 5.2 Potential substrates for wild-type and engineered Fcc_3

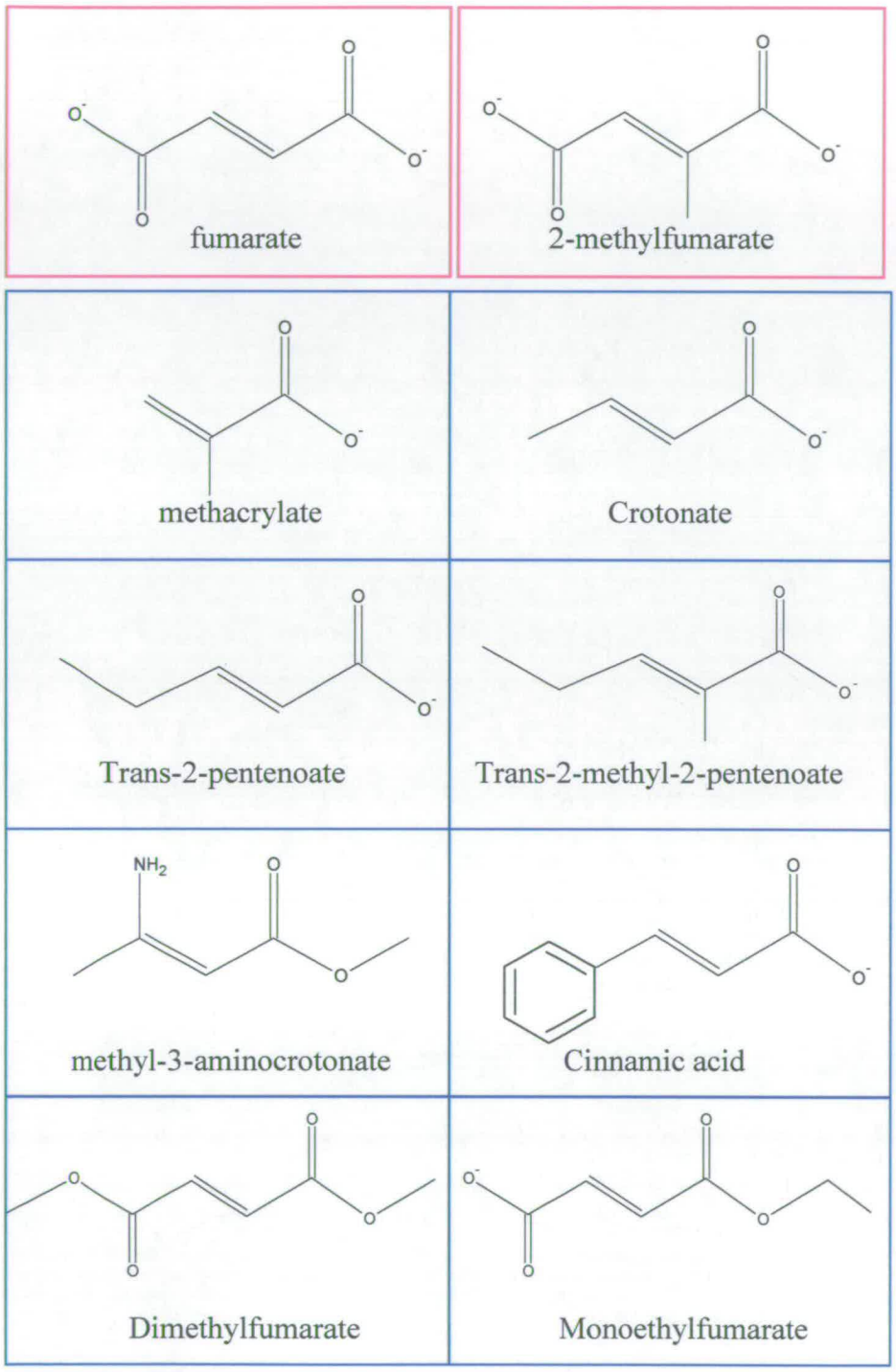

The table shows examples of some unsaturated organic acids tested as potential substrates for Fcc_3. Highlighted in pink are fumarate and 2-methylfumarate which are turned over by WT and most of the mutants. IUPAC names for all of the above chemicals are listed in appendix

Figure 5.2 Crystal structure showing hydrogen bonding interactions at active site

a)

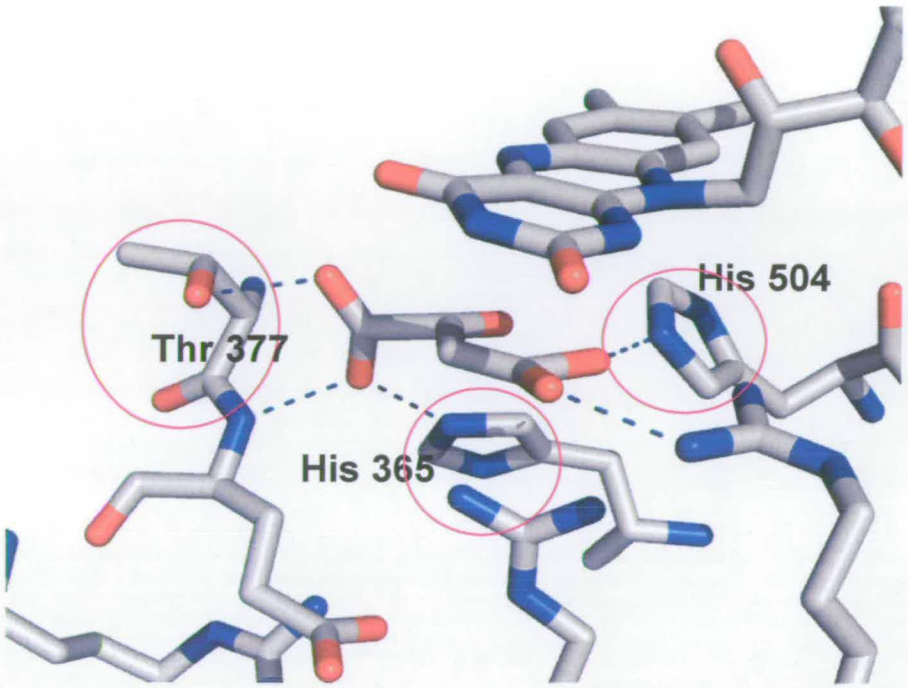

b)

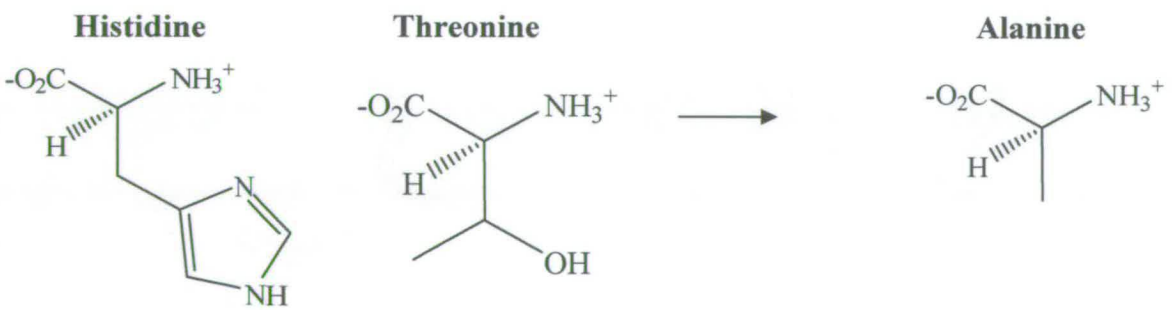

a) Active site of Fcc_3 showing hydrogen bonding interactions (blue dashes) between the malate-like substrate and active site residues. Circled are residues which were substituted with alanine to generate the mutants listed in table 4.3 b) Structures of amino-acids histidine, threonine and alanine.

5.1 Substitution of active site residues with alanine

It was thought that replacing one or more of the hydrogen-bonding residues with alanine (figure 5.2) would possibly increase the size of the active site cavity and thus allow binding of substrates with bulkier functional groups. Previous work carried out by our laboratory had demonstrated that substitution of histidine 365, histidine 504 and threonine 377 with alanine (a smaller non-polar residue) did not entirely abolish activity for the reduction of fumarate [Doherty 1999, Pankhurst, 2003]. All amino-acid substitutions were done using site directed mutagenesis (see materials and methods). Table 5.3 contains rates of fumarate reduction by mutant forms of fcc_3 at pH 7.2.

Table 5.3 kinetic parameters for reduction of fumarate by mutant forms of fcc_3 at pH 7.2

	k_{cat} (s^{-1})	K_m (μM)	k_{cat}/K_m ($M^{-1}s^{-1}$)
WT	509 ± 15	25 ± 2	2.0×10^7
H365A	52 ± 2	259 ± 20	2.0×10^5
H504A	65 ± 3	256 ± 23	2.5×10^5
T377A	38 ± 1	676 ± 27	5.6×10^4
H365A/ H504A	0.8 ± 0.1	~1100	7.3×10^2
H365A/ T377A	0.24 ± 0.02	2000 ± 300	1.2×10^2

Data for WT (wild-type), H365A, H504A and H365A/H504A taken from M. Doherty 1999. Data for T377A and H365A/T377A taken from K. Pankhurst, 2002. k_{cat}/K_m indicates the catalytic efficiency of each enzyme. For ease of comparison all K_m's are in micromolar units.

It can be seen from table 5.3 that all of the mutated forms of fcc_3 reduced fumarate at rates lower than the Wild-type. Reduction by H365A and H504A proceeded with rates approximately 10-fold lower and exhibited K_m values that were higher by a factor of 10. Substitution of threonine 377 had more pronounced effects, resulting in an even lower k_{cat} for fumarate reduction and a K_m almost 30 times higher than that observed for wild-type fcc_3. When mutants were constructed with two residues substituted with alanine, (double mutants H365A/H504A and H365A/T377A), fumarate reduction rates were over 600 and 2000 times slower than that of wild-type respectively. In addition, they exhibit K_m values at the millimolar level, indicating that these mutants do not form the enzyme-substrate complex efficiently. The catalytic efficiency of fcc_3 is measured by k_{cat}/K_m and it can be seen from the table that this value is lower relative to wild-type for the mutated forms of the enzyme. These effects will be discussed further in this chapter in relation to the crystal structures of H365A and T377A.

5.2 Reduction of 2-methylfumarate by H365A, H504A and T377A

It was hoped that the mutants listed in table 5.3 would be able to catalyse the reduction of substrates not turned over by the wild-type enzyme. Molecular modelling studies suggested that all forms of fcc_3 would be able to accommodate methacrylate (table 5.2) and perhaps methyl-3-aminocrotonate. T377A might be expected to bind both crotonate and trans-2-pentenoate since the OH group of threonine, which normally forms a hydrogen bond with the polar substrate, has been replaced by the non-polar alanine. Although the double mutant enzymes display poor activity for fumarate reduction, it was thought possible that H365A/T377A may be able to bind acids with bulky non-polar groups attached, for example cinnamic acid.

Table 5.4 Kinetic parameters for reduction of 2-methylfumarate at pH 7.2

	k_{cat} (s^{-1})	K_m (μM)	k_{cat}/K_m ($M^{-1}s^{-1}$)
WT	9.0 ± 0.4	32 ± 8.5	2.8×10^5
H365A	0.11 ± 0.01	90 ± 18	1.2×10^3
H504A	0.22 ± 0.01	136 ± 26	1.6×10^3
T377A	0.34 ± 0.03	1260 ± 284	2.7×10^2
H365A/ H504A	No measurable activity		
H365A/ T377A	No measurable activity		

Reduction rates for 2-methylfumarate reduction by Fcc_3. No activity was detected for the double mutants.

Subsequent activity screens demonstrated that this was not the case. None of the mutants were able to catalyse reduction of any potential substrates other than fumarate and 2-methylfumarate. Kinetic parameters for 2-methylfumarate reduction by mutant forms of fcc_3 at pH 7.2 are listed in table 4.4. The single mutants are all able to catalyse reduction of 2-methylfumarate at low rates, but the double mutant enzymes exhibited no measurable activity. This is reasonable considering that they are inefficient at fumarate reduction.

5.2.1 pH profiles

Michaelis plots for 2-methylfumarate reduction by H365A, H504A and T377A are shown in figure 5.3 along with pH profiles. It can be seen from the table 5.4 that

Figure 5.3 Observed rates of reduction of 2-methylfumarate by H365A, H504A and T377A

a) Michaelis plot of 2-methylfumarate reduction by fcc_3 mutants at pH 7.2

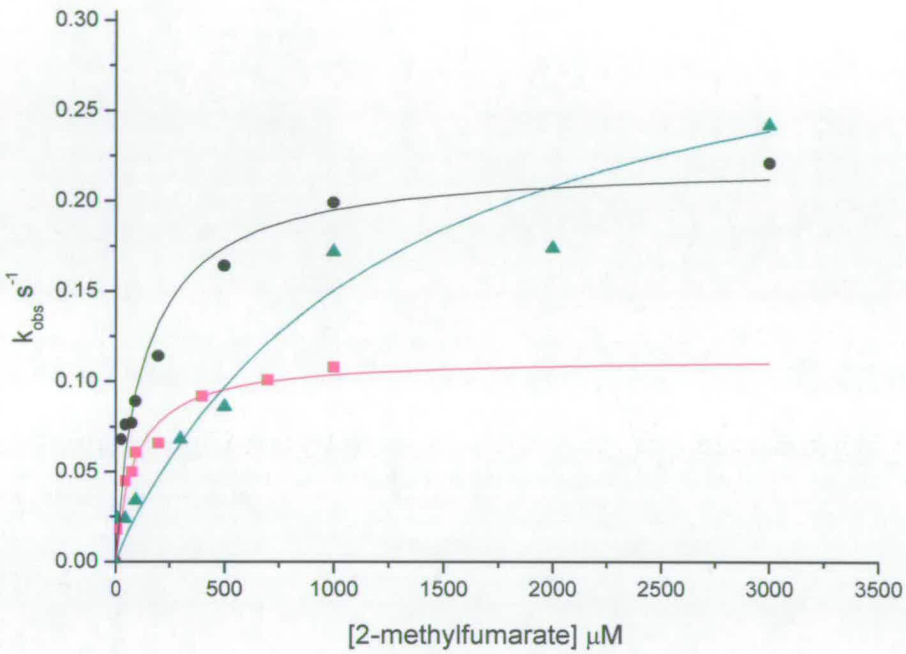

b) Rate of 2-methylfumarate reduction by mutants versus pH

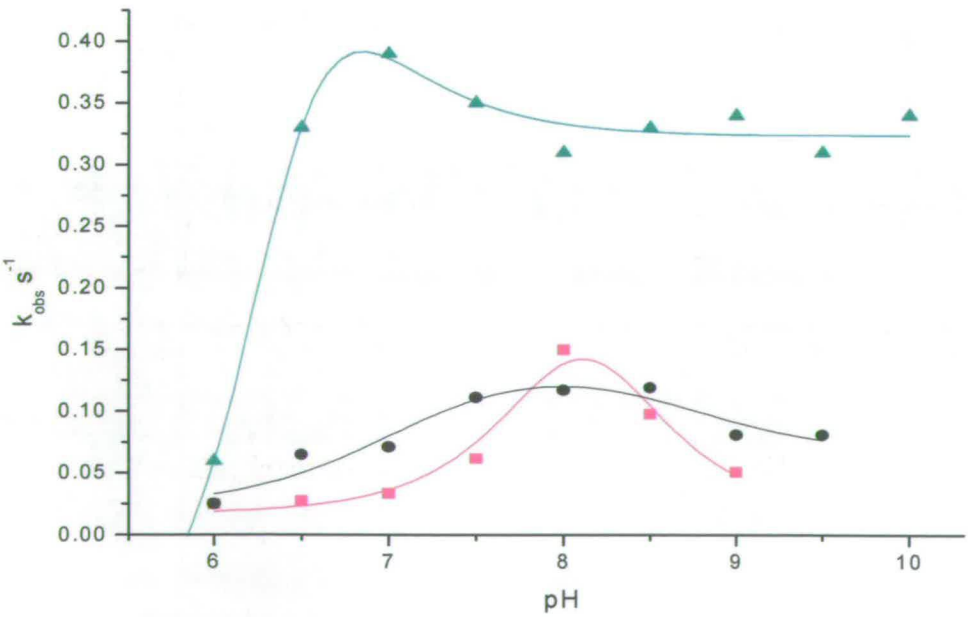

a) 2-methylfumarate reduction rates at various substrate concentrations for H365A (pink), H504A (black) and T377A (green). b) Reduction rates ct various pH for H365A (pink), H504A (black) and T377A (green).

H365A and H504A display lower K_m values for 2-methylfumarate than for fumarate reduction, which suggests that they have a higher affinity for this substrate. However, the k_{cat} values are low so the catalytic efficiencies for the reduction of 2-methylfumarate by these mutants are approximately 150 times lower than those calculated for fumarate reduction. 2-methylfumarate is likely to act as an inhibitor of fumarate reduction in both H365A and H504A as it does in WT because the K_m values are lower than those observed when fumarate is the substrate. In the case of T377A, 2-methylfumarate does not appear to bind efficiently to the active site. The K_m is twice as large compared to that observed when fumarate is the substrate so although the presence of 2-methylfumarate may reduce the rate of fumarate reduction, it is unlikely to be an effective inhibitor of reduction by this mutant.

Figure 5.3 b shows how rates of 2-methylfumarate reduction are affected by variation in pH. The pH profile for H365A (shown in pink) fits to a bell shaped curve with two pK_a's of 7.4 ± 1.8 and 8.5 ± 1.4. H504A (shown in black) is also pH dependent with two pK_a's of 6.9 ± 0.3 and 8.9 ± 0.8, but to a lesser degree as the curve is much flatter. It can be seen from the pH profile for T377A (shown in green in figure 5.3 b) that between pH 6.5 and 10, enzymatic activity remains approximately the same for 2-methylfumarate reduction (For limitations of this assay see section 2.5) When fumarate is the substrate, the pH profile of reduction by T377A fits to a single pK_a value of 9.1 ± 0.1 [Pankhust, 2003].

Figure 5.4 Overlay of WT and H365A - hydrogen bonding of substrate at active site

a)

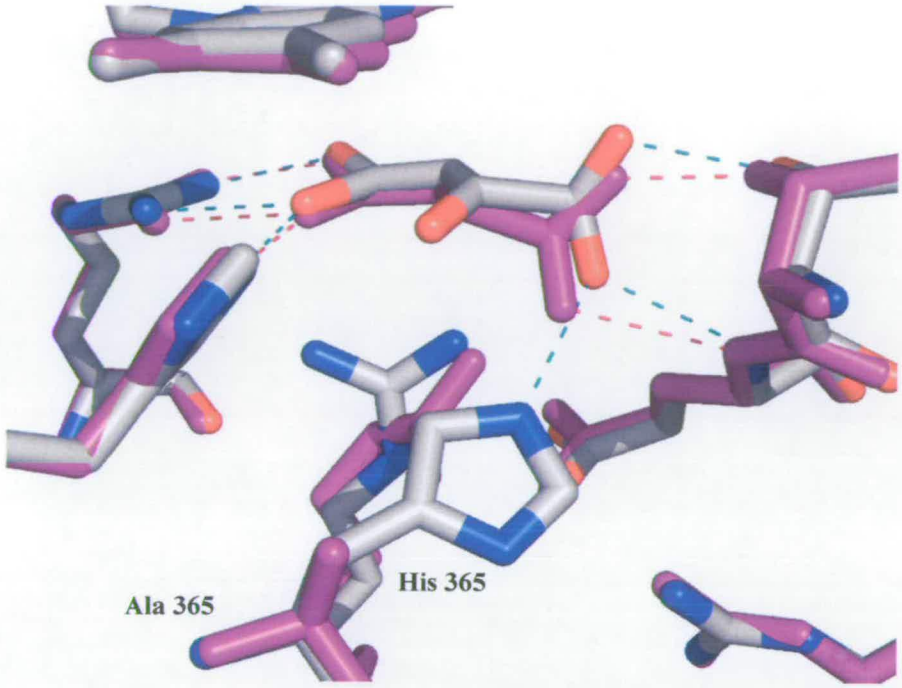

b)

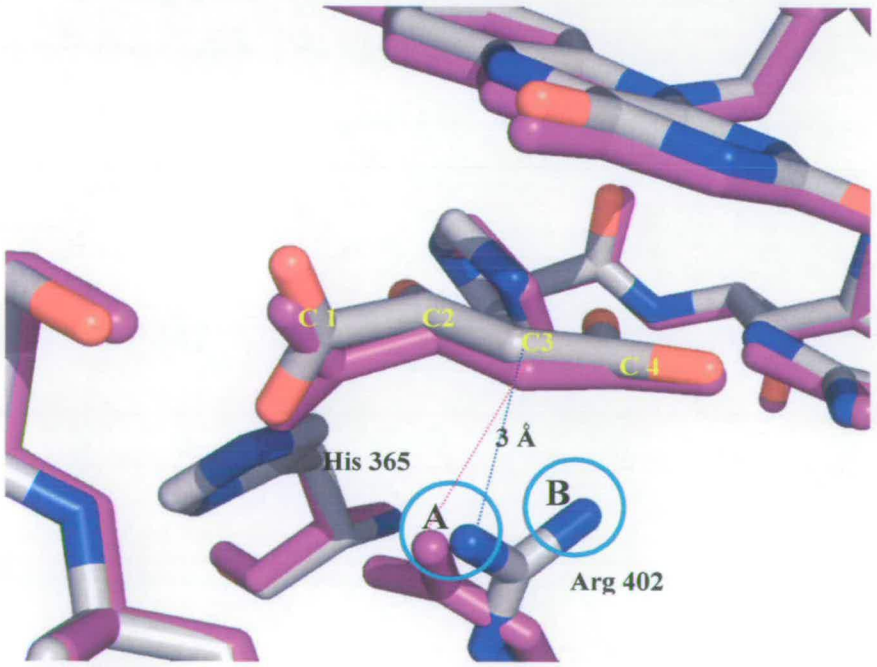

a) H365A (purple) overlaid on WT. Hydrogen bonding interactions are shown in light blue dashes for WT and purple dashes for H365A. b) Crystal structure showing relative positions of arginine 402 to substrate for H365A (purple) and WT. The NH_2 group at position A transfers a proton to C3. The NH_2 at position B acts as a Lewis acid to stabilise build-up of negative charge during the transition state. Arginine 402 in H365A can transfer a proton to C3 but is unable to act as a Lewis acid also due to its position relative to substrate.

5.3 Crystal structure of histidine 365 to alanine mutant

The crystal structure of H365A Fcc_3 had been previously solved to 1.8 Å [PDB ID: 1E39, Doherty *et al*, 2000]. Figure 5.4 shows crystal structures of the active site of H365A (purple) with fumarate bound, overlaid on Wild-type Fcc_3 with a malate-like molecule bound at the active site. Although there is the loss of a hydrogen bond when Histidine 365 is replaced with alanine, fumarate is still bound in an analagous manner to that observed in WT. There is a slight shift in position of the C1 carboxylate group of fumarate but it retains its twisted conformation, thus aiding polarisation of the C2 – C3 double bond, an important aspect of the reaction mechanism. Hydride transfer should not be affected because the distance between the N5 of the flavin alloxazine ring and C2 of substrate is the same as that measured in the WT active site. There is a change in the positioning of the active site acid arginine 402. As mentioned in the introduction, one NH_2 of the guanidinium group occupies position **A** (figure 5.4 b) relative to the substrate and acts as a Brønsted acid in that it donates a proton to C3 to complete the two-electron reduction of fumarate to succinate. The other NH2 occupies position **B** and behaves as a lewis acid, stabilising the build up of negative charge (at the carbanion) that occurs during during the transition state. In H365A, the NH_2 that would normally occupy position **A** is not ideally placed for direct proton transfer because it is 4.91 Å from C3 of fumarate. The NH_2 that occupies position **B** in WT now occupies position **A** relative to fumarate, and at a distance of 3.0 Å, donates a proton to C3 to complete the formation of succinate. Therefore arginine 402 is still able to act as a Brønsted acid during catalysis in H365A, but its position relative to substrate means that it does not additionally function as a Lewis acid as it does in the WT enzyme. Therefore, reduction of fumarate to succinate would require a greater amount of free energy because the carbanion that forms during the transition

state is less stable than during catalysis by WT Fcc_3. This would explain why H365A reduces fumarate at lower rates than wild-type Fcc_3 (table 5.3) and the loss of a hydrogen bond would explain the higher K_m because fumarate would not bind as strongly to the active site. The low rates observed for 2-methylfumarate reduction (table 5.4) by H365A suggests that, despite binding more strongly to the active site than fumarate, the presence of the methyl group interferes with catalysis to a greater extent than it does in WT. This is illustrated by the fact that reduction of 2-methylfumarate in WT is approximately 50 times slower than reduction of fumarate but for H365A it is approximately 450 times slower. The same is also true for H504A where reduction of 2-methylfumarate is ~300 times slower than fumarate reduction.

5.4 Crystal structure of T377A

As previously discussed in chapter 3.2, the crystal structure of T377A was solved to 2.0 Å. The active site of T377A (green) with fumarate bound is shown in figure 5.5 overlaid on to the wild-type active site. Because threonine has been replaced by alanine, there are two less hydrogen bonding interactions with fumarate. Substrate binds less well, so the enzyme-substrate complex that promotes catalytic reduction is less likely to form than it does in H365A, H504A (where a single Hydrogen bond has been removed) and WT. This results in the much larger K_m values observed for reduction of fumarate and 2-methylfumarate by T377A (tables 5.3 and 5.4) relative to WT and the other single mutants. The orientation of fumarate relative to flavin and arginine 402 is the same as that seen in WT and distances for hydride and proton transfer are unaffected. However it can be seen that the C1 carboxylate of substrate bound to T377A is not twisted out of plane as it is in the WT and H365A structures. This could partly explain why rates for fumarate reduction are lower. It might be

Figure 5.5 Crystal structure of T377A active site

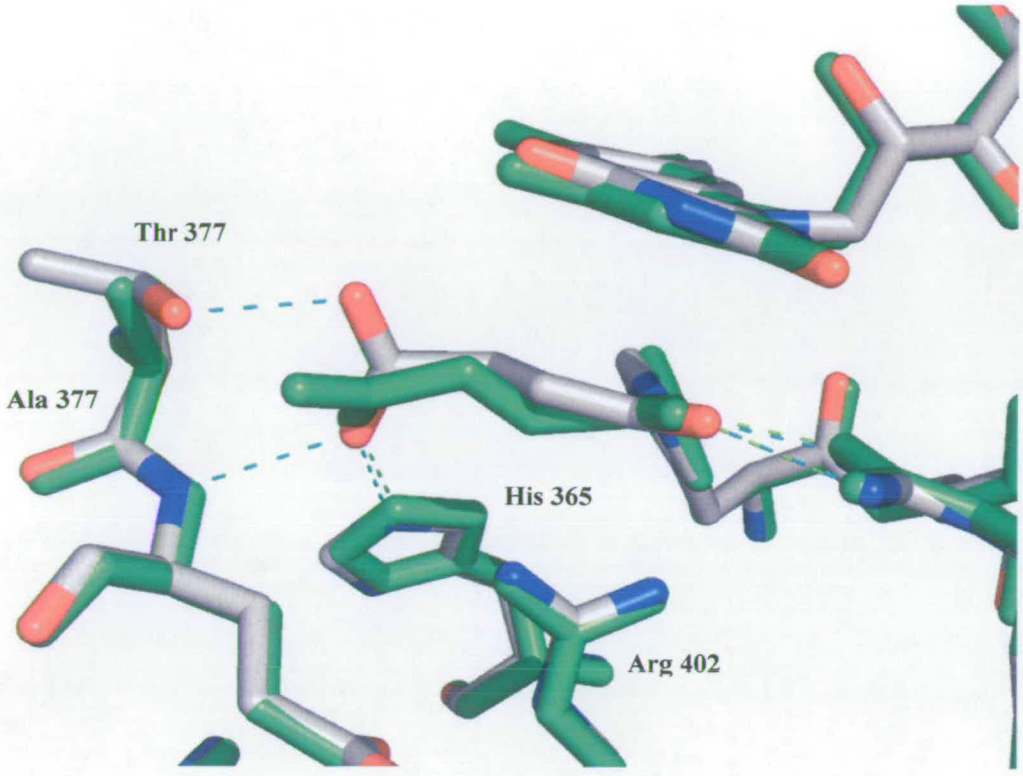

T377A (green) overlaid on WT. Hydrogen bonding interactions are shown in light blue dashes for WT and in green dashes for T377A. There are two less Hydrogen bonds in T377A so the substrate is no longer bound in the twisted conformation. The relative positioning of the other active site residues are unchanged.

expected that the less polar environment caused by substitution of threonine to alanine would facilitate binding (and possibly reduction) of the unsaturated monoacids listed in table 5.2 But none of these substrates were bound or reduced. Unfortunately, there are no crystal structures available for the double mutants. In the case of H365A/T377A, the removal of three hydrogen-bonds would explain why it does not turn over fumarate very efficiently and why it cannot catalyse reduction of 2-methylfumarate.

5.5 Substitution of Histidine365 with glycine

As previously mentioned at the beginning of this chapter, only two methacrylate reductases have been discovered to date. One of these – FccA from *Wollinella succinogenes* – appears to have a similar active site to that of Fcc_3. However, instead of a histidine at position 365 (or equivalent) there is a glycine residue (figure 5.1) for sequence alignment). It was hoped that substitution of H365 with glycine may alter the properties of the active site in such a way as to promote binding of one or more of the mono-acids listed in table 5.2. However, H365G was not able to catalyse reduction of methacrylate or any other substrate apart from fumarate. Compared with

Figure 5.6 Michaelis plot of fumarate reduction by H365G at pH 7.2

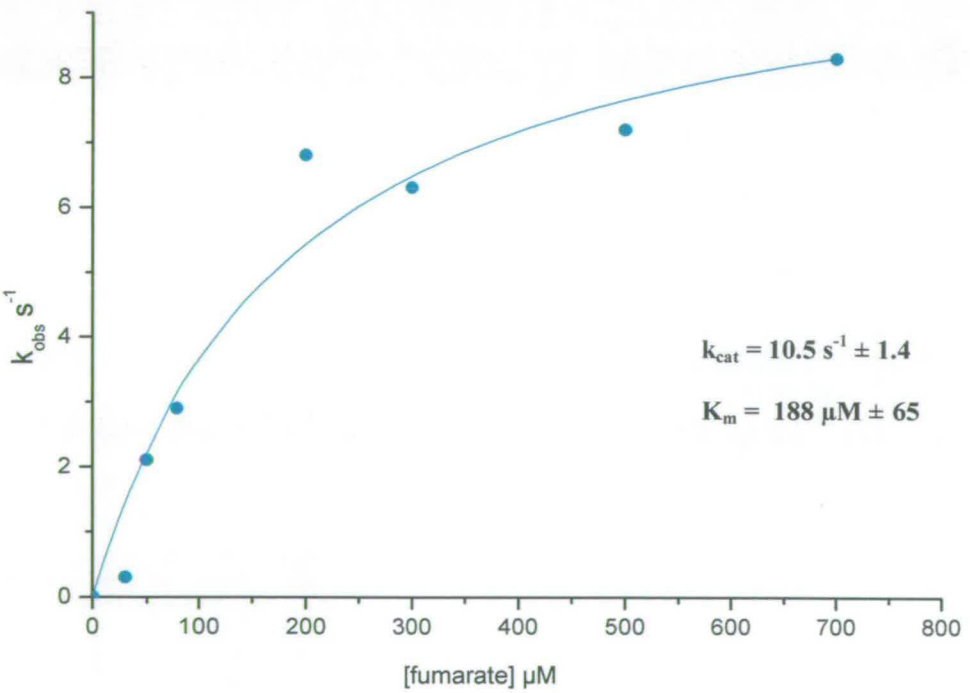

Michaelis plot of observed rates of fumarate reduction by H365G versus fumarate concentration. Fitted as before using Microcal Origin

Figure 5.7 Crystal structure of H365G active site overlaid on to the IFcc$_3$ active site

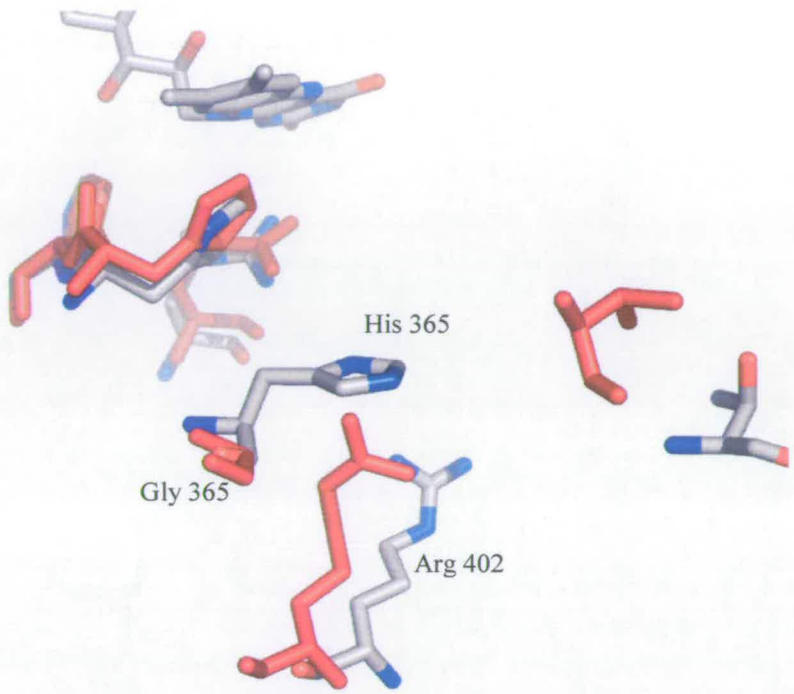

Crystal structure of H365G active site residues (red) overlaid on to iron-induced IFcc$_3$ (wild-type) active site

WT Fcc$_3$, H365G is not a very good fumarate reductase with a k_{cat} of only 10.5 s^{-1} ± 1.4, and a K_m of 188 μM ± 65 (figure 5.6). The crystal structure of H365G was obtained in the "open" conformation without substrate bound as discussed in chapter 3. Figure 5.7 shows the active site of H365G overlaid on to the active site of iron-induced Fcc$_3$ also in the open conformation [Bamford *et al.* 1999]. The active site residues occupy slightly different positions and it can be seen that conversion of Histidine 365 to glycine creates a larger cavity. It is interesting that H365A is able to turn over 2-methylfumarate but H365G cannot. Perhaps the increased size of the active site cavity hinders correct orientation of the substrate required to facilitate reduction to 2-methylsuccinate.

5.6 Substitution of H365 and T377 with leucine, isoleucine and valine

The mutants mentioned so far have all been substituted with a smaller residue (alanine and glycine) and so probably result in creating more space at the active site. Instead of just altering the space available it was thought worthwhile to attempt to change the properties of the active site by substituting H365 and T377 with residues that were non-polar but of similar size. Therefore H365 was substituted with leucine and with isoleucine and T377 was substituted with valine (figure 5.8), again using site-directed mutagenesis. The T377V mutant was found to be capable of fumarate

Figure 5.8 Substitution of polar H365 and T377 with hydrophobic residues

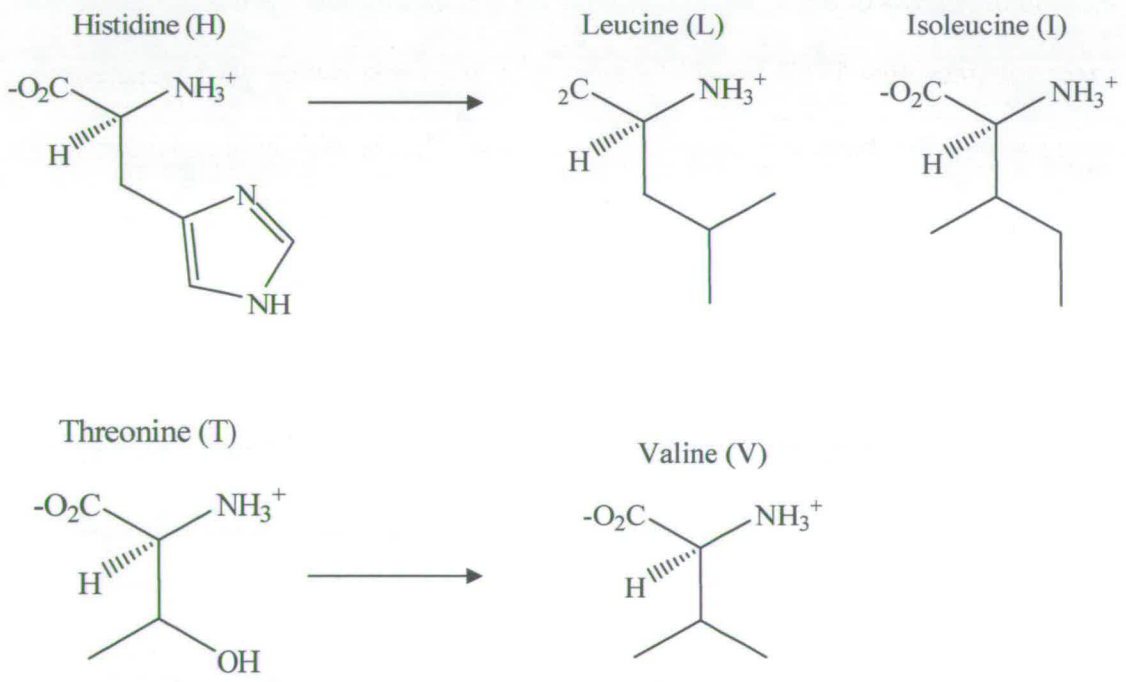

Structures of amino-acids. Histidine 365 was substituted with Leucine or Isoleucine. Threonine 377 was substituted with valine.

Figure 5.9 Reduction of fumarate by H365L and H365I

a) H365L

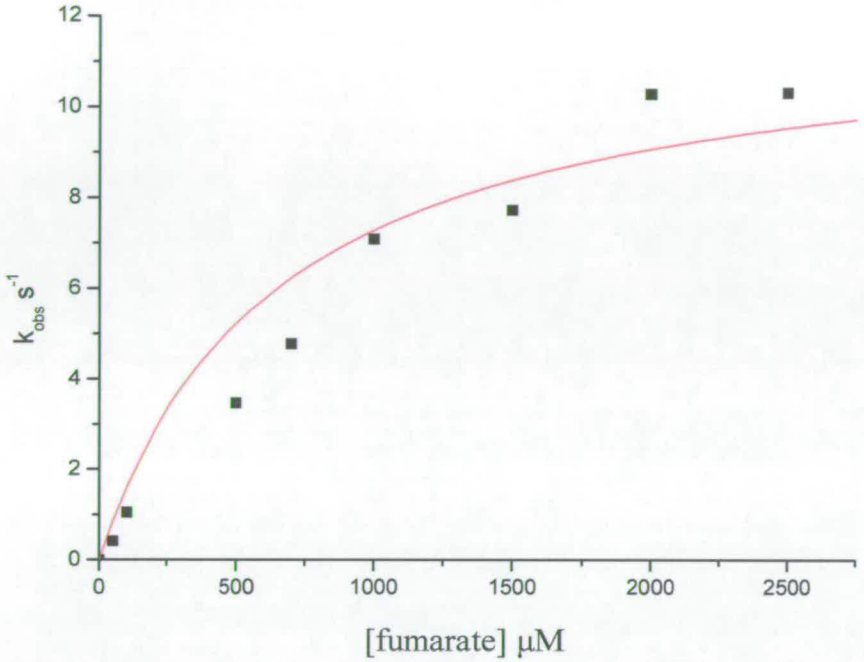

b) H365I

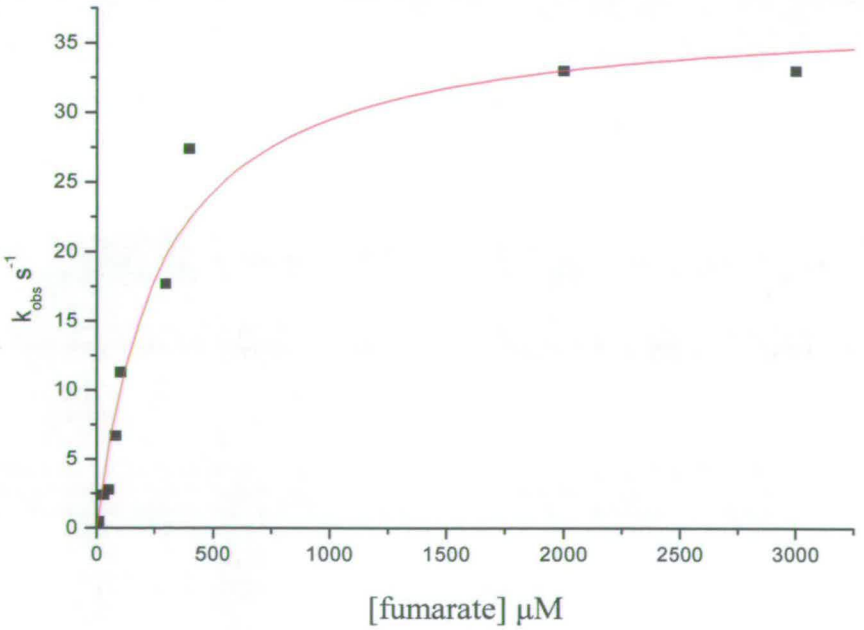

Michaelis plots for reduction of fumarate by H365L (a) and H365I (b). It can be seen that the maximum observed rates for fumarate reduction are about five times faster when H365I is used relative to H365L. Also there is a large difference in the observed K_m values (table 5.5)

reduction but the enzyme lost activity quite quickly and reproducible Michaelis plots have not yet been obtained. Also, disappointingly, it did not appear to turn over any other substrate including those listed in table 5.1. Both H365L and H365I were able to catalyse reduction of fumarate (figure 5.9 *a* and *b*) and 2-methylfumarate (figures 5.10 *a* and *b*). Interestingly, H365I catalysed reduction of fumarate at double the rate of H365L, with a k_{cat} of 37.5 s^{-1} ± 2.4 compared to 16.5 s^{-1} ± 2.0. There is also a large difference in the K_m values. The K_m measured for fumarate reduction by H365I was 272 μM ± 55 compared with 1566 μM ± 367 (1.6 mM). When the catalytic efficiencies (table 5.5) are calculated it can be seen that H365I is over ten times more efficient at catalysing the reduction of fumarate than H365L. When 2-methylfumarate is used as the substrate, both H365L and H365I operate with similar k_{cat} values (0.16 s^{-1} ± 0.02 and 0.18 s^{-1}± 0.003 respectively). Despite the low rate however, H365I has a K_m of 50 μM ± 5 which is close to that observed for 2-methylfumarate reduction by WT Fcc_3 and the lowest value seen for the mutant forms of the enzyme. Because the K_m for 2-methylfumarate reduction by H365L is so large (~5,300 μM), it is a hundred times less efficient at catalysing reduction of this substrate than H365I. Activity tests were again performed to see if H365L and H365I could catalyse reduction of any other substrates including those listed in table 5.2, but no activity was observed. There are no crystal structures available for these mutants so it is difficult to say why H365I is more likely to form the enzyme-substrate complex than H365L. Double mutants H365L/T377V and H365I/T377V were also constructed but no activity tests have been performed on purified protein as yet. However, given the low rates of reduction catalysed by the single mutants, it is unlikely that they will reduce any of the substrates listed in this chapter with any efficiency or even at rates that would be detectable.

Figure 5.10 Reduction of 2-methylfumarate at pH 7.2

a) H365L

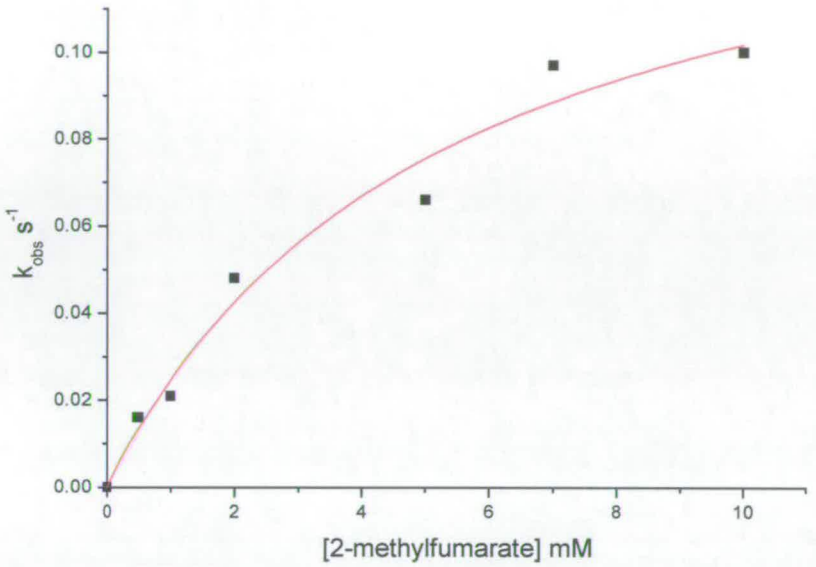

b) H365I

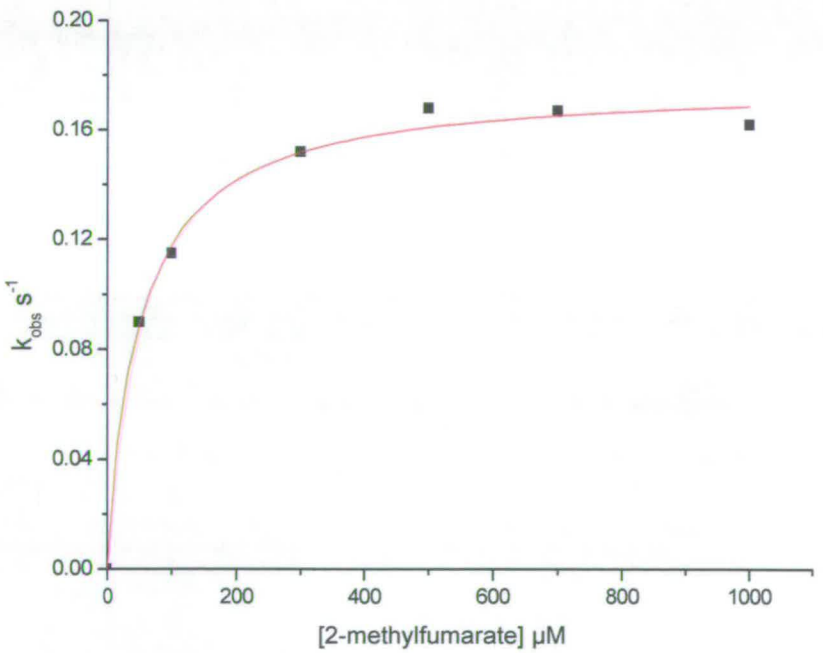

a) Rates of 2-methylfumarate reduction by H365L at different substrate concentrations (in milllimolar). b) Reduction rates for H365I at different substrate concentrations (in micromolar). Michaelis plots were generated using Microcal Origin 7.0. k_{cat} and K_m values are listed in table 5.5.

Table 5.5 kinetic parameters for reduction of fumarate and 2-methylfumarate at pH 7.2.

	k_{cat} (s^{-1})	K_m (μM)	k_{cat}/K_m ($M^{-1}s^{-1}$)
fumarate			
WT	509 ± 15	25 ± 2	2.0×10^7
H365L	16.5 ± 2.0	1566 ± 367	1.0×10^4
H365I	37.5 ± 2.4	272 ± 55	1.4×10^5
2-methylfumarate			
WT	9.0 ± 0.4	32 ± 8.5	2.8×10^5
H365L	0.16 ± 0.02	~5300	3.0×10^1
H365I	0.18 ± 0.003	50 ± 5	3.6×10^3

Rates of fumarate and 2-methylfumarate reduction by H365L and H365I. the K_m's are listed in micromolar units for ease of comparison.

5.7 Future Work and conclusion

Although molecular modelling studies had suggested that the active site of Fcc_3 might accommodate some of the potential substrates listed in table 5.2, none of the substituted enzymes were able to catalyse the reduction of molecules not turned over by wild-type Fcc_3. Substitution of active site residues resulted in changes to the kinetics of fumarate and 2-methylfumarate reduction, but did not enable the enzyme to bind alternative substrates. It is possible however, that other combinations of active site substitutions (not yet tested) could yield different results. In the case of H365G, substitution resulted in a 50-fold decrease in the rate of reduction of fumarate relative to the wild-type enzyme and it does not appear to catalyse the reduction of any of the

chemicals listed in table 5.2. However, additional substitutions that could be made at position 377 (threonine in wild-type Fcc_3) may further alter the enzyme's substrate binding range and activity (the Wollinella succinogenes methacrylate reductase has a valine residue at the equivalent position [Gross *et al*, 2001]). Also it would be useful to obtain a crystal structure of H365G in the "closed" conformation with fumarate bound. This would provide additional information about changes in the relative positioning of other active site residues which would enable determination of why the rate of fumarate reduction is 5-fold lower than that of the H365A enzyme. On the other hand, all research so far seems to indicate that Fcc_3 is a highly specific fumarate reductase. If this is the case, then it is unlikely that any substitutions will result in the enzyme being able to catalyse the reduction of any potential substrates other than fumarate or 2-methylfumarate.

Summary

During the course of this project, three new crystal structures of Fcc_3 have been obtained including one (H365G) in the "open" conformation. It has been shown that Flavocytochrome c_3 can catalyse the reduction of 2-methylfumarate, a molecule previously thought to be only an inhibitor of the enzyme. Crystallography of the Fcc_3/2-methylfumarate complex has allowed us to visualise the binding of this substrate at the active site of the enzyme. This structure, in combination with the previously proposed mechanism for catalysis by Fcc_3 [Taylor *et al*, 1999], has enabled us to predict the trajectories for hydride and proton transfer to 2-methylfumarate. This suggested that the resulting product should be (S)-methylsuccinate and this has been confirmed by CD spectroscopy adding strong support to the validity of the proposed mechanism. It was thought that substitution of active site residues could possibly

alter the substrate specificity of Fcc_3. However, activity tests have shown that none of the substitutions enabled the enzyme to reduce any of the alternative substrates tested, or improved the enzyme's ability to reduce fumarate or 2-methylfumarate. Also, none of the chemicals tested altered the activity of fumarate reduction when included (in excess) in the fumarate reductase assay, indicating that none of them bound to the active site. All substitutions resulted in a detrimental effect on the rates of reduction of fumarate and 2-methylfumarate compared to that of the wild-type enzyme, indicating that Fcc_3 is already perfectly designed for its purpose as a fumarate reductase.

Appendices

Appendix 1

References

Bamford V., Dobbin P.S., Richardson D.J., Hemmings A.M. 1999 "Open conformation of a flavocytochrome c_3 fumarate reductase" *Nature Structural Biology*, **6**, 1104-1107

Bilsland M. 2003 "Novel Respiratory Flavocytochromes of *Shewanella oneidensis* MR-1" *PhD thesis* University of Edinburgh

Blaut M., Whittaker K., Valdovinos A., Ackrell B.A., Gunsalus R.P., Cecchini G 1989 "Fumarate reductase mutants of Escherichia coli that lack covalently bound flavin" *J. Biol. Chem*, **264**, 13599-13604

Bowman J.P., McCammon S.A., Nichols D.S., Skerratt J.H., Rea S.M., Nichols P.D., McMeekini T.A. (1997) *"Shewanella gelidimarina* sp. nov. and *Shewanella frigidimarina* sp. nov., Novel Antarctic species with the ability To produce eicosapentaenoic Acid (20:5v3) and grow anaerobically by dissimilatory Fe(III) reduction" *International Journal of Systematic Bacteriology*, **47**, 1040–1047

Brink A.J., van Straten A., van Rensburg A.J. 1995 "*Shewanella* (*Pseudomonas*) *putrefaciens* bacteremia" *Clin. Infect. Dis.* **20**, 1327–1332.

Boyer P.D. 1993 "The binding change mechanism for ATP synthase: some probabilities and possibilities" *Biochim. Biophys. Acta* **1140**, 215–250

Boyington J.C., Gladyshev V.N., Khangulov S.V., Stadtman T.C., Sun P.D. 1997 "Crystal structure of formate dehydrogenase H: catalysis involving Mo, molybdopterin, selenocysteine, and an Fe4S4 cluster" *Science*, **275**, 1305-1308

Butler J.E., Glaven R.H. Esteve-Núñez A., Núñez C., Shelobolina E.S., Bond D.R., Lovely D.R. 2006 "Genetic Characterization of a Single Bifunctional Enzyme

for Fumarate Reduction and Succinate Oxidation in *Geobacter sulfurreducens* and Engineering of Fumarate Reduction in *Geobacter metallireducens" Journal of Bacteriology*, **188**, . 450–455

Butt A.A., Figueroa J., Martin D.H. 1997 "Ocular infection caused by three unusual marine organisms" *Clin. Infect. Dis.* **24**, 470

Cecchini G., Maklashinaa E., Yankovskayaa V., Iverson T.M., Iwata S. 2003 "Variation in proton donor/acceptor pathways in succinate:quinone oxidoreductases" *FEBS Letters*, **545**, 31-38

Chen S. C. A., Lawrence R.H., Packlam D.R., Sorrell T.C. 1991 "Cellulitis due to *Pseudomonas putrefaciens*: possible production of exotoxins" *Rev. Infect. Dis.* **13**, 642–643

Chen Y.S., Liu Y.C., Yen M.Y., Wang J.H., Wann S.R., Cheng D.L. 1997 "Skin and soft-tissue manifestations of *Shewanella putrefaciens* infection" *Clin. Infect. Dis.* **25**, 225–229

Derby, H. A., B. W. Hammer 1931 "Bacteriology of butter. IV. Bacteriological studies on surface taint butter" *Iowa Agric. Exp. Stn. Res. Bull.* **145**, 389–416

Doherty M.K. 1999 "Mechanistic Characterisation of Flavocytochrome c_3, the Fumarate Reductase from *Shewanella frigidimarina* NCIMB400" *PhD thesis* University of Edinburgh

Doherty M.K., Pealing S.L., Miles C.S., Moysey R., Taylor P., Walkinshaw M.D., Reid G.A.,Chapman S.K. 2000 "Identification of the active site acid/base catalyst in a bacterial fumarate reductase: a kinetic and crystallographic study" *Biochemistry*, **39**, 10695 – 10701.

Dodd F.E., Abraham Z.H.L., Eady R.R., Hasnaina S.S. 2000 "Structures of oxidized and reduced azurin II from *Alcaligenes xylosoxidans* at 1.75 Å resolution" *Acta Cryst.* **56**, 690-696

Domínguez H., Vogel B.F., Gram L., Hoffmann S., Schaebel S. 1996 "*Shewanella alga* bacteremia in two patients with lower leg ulcers" *Clin. Infect. Dis*, **22**, 1036–1039

Friedricha T, Böttcher B. 2004 "The gross structure of the respiratory complex I: a Lego System" *Biochimica et Biophysica Acta*, **1608**, 1–9

Galouchko A.S., Mikulinskaya O.V., Laurinavichyus K.S., Obraztsova A.Y., Akimenko V.K. 1996 "Periplasmic location of methacrylate reductase in cells of the strictly anaerobic bacterial strain AM-1." *Microbiology* (Russian), **65**, 432-435.

Gao X., Wen X., Esser L., Quinn B., Yu L., Yu C., Xia D. 2003 "Structural basis for the quinone reduction in the *bc*1 complex: A comparative analysis of crystal structures of mitochondrial cytochrome *bc*1 with bound substrate and inhibitors at the Qi site." *Biochemistry*, **42**, 9067-9080

Ghisla S., Massey V. 1989 "Mechanisms of flavoprotein-catalysed reactions" *Eur. J. Biochem.*, **181**, 1-17

Gibbons C., Montgomery M.G., Leslie A.G.W., Walker J.E. 2000 "The structure of the central stalk in bovine F1-ATPase at 2.4 Å resolution" *Nature structural biology* **7**, 1055-1061

Gordon E.H.J., Pealing S.L., Chapman S.K., Ward F.B., Reid G.A. 1998 "Physiological function and regulation of flavocytochrome *c*3, the soluble fumarate reductase from *Shewanella putrefaciens* NCIMB 400" *Microbiology*, **144**, 937–945

Gross R., Simon J., Kröger A. 2001 "Periplasmic methacrylate reductase activity in *Wolinella succinogenes*" *Arch. Microbiol.* **176**, 310-313

Guest J. R. 1992 "Oxygen-regulated gene expression in *Escherichia Coli*" *J. Gen. Microbiol.* **138**, 2253-2263

Gunsalus, R. P. 1992 "Control of electron flow in *Escherichia coli*: coordinated transcription of respiratory pathway genes" *J. Bacteriol.* **174**, 7069-7074

Higuchi Y., Yagi T., Yasuoka N. 1997 "Unusual ligand structure in Ni–Fe active center and an additional Mg site in hydrogenase revealed by high resolution X-ray structure analysis" *Structure*, **5**, 1671–1680

Hille R. 1999 "Molybdenum Enzymes" *Essays in Biochemistry: Metalloproteins* (D.P.Ballou, H., Eds.) pp 125 – 137, Portland Press, London.

Iverson T.M., Luna-Chavez C, Cecchini G. 1999 "Structure of the *Escherichia coli* Fumarate Reductase Respiratory Complex" *Science*, **284,** 1961-1966

Iverson T.M., Luna-Chavez C., Croal L.R., Cecchini G., Rees D.C. 2002 "Crystallographic studies of the Escherichia coli quinol-fumarate reductase with inhibitors bound to the quinol-binding site" *J.Biol.Chem.* **277**, 16124-16130

Iwata, S., Ostermeier, C., Ludwig, B., Michel, H. (1995) "Structure at 2.8 Å. resolution of cytochrome *c* oxidase from *Paracoccus denitrificans*" *Nature*, **376**, 660-669.

Iwata S., Lee J.W., Okada K., Lee J.K., Iwata M., Rasmussen B., Link T.A., Ramaswamy S., Jap B.K. 1998 "Complete structure of the 11-subunit bovine mitochondrial cytochrome bc1 complex" *Science*, **281**, 64-71

Jensen, M.J., Tebo B.M., Baumann P., Mandel M., Nealson K.H. 1980 "Characterization of *Alteromonas hanedai* (sp. nov.), a non-fermentative luminous species of marine origin. *Curr. Microbio*, **3**, 311–315

Jeuken L.C.J., Jones A.K., Chapman S.K., Cecchini G., Armstrong F.A. 2002 "Electron-transfer mechanisms through biological redox chains in multicenter enzymes" *J. Am. Chem. Soc.* **124**, 5702-5713

Jones A.K., Camba R., Reid G.A., Chapman S.K., Armstrong F.A. 2000 "Interruption and Time-Resolution of Catalysis by a Flavoenzyme Using Fast Scan Protein Film Voltammetry" *J. Am. Chem. Soc.* **122**, 6494-6495

Khashe S., Janda M. 1998 "Biochemical and Pathogenic Properties of *Shewanella alga* and *Shewanella putrefaciens*" *Journal of clinical microbiology*, **46**, 783–787

Komar-Panicucci S., McLendon G., Gray H.B. 1994 "Electron transfer in cytochrome c depends upon the structure of the intervening medium" *Structure* **2**, 415-422

Lancaster, C.R.D., Kröger, A., Auer, M., Michel, H. 1999 "Structure of fumarate reductase from *Wolinella succinogenes* at 2.2 Å resolution" *Nature*, **402**, 377 – 385.

Lancaster C.R.D. 2002 "Succinate:quinone oxidoreductases: an overview" *Biochimica et Biophysica Acta*, **1553**, 1-6

Leys D., Tsapin A.S., Nealson K.H., Meyer T.E., Cusanovich M.A., Van-Beeumen J.J. 1999 "Structure and mechanism of the flavocytochrome c fumarate reductase of *Shewanella putrefaciens*" *Nature Structural Biology*, **6**, 1103-1117

Leys D., Meyer T.E., Tsapin A.S., Nealson K.H., Cusanovich M.A., Van Beeumen J.J. 2002 "Crystal structures at atomic resolution reveal the novel concept of "electron-harvesting" as a role for the small tetraheme cytochrome *c*" *Journal of biological chemistry*, **277**, 35703–35711

Lovely, D. R. 1993 "Dissimilatory metal reduction", *Annu. Rev. Microbiol.* **47**, 263–290

Lovely, D. R., Phillips E. J. P. 1986 "Organic matter mineralization with reduction of ferric iron in anaerobic sediments", *Appl. Environ. Microbiol,* **51**, 683–689

Lucas M.F., Ramos M.J. 2006 "Mechanism of a soluble fumarate reductase from *Shewanella frigidimarina*: a theoretical study" *J. Phys. Chem.* **110**, 10550-10556

MacDonell M. T., Colwell R. R. 1985 "Phylogeny of the Vibrionaceae, and recommendation for two new genera, *Listonella* and *Shewanella" Syst. Appl. Microbiol*, **6**, 171–182

Massey V. 1995 "Introduction: flavoprotein structure and mechanism". *FASEB J.* **9**, 473 – 475

Mattevi1 A., Tedeschi G., Bacchella L., Coda ., Negri A., Ronchi S. 1999 "Structure of L-aspartate oxidase: implications for the succinate dehydrogenase/fumarate reductase oxidoreductase family" *Structure*, **7**, 745-756

Mewies M., McIntire W.S., Scrutton N.S., 1998 "Covalent attachment of flavin adenine dinucleotide (FAD) and flavin mononucleotide (FMN) to enzymes: The current state of affairs" *Protein Science*, **7**, 7-20

Michel H. 1998 "The mechanism of proton pumping by cytochrome *c* oxidase" *Proc. Natl. Acad. Sci. USA*, **95**, 12819–12824

Mikoulinskaia O., Akimenko V., Galouchko A., Thauer R.K., Hedderich R. 1999 "Cytochrome *c*-dependent methacrylate reductase from *Geobacter sulfurreducens*" *Eur. J. Biochem.* **263**, 346-352

Moser D.P., Nealson K.H. 1996 "Growth of the facultative anaerobe *Shewanella putrefaciens* by elemental sulfur reduction" *Appl. Environ. Microbiol.* **62**, 2100–2105

Mowat, C.G., Moysey, R., Miles, C.S., Leys, D., Doherty, M.K., Taylor, P., Walkinshaw, M.D., Reid, G.A. Chapman S.K. (2001) "Kinetic and crystallographic analysis of the key active site acid/base arginine in a soluble fumarate reductase" *Biochemistry 40*, 12292 – 12298

Mowat C.G., Pankhurst, K.L, Miles, C.S., Leys, D., Walkinshaw, M.D., Reid, G.A., Chapman, S.K. (2002) "Engineering water to act as an active site acid in a soluble fumarate reductase " *Biochemistry*, **41**, 11990 – 11996.

Mowat, C.G., Miles, C.S., Reid, G.A., Walkinshaw, M.D., Pankhurst, K.L., Chapman, S.K., Leys, D. (2002) "A universal mechanism for the fumarate reductase and succinate dehydrogenase family" in *Flavins and Flavoproteins 2002* (Chapman, S.K., Perham, R., and Scrutton, N., Eds.) pp 739 – 748, Rudolf Weber, Agency for Scientific Publications, Berlin.

Moysey, R., 2001 "A study of Flavocytochrome b2 and Flavocytochrome c_3" PhD thesis, University of Edinburgh

Murshudov G. N., Vagin A. A., Dodson E. J. 1997."Refinement of macromolecular structures by the maximum-liklihood method" *Acta Crystallographica* **D53**, 240-255.

Myers, C.R., Myers, J.M. (1997) "Cloning and sequence of cymA, a gene encoding a tetraheme cytochrome c required for reduction of iron(III), fumarate, and nitrate by *Shewanella putrefaciens* MR-1" *J. Bacteriology*, **179**, 1143 – 1152.

Ogata H., Mizoguchi Y., Mizuno N., Miki K., Adachi S., Yasuoka N., Yagi T., Yamauchi O., Hirota S., Higuchi Y. 2002 "Structural Studies of the Carbon Monoxide Complex of [NiFe]hydrogenase from Desulfovibrio vulgaris Miyazaki F: Suggestion for the Initial Activation Site for Dihydrogen" *J.Am.Chem.Soc*, **124**, 11628-11635

Otwinowski Z., Minor W., 1997 "Processing of X-ray Diffraction Data Collected in Oscillation Mode." *Methods in Enzymology*, **276**

Overbye L., Sandkvist M., Bagdasarian M. 1995 "Specificity of the protein secretory apparatus: secretion of the heat-labile enterotoxin B subunit pentamers by different species of Gram- bacteria" *Gene*, **152**, 41-45

Page C.C., Moser C.C., Chen X., Dutton P.L. 1999 "Natural engineering principles

of electron tunnelling in biological oxidation-reduction" *Nature* **402**, 47 - 52

Pankhurst, K.L. 2003 "Mechanistic studies on flavocytochrome c_3" Ph.D. Thesis, University of Edinburgh.

Pankhurst K.L., Rothery E.L., Doherty M.K., Mowat C.G., Miles C.S., Reid G.A., Chapman S.K. 2002 "Investigating the proton pathway in flavocytochrome c_3 from *Shewanella frigidimarina* by site directed mutagenesis" in *Flavins and Flavoproteins 2002* (Chapman, S.K., Perham, R., and Scrutton, N., Eds.) pp 779 – 784, Rudolf Weber, Agency for Scientific Publications, Berlin.

Pealing S.L., Cheesman M.R., Reid G.A., Thomson A.J., Ward F.B., Chapman S.K. 1995 "Spectroscopic and Kinetic Studies of the Tetraheme Flavocytochrome *c* from *Shewanella putrefaciens* NCIMB400" *Biochemistry*, **34**, 6153-6158

Pessanhaa M., Brennana L., Xaviera A.V., Cuthbertson P.M., Reid G.A., Chapman S.K., Turner D.L. Salgueiroa C.A. 2001 "NMR structure of the haem core of a novel tetrahaem cytochrome isolated from Shewanella frigidimarina: identification of the haem-specific axial ligands and order of oxidation" *FEBS Letters*, **489**, 8-13

Raaijmakers H.C.A., Romao M.J. 2006 "Formate-Reduced E. Coli Formate Dehydrogenase H: The Reinterpretation of the Crystal Structure Suggests a New Reaction Mechanism" *JBIC,* **11**, *849-854*

Reid G.A., Gordon E.H.J. 1999 "Phylogeny of marine and freshwater *Shewanella*: reclassification of *Shewanella putrefaciens* NCIMB400 as *Shewanella frigidimarina*" *Int. J. Syst. Bacteriol.*, **49**, 189 – 191.

Reid G.A., Miles C.S., Moysey R.K., Pankhurst K.L., Chapman S.K. (2000) "Catalysis in fumarate reductase" *Biochim. Biophys. Acta* **1459**, 310 – 315.

Rothery E.L., Mowat C.G., Miles C.S. Walkinshaw M.D., Reid G.A., Chapman S.K. 2003 "Histidine 61: An Important Heme Ligand in the Soluble Fumarate Reductase from *Shewanella frigidimarina*" *Biochemistry*, **42**, 13160-13169

Rothery E.L., Mowat C.G., Miles C.S., Mott S., Walkinshaw M.D., Reid G.A., Chapman S.K. 2004 "Probing domain mobility in a flavocytochrome" *Biochemistry*, **43**, 4983-4989

Roussel A., Cambillau C. 1991 "*Silicon Graphics Geometry Partners Directory*" (Graphic, S., ed) pp. **86**, Silicon Graphics, Mountain View, CA

Rousset M., Montet Y., Guigliarelli B., Forget N., Asso M., Bertrand P., Fontecilla-Camps J.C., Hatchikian E.C. 1998 "[3Fe-4S] to [4Fe-4S] cluster conversion in *Desulfovibrio fructosovorans* [NiFe] hydrogenase by site-directed mutagenesis" *Proc. Natl. Acad. Sci. USA* **95**, 11625–11630

Saffarini D.A., Nealson K.H. 1993 "Sequence and genetic characterization of etrA, an fnr analog that regulates anaerobic respiration in *Shewanella putrefaciens* MR-1" *Journal of Bacteriology*, **175**, 7938-7944

Schwalb C., Chapman S.K., Reid G.A. (2002) "The membrane-bound tetraheme *c*-type cytochrome CymA interacts directly with the soluble fumarate reductase in *Shewanella*" *Biochem. Soc. Trans.*, **30**, 658 – 662.

Schwalb C., Chapman S.K., Reid G.A. 2003 "The tetraheme cytochrome CymA is required for anaerobic respiration with dimethyl sulfoxide and nitrite in *Shewanella oneidensis*" *Biochemistry*, **42**, 9491 – 9497.

Smith D.M.A., Rosso K.M., Dupuis M., Valiev M., Straatsma T.P. 2006 "Electronic Coupling between Heme Electron-Transfer Centers and Its Decay with Distance Depends Strongly on Relative Orientation" *J. Phys. Chem.* **110**, 15582-15588

Stenström I.M., Molin G 1990 "Classification of the spoilage flora of fish, with special reference to *Shewanella putrefaciens*" *J. Appl. Bacteriol.* **68**, 601–618

Taylor P., Pealing S.L., Reid G.A., Chapman S.K., Walkinshaw M.D. (1999) "Structural and mechanistic mapping of a unique fumarate reductase" *Nature Structural Biology*, **6**, 1108-1112

Thorsten F., Böttcherb B. 2004 "The gross structure of the respiratory complex I: a lego system" *Biochim. et Biophys. Acta.* **1608**, 1-9

Trumpower B.L., Gennis,R. 1994 "Energy transduction by cytochrome complexes in mitochondrial and bacterial respiration: the enzymology of coupling electron transfer reactions to transmembrane proton translocation". *Annu. Rev. Biochem.*, **63**, 675-716.

Turner K.L., Doherty M.K., Heering H.A., Armstrong F.A., Reid G.A., Chapman S.K. 1999 "Redox Properties of Flavocytochrome *c*3 from *Shewanella frigidimarina* NCIMB400" *Biochemistry*, **38**, 3302-3309

van Hellemond J.J., van der Klei A, van Weelden S.H., Tielens A.G.M. 2003 "Biochemical and evolutionary aspects of anaerobically functioning mitochondria" *Phil. Trans. R. Soc. Lond.* B) **358**, 205–215

Venkateswaran K., Dollhopf M.E., Aller R., Stackebrant E., Nealson K.H. 1998 "*Shewanella amazonensis* sp. nov., a novel metal-reducing facultative anaerobe from Amazonian shelf muds" *International Journal of Systematic Bacteriology* **48**, 2940

Volbeda A., Charon M.H., Piras C., Hatchikian E.C., Frey M., Fontecillacamps J.C. 1995 "Crystal structure of the nickel-iron hydrogenase from *Desulfovibrio gigas*" *Nature*, **373,** 580 – 587.

Wardrope C., Mowat C.G., Walkinshaw M.D., Reid G.A., Chapman S.K. 2006 "Fumarate reductase: Structural and mechanistic insights from the catalytic reduction of 2-methylfumarate" *FEBS letters* **580**, 1677–1680

Wistance G.R., Terelfall D.R. 1968 "Effect of anaerobiosis on the concentrations of dimethylmenaquinone, menaquinone and ubiquinone in *Escherichia freundii, Proteus mirabilis* and *Aeromonas punctata*". *Biochemical Journal*, **108**, 505-507

Yankovskaya V., Horsefield R., Tornroth S., Luna-Chavez C., Miyoshi H., Leger C., Byrne B., Cecchini G., Iwata S. 2003 . "Architecture of succinate dehydrogenase and reactive oxygen species generation" *Science*, **281**, 700-704

Yasuda R., Noji H., Kinosita K., Yoshida, M. 1998 "F1-ATPase is a highly efficient molecular motor that rotates with discrete 120° steps" *Cell*, **93**, 1117–1124

Yoshikawa S., Shinzawa-Itoh K., Nakashima R., Yaono R., Yamashita E., Inoue N., Yao M., Fei M.J., Libeu C.P., Mizushima T., Yamaguchi H., Tomizaki T., Tsukihara 1998 "Redox-coupled crystal structural changes in bovine heart cytochrome c oxidase" *Science*, **280**, 1723-1729

Appendix 2

Michaelis-Menten equation

The kinetics of many enzymes can be described by the Michaelis-Menten model.

$$E + S \underset{k_{-1}}{\overset{k_1}{\rightleftharpoons}} ES \xrightarrow{k_2} E + P$$

This model describes the reversible formation of an enzyme-substrate (ES) complex intermediate (k_1 and k_{-1}), which then dissociates in a rate-limiting step to form product and free enzyme (k_2). When the concentration of substrate is saturating compared to that of enzyme the concentration of ES remains constant so that:

$$\frac{d[ES]}{dt} = k_1 [E] [S] - k_{-1} [ES] - k_2 [ES] = 0$$

Therefore:

$$[ES] = \frac{k_1 [E] [S]}{k_{-1} + k_2}$$

The Michaelis constant K_m is the concentration of substrate when the rate of reaction is 50 % of that of the maximum (V_{max}) and can be represented as:

$$K_m = \frac{k_{-1} + k_2}{k_1}$$

This enables equation – to be simplified to:

$$[ES] = \frac{[E] [S]}{K_m}$$

The total concentration of enzyme present is taken as the initial concentration at time zero (E_0) and is equal to the concentration of enzyme bound to substrate (ES) minus the concentration of free enzyme [E].

$$[E] = [E_0] - [ES]$$

The concentration of substrate-bound enzyme can thus be written as:

$$[ES] = \frac{([E_0] - [ES]) [S]}{K_m}$$

Which rearranges to give:

$$[ES] = \frac{[E_0]\,[S]}{K_m + [S]}$$

The rate of the reaction (V) is the rate of product formation:

$$\frac{d[P]}{dt} = k_2\,[ES]$$

Combining equations – results in the Michaelis-Menten equation

$$V = \frac{k_2\,[E_0][S]}{K_m + [S]}$$

Where k_2 is the k_{cat} or turnover number of the particular enzyme.

Appendix 3

Nucleotide and protein sequences of wild-type Flavocytochrome c_3

Fcc$_3$ including signal sequence and modified internal *Eco*RI and *Hin*dIII sites (571 amino acid residues, 1713bp).

```
atgaaaaagatgaatcttgcagtctgtattgctacattaatgggcacagcaggcctaatg
----:----|----:----|----:----|----:----|----:----|----:----|
         10        20        30        40        50        60
tacttttctacttagaacgtcagacataacgatgtaattacccgtgtcgtccggattac

M  K  K  M  N  L  A  V  C  I  A  T  L  M  G  T  A  G  L  M

ggcactgctgttgcggctgataacttagctgaatttcatgtacaaaaccaagaatgtgat
----:----|----:----|----:----|----:----|----:----|----:----|
         70        80        90        100       110       120
ccgtgacgacaacgccgactattgaatcgacttaaagtacatgttttggttcttacacta

G  T  A  V  A  A  D  N  L  A  E  F  H  V  Q  N  Q  E  C  D

agctgccatacaccagatggtgaactgtcaaacgacagcttaacctatgaaaatacccaa
----:----|----:----|----:----|----:----|----:----|----:----|
         130       140       150       160       170       180
tcgacggtatgtggtctaccacttgacagtttgctgtcgaattggatacttttatgggtt

S  C  H  T  P  D  G  E  L  S  N  D  S  L  T  Y  E  N  T  Q

tgcgtatcttgccatggcacacttgctgaagtagctgaaaccacaaaacatgaacattat
----:----|----:----|----:----|----:----|----:----|----:----|
         190       200       210       220       230       240
acgcatagaacggtaccgtgtgaacgacttcatcgactttggtgttttgtacttgtaata

C  V  S  C  H  G  T  L  A  E  V  A  E  T  T  K  H  E  H  Y

aatgctcatgcttctcatttccctggcgaagtagcttgtacctcatgccacagcgcacac
----:----|----:----|----:----|----:----|----:----|----:----|
         250       260       270       280       290       300
ttacgagtacgaagagtaaagggaccgcttcatcgaacatggagtacggtgtcgcgtgtg

N  A  H  A  S  H  F  P  G  E  V  A  C  T  S  C  H  S  A  H

gaaaaatcgatggtgtattgtgactcttgccacagcttcgatttcaacatgccttatgct
----:----|----:----|----:----|----:----|----:----|----:----|
         310       320       330       340       350       360
ctttttagctaccacataacactgagaacggtgtcgaagctaaagttgtacggaatacga

E  K  S  M  V  Y  C  D  S  C  H  S  F  D  F  N  M  P  Y  A

aaaaaatggctacgtgacgagccgactattgctgaattggccaaagacaaatcagaacgt
----:----|----:----|----:----|----:----|----:----|----:----|
         370       380       390       400       410       420
tttttttaccgatgcactgctcggctgataacgacttaaccggtttctgtttagtcttgca

K  K  W  L  R  D  E  P  T  I  A  E  L  A  K  D  K  S  E  R
```

```
caggctgctcttgctagcgcacctcacgatactgttgacgtagtggttgtcggttctggc
----:----|----:----|----:----|----:----|----:----|----:----|
         430       440       450       460       470       480
gtccgacgagaacgatcgcgtggagtgctatgacaactgcatcaccaacagccaagaccg

Q  A  A  L  A  S  A  P  H  D  T  V  D  V  V  V  V  G  S  G

ggcgcaggtttctcagcggcaatatcagcaacagacagtggtgctaaagtcattcttatt
----:----|----:----|----:----|----:----|----:----|----:----|
         490       500       510       520       530       540
ccgcgtccaaagagtcgccgttatagtcgttgtctgtcaccacgatttcagtaagaataa

G  A  G  F  S  A  A  I  S  A  T  D  S  G  A  K  V  I  L  I

gaaaaagagcctgttattggtggtaatgctaagttagctgcgggtggcatgaacgctgct
----:----|----:----|----:----|----:----|----:----|----:----|
         550       560       570       580       590       600
ctttttctcggacaataaccaccattacgattcaatcgacgcccaccgtacttgcgacga

E  K  E  P  V  I  G  G  N  A  K  L  A  A  G  G  M  N  A  A

tggactgatcaacaaaaagccaaaaaaattactgacagcccagagttaatgttcgaagac
----:----|----:----|----:----|----:----|----:----|----:----|
         610       620       630       640       650       660
acctgactagttgtttttcggttttttaatgactgtcgggtctcaattacaagcttctg

W  T  D  Q  Q  K  A  K  K  I  T  D  S  P  E  L  M  F  E  D

accatgaaaggtggccaaaacataaatgaccctgcattagttaaagtattaagctcacac
----:----|----:----|----:----|----:----|----:----|----:----|
         670       680       690       700       710       720
tggtactttccaccggttttgtatttactgggacgtaatcaatttcataattcgagtgtg

T  M  K  G  G  Q  N  I  N  D  P  A  L  V  K  V  L  S  S  H

tctaaagactctgttgattggatgaccgctatgggtgccgatttaactgatgttggcatg
----:----|----:----|----:----|----:----|----:----|----:----|
         730       740       750       760       770       780
agatttctgagacaactaacctactggcgatacccacggctaaattgactacaaccgtac

S  K  D  S  V  D  W  M  T  A  M  G  A  D  L  T  D  V  G  M

atgggtggcgcatctgttaatcgtgcgcatcgtccaaccggtggtgcgggtgttggtgct
----:----|----:----|----:----|----:----|----:----|----:----|
         790       800       810       820       830       840
tacccaccgcgtagacaattagcacgcgtagcaggttggccaccacgcccacaaccacga

M  G  G  A  S  V  N  R  A  H  R  P  T  G  G  A  G  V  G  A

catgttgttcaagtactttatgataatgcagtgaaacgcaatatcgacttacgcatgaac
----:----|----:----|----:----|----:----|----:----|----:----|
         850       860       870       880       890       900
gtacaacaagttcatgaaatactattacgtcactttgcgttatagctgaatgcgtacttg

H  V  V  Q  V  L  Y  D  N  A  V  K  R  N  I  D  L  R  M  N
```

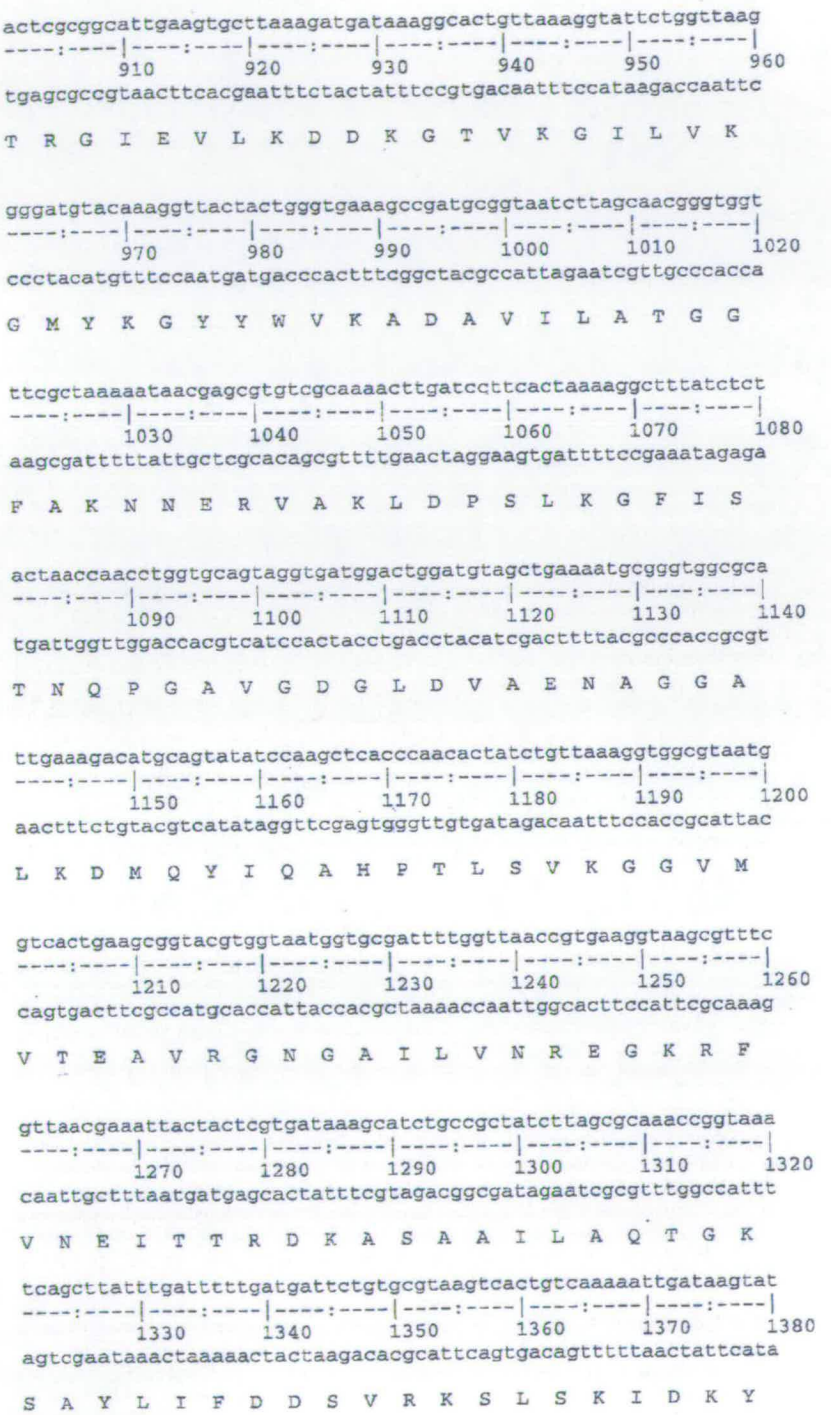
actcgcggcattgaagtgcttaaagatgataaaggcactgttaaaggtattctggttaag
910 920 930 940 950 960
tgagcgccgtaacttcacgaatttctactatttccgtgacaatttccataagaccaattc
T R G I E V L K D D K G T V K G I L V K
gggatgtacaaaggttactactgggtgaaagccgatgcggtaatcttagcaacgggtggt
970 980 990 1000 1010 1020
ccctacatgtttccaatgatgacccactttcggctacgccattagaatcgttgcccacca
G M Y K G Y Y W V K A D A V I L A T G G
ttcgctaaaaataacgagcgtgtcgcaaaacttgatccttcactaaaaggctttatctct
1030 1040 1050 1060 1070 1080
aagcgatttttattgctcgcacagcgttttgaactaggaagtgattttccgaaatagaga
F A K N N E R V A K L D P S L K G F I S
actaaccaacctggtgcagtaggtgatggactggatgtagctgaaaatgcgggtggcgca
1090 1100 1110 1120 1130 1140
tgattggttggaccacgtcatccactacctgacctacatcgacttttacgcccaccgcgt
T N Q P G A V G D G L D V A E N A G G A
ttgaaagacatgcagtatatccaagctcacccaacactatctgttaaaggtggcgtaatg
1150 1160 1170 1180 1190 1200
aactttctgtacgtcatataggttcgagtgggttgtgatagacaatttccaccgcattac
L K D M Q Y I Q A H P T L S V K G G V M
gtcactgaagcggtacgtggtaatggtgcgattttggttaaccgtgaaggtaagcgtttc
1210 1220 1230 1240 1250 1260
cagtgacttcgccatgcaccattaccacgctaaaaccaattggcacttccattcgcaaag
V T E A V R G N G A I L V N R E G K R F
gttaacgaaattactactcgtgataaagcatctgccgctatcttagcgcaaaccggtaaa
1270 1280 1290 1300 1310 1320
caattgctttaatgatgagcactatttcgtagacggcgatagaatcgcgtttggccattt
V N E I T T R D K A S A A I L A Q T G K
tcagcttatttgatttttgatgattctgtgcgtaagtcactgtcaaaaattgataagtat
1330 1340 1350 1360 1370 1380
agtcgaataaactaaaaactactaagacacgcattcagtgacagtttttaactattcata
S A Y L I F D D S V R K S L S K I D K Y

```
attggtttaggtgttgcaccaacggcagatagcctagttaaattaggtaaaatggaaggt
----:----|----:----|----:----|----:----|----:----|----:----|
         1390      1400      1410      1420      1430      1440
taaccaaatccacaacgtggttgccgtctatcggatcaatttaatccattttaccttcca

I  G  L  G  V  A  P  T  A  D  S  L  V  K  L  G  K  M  E  G


attgacggcaaagcactgactgaaactgtcgcgcgttacaacagcttagtgagtagcggt
----:----|----:----|----:----|----:----|----:----|----:----|
         1450      1460      1470      1480      1490      1500
taactgccgtttcgtgactgactttgacagcgcgcaatgttgtcgaatcactcatcgcca

I  D  G  K  A  L  T  E  T  V  A  R  Y  N  S  L  V  S  S  G


aaagacactgattttgagcgtccaaacctaccgcgcgcacttaacgaaggtaactactat
----:----|----:----|----:----|----:----|----:----|----:----|
         1510      1520      1530      1540      1550      1560
tttctgtgactaaaactcgcaggtttggatggcgcgcgtgaattgcttccattgatgata

K  D  T  D  F  E  R  P  N  L  P  R  A  L  N  E  G  N  Y  Y


gcaattgaagttacacctggtgttcaccacactatgggtggcgtgatgatcgacactaaa
----:----|----:----|----:----|----:----|----:----|----:----|
         1570      1580      1590      1600      1610      1620
cgttaacttcaatgtggaccacaagtggtgtgatacccaccgcactactagctgtgattt

A  I  E  V  T  P  G  V  H  H  T  M  G  G  V  M  I  D  T  K


gctgaagtcatgaatgctaagaagcaggttatccctggcttgtatggtgctggtgaggtt
----:----|----:----|----:----|----:----|----:----|----:----|
         1630      1640      1650      1660      1670      1680
cgacttcagtacttacgattcttcgtccaatagggaccgaacataccacgaccactccaa

A  E  V  M  N  A  K  K  Q  V  I  P  G  L  Y  G  A  G  E  V


actggcggtgttcatggtgctaaccgcttaggtggtaatgctatttcagacatcatcacc
----:----|----:----|----:----|----:----|----:----|----:----|
         1690      1700      1710      1720      1730      1740
tgaccgccacaagtaccacgattggcgaatccaccattacgataaagtctgtagtagtgg

T  G  G  V  H  G  A  N  R  L  G  G  N  A  I  S  D  I  I  T


ttcggtcgcttagcgggtgaagaagctgcaaaatattctaaaaagaactaa
----:----|----:----|----:----|----:----|----:----|----:----|
         1750      1760      1770      1780      1790      1800
aagccagcgaatcgcccacttcttcgacgttttataagatttttcttgatt

F  G  R  L  A  G  E  E  A  A  K  Y  S  K  K  N  *
```

Appendix 4

Mutagenic primers for H365L, H365I and T377V

The following primers were designed to substitute Histidine 365 with either leucine or isoleucine and threonine 377 to valine. Other mutants used for studies had been previously made.

Histidine 365 to leucine

Forward primer:

$^{5'}$GCAGTATATCCAAGCTCTGCCAACACTATCTG$^{3'}$

Reverse primer:

$^{5'}$CAGATAGTGTTGGCAGAGCTTGGATATACTGC$^{3'}$

Histidine 365 to isoleucine

Forward primer:

$^{5'}$GCAGTATATCCAAGCTATCCCAACACTATCTG$^{3'}$

Reverse primer:

$^{5'}$CAGATAGTGTTGGGATAGCTTGGATATACTGC$^{3'}$

Threonine 377 to valine

Forward primer:

$^{5'}$GTGGCGTAATGGTCGTTGAAGCGGTACGTGG$^{3'}$

Reverse primer:

$^{5'}$CCACGTACCGCTTCAACGACCATTACGCCAC$^{3'}$

Appendix 5

IUPAC names for chemicals listed in table 5.2

2-butenedioic acid (fumarate)

2-methyl-2-butenedioic acid (2-methylfumarate)

2-methyl-2-propenoic acid (methacrylate

2-butenoic acid (crotonate)

Trans-2-pentenoic acid (trans-2-pentenoate)

Trans-2-methyl-2-pentenoic acid (trans-2-methyl-2-pentenoate)

Methyl-3-amino-2-butenoic acid (methyl-3-aminocrotonate)

3-phenyl-2-propenoic acid (cinnamic acid)

2-butenedioic acid dimethyl ester (dimethylfumarate)

2-butenedioic acid monoethyl ester (monoethylfumarate)

CONFERENCES ATTENDED

Inorganic Biochemistry discussion group (IBDG) conference, Imperial College, London, January 2004

8th Redox enzymes meeting, Firbush, Loch Tay (University of Edinburgh), June 2004

Chemical Biology section meeting, Firbush (University of Edinburgh), April 2005 – Presented poster

EastChem Meeting, Firbush (University of Edinburgh), June 2005

12th International Conference on Biological Inorganic Chemistry (ICBIC), University of Michigan, Ann Arbor, August 2005 – Presented poster

Chemical Biology section meeting, Firbush (University of Edinburgh), April 2006 – Speaker, 3rd year PhD talk

FEBS Letters 580 (2006) 1677–1680

Fumarate reductase: Structural and mechanistic insights from the catalytic reduction of 2-methylfumarate☆

Caroline Wardrope[a], Christopher G. Mowat[a,b], Malcolm D. Walkinshaw[b], Graeme A. Reid[b], Stephen K. Chapman[a,*]

[a] *EaStCHEM, School of Chemistry, University of Edinburgh, West Mains Road, Edinburgh EH9 3JJ, UK*
[b] *Institute of Structural and Molecular Biology, University of Edinburgh, Mayfield Road, Edinburgh EH9 3JR, UK*

Received 20 December 2005; revised 19 January 2006; accepted 9 February 2006

Available online 17 February 2006

Edited by Miguel De la Rosa

Abstract The soluble fumarate reductase (FR) from *Shewanella frigidimarina* can catalyse the reduction of 2-methylfumarate with a k_{cat} of 9.0 s^{-1} and a K_M of 32 μM. This produces the chiral molecule 2-methylsuccinate. Here, we present the structure of FR to a resolution of 1.5 Å with 2-methylfumarate bound at the active site. The mode of binding of 2-methylfumarate allows us to predict the stereochemistry of the product as (*S*)-2-methylsuccinate. To test this prediction we have analysed the product stereochemistry by circular dichroism spectroscopy and confirmed the production of (*S*)-2-methylsuccinate.

Keywords: Fumarate reductase; Flavocytochrome c_3; 2-Methylfumarate; Mesaconate; 2-Methylsuccinate

1. Introduction

During anaerobic respiration many bacteria can utilise fumarate as a terminal electron acceptor. In most cases bacterial fumarate reductases (FRs) are cytoplasmic, membrane-associated complexes related to the succinate dehydrogenases, and contain iron–sulfur centres and flavin adenine dinucleotide (FAD) as cofactors [1,2]. In contrast, *Shewanella* species produce a soluble periplasmic FR which contains four *c*-type heme groups and one FAD, and as such is designated a flavocytochrome c_3. A number of crystal structures of the FR from *Shewanella frigidimarina* have been reported [3–5]. The highest resolution structure is to 1.8 Å (PDB ID 1QJD), and based upon this structure a mechanism for fumarate reduction has been proposed [3]. This mechanism involves the use of Arg402 as the active-site acid according to the scheme shown in Fig. 1, and is corroborated by further studies on site-directed mutant forms of the enzyme [6].

Fumarate reduction by FR is known to be competitively inhibited by 2-methylfumarate (also known as mesaconate) with a K_i of 1.0 μM. However, we show in the present paper that 2-methylfumarate is actually a substrate for FR. Unlike fumarate reduction by FR, which leads to the formation of the achiral product succinate, the reduction of 2-methylfumarate should result in the production of the chiral molecule 2-methylsuccinate. Depending upon the mode of binding of 2-methylfumarate at the active site of the enzyme, the product will be either (*S*)- or (*R*)-2-methylsuccinate. In order to investigate this we have obtained the crystal structure of FR with 2-methylsuccinate bound and have examined the FR-catalysed reduction of 2-methylfumarate by steady-state kinetics. In addition, we have carried out an electrocatalytic bulk reduction of 2-methylfumarate by FR, and identified the stereochemistry of the resultant 2-methylsuccinate by circular dichroism spectroscopy (CD). The results confirm our predicted trajectories for hydride and proton transfer in the catalytic mechanism.

2. Materials and methods

2.1. Protein expression and purification and determination of FAD content

Wild type FR was expressed and purified as previously reported [7]. The FAD content of the FR preparations was determined by the method of Macheroux [8]. All steady-state rate constants were corrected for the percentage of FAD present.

2.2. Crystallisation and refinement

Crystallisation of wild-type FR was carried out by hanging-drop vapour diffusion at 4 °C in Linbro plates. Crystals were obtained with well solutions comprising 100 mM Tris–HCl buffer (pH 7.8–8.5) (measured at 25 °C), 80 mM NaCl, 16–19% PEG 8000, and 1 mM 2-methylfumarate. Hanging drops (4 μl volume) were prepared by adding 2 μl of 6 mg/ml protein (in 10 mM Tris–HCl pH 8.5) to 2 μl of well solution. After approximately seven days needles of up to 1 mm × 0.2 mm × 0.2 mm and plates of up to 0.5 mm × 0.5 mm × 0.2 mm were formed. Crystals were immersed in a solution of 100 mM sodium acetate buffer (pH 6.5), 20% PEG 8000, 1 mM 2-methylfumarate, and 80 mM NaCl, containing 23% glycerol as a cryoprotectant, prior to being mounted in nylon loops and flash cooled in liquid nitrogen. A data set was collected to 1.5 Å at station 14.1 ($\lambda = 0.975$ Å) at SRS Daresbury using an ADSC Quantum 4 CCD detector. Crystals belonged to space group $P2_1$ with cell dimensions $a = 45.449$ Å, $b = 91.687$ Å, $c = 78.287$ Å, and $\beta = 91.13°$. Data processing was carried out using the HKL package [9]. The wild-type FR structure (PDB ID 1QJD), stripped of water, was used as the initial model. Electron-density fitting was carried out using the program Turbofrodo [10] and structure refinement by using Refmac [11].

☆ The atomic coordinates have been deposited in the protein data bank, entry 1Y0P.

*Corresponding author. Fax: +44 131 650 6453.
E-mail addresses: S.K.Chapman@ed.ac.uk, skc01@staffmail.ed.ac.uk (S.K. Chapman).

Abbreviations: FR, fumarate reductase; FAD, flavin adenine dinucleotide; CD, circular dichroism spectroscopy

0014-5793/$32.00
doi:10.1016/j.febslet.2006.02.016

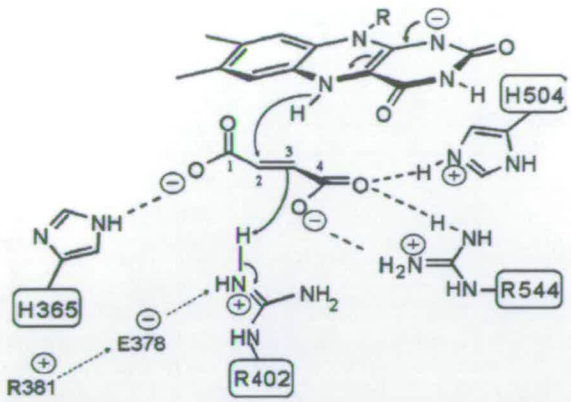

Fig. 1. The reaction mechanism for fumarate reduction in FR (this is an abbreviated version of the mechanism proposed by Taylor et al. [3]). The substrate is polarised by interactions with charged residues facilitating hydride transfer from N5 of the reduced FAD to C2 of the substrate. Arg402 is ideally positioned to donate a proton to C3 of the substrate, resulting in the formation of succinate. Arg402 is immediately reprotonated via a proton pathway involving Arg381 and Glu378.

2.3. Steady-state kinetics

The steady-state kinetics of 2-methylfumarate reduction were followed at 25 °C as described by Turner et al. [12]. The 2-methylfumarate-dependent reoxidation of reduced methyl viologen was monitored at 600 nm using a Shimadzu UV-PC 1501 spectrophotometer. To ensure anaerobicity, the spectrophotometer was housed in a Belle Technology glovebox under a nitrogen atmosphere with the O_2 level below 5 ppm. Assay buffers contained 0.45 M NaCl and 0.2 mM methyl viologen and were adjusted to the appropriate pH values using 0.05 M HCl or NaOH as follows: Tris–HCl at pH 7.0–9.0, MES/NaOH at pH 5.4–6.8, and CHES/NaOH at pH 8.6–10.0. The viologen was reduced by addition of sodium dithionite until a reading of ~1 absorbance unit was obtained (corresponding to ~80 μM reduced methyl viologen). The concentration of reduced methyl viologen could be varied from 20 to 100 μM with no effect on the rate of reaction. A known concentration of the enzyme was added and the reaction initiated by addition of 2-methylfumarate (0–1 mM).

Kinetic parameters K_M and k_{cat} were determined from steady-state results using non-linear-regression analysis (Microcal Origin software).

2.4. Electrocatalytic reduction of 2-methylfumarate

In order to carry out subsequent CD analysis, millimolar concentrations of product were required. Therefore, bulk reduction of 2-methylfumarate was carried out under anaerobic conditions at 25 °C in 0.05 M MOPS/NaOH buffer, pH 7.0, containing 0.5 M KF, 50 μM methyl viologen, and 5 mM 2-methylfumarate. The concentration of FR was approximately 1 μM. The electrodes used were platinum with a Ag/AgCl reference electrode. The potential was held at −0.6 V until reaction completion was indicated by cessation of current flow. After completion protein was separated from product by centrifugation through a 10 kDa membrane (Millipore).

2.5. Circular dichroism spectroscopy

CD spectroscopy was carried out using a Jasco J-810 spectropolarimeter and a 1 cm pathlength quartz cell. CD spectra of the product was compared with the spectra of enantiomerically pure solutions of 500 μM (*R*) and (*S*)-methylsuccinate (Sigma).

3. Results and discussion

3.1. Crystal structure of FR with 2-methylfumarate bound

A data set to 1.5 Å resolution was used to refine the structure to a final *R*-factor of 15.08% (R_{free} = 18.35%), data collection and refinement statistics are summarised in Table 1. The final model consists of one protein molecule comprising residues 1–568, four hemes, one FAD, one sodium ion, one 2-methylfumarate molecule, and 1249 water molecules. The atomic coordinates have been deposited in the protein data bank, accession code 1Y0P.

Table 1
Data collection and refinement statistics

Resolution (Å)	24.0–1.5
Total number of reflections	678 137
Number of unique reflections	99 564 (9590)[a]
Completeness (%)	97.2 (94.0)[a]
$I/[\sigma(I)]$	21.0 (3.1)[a]
R_{merge} (%)[b]	4.8 (37.3)[a]
R_{cryst} (%)[c]	15.08
R_{free} (%)[c]	18.35
RMSD from ideal values	
Bond lengths (Å)	0.014
Bond angles (°)	1.5
Ramachandran analysis	
Most favoured (%)	88.1
Additionally allowed (%)	11.7

[a]Values in parentheses indicate statistics for the highest resolution shell (1.55–1.50 Å).
[b]$R_{merge} = \sum_h \sum_i |I(h) - I_i(h)| / \sum_h \sum_i I_i(h)$, where $I_i(h)$ and $I(h)$ are the *i*th and mean measurement of reflection *h*, respectively.
[c]$R_{cryst} = \sum_h |F_o - F_c| / \sum_h F_o$, where F_o and F_c are the observed and calculated structure factor amplitudes of reflection *h*, respectively. R_{free} is the test reflection data set, 5% selected randomly for cross validation during crystallographic refinement.

The binding of 2-methylfumarate is illustrated by the F_o–F_c omit map shown in Fig. 2A. As found for other FR structures, residues 569–571 at the C-terminus of the enzyme could not be located in the electron density maps. The RMSD fit of all backbone atoms between this model and the earlier wild-type enzyme structure (PDB ID 1QJD) [3] is 0.2 Å, indicating no major differences between the two protein structures. 2-Methylfumarate is found at the active site of the enzyme in the same twisted conformation observed for the malate-like molecule (henceforth referred to as malate for the sake of simplicity) in the original crystal structure (PDB ID 1QJD) [3] and for fumarate in structures of mutant forms of the enzyme (e.g., PDB ID 1JRX) [6]. The binding of 2-methylfumarate and malate (from the structure of Taylor et al. [3]) to FR is shown in Fig. 2B. The ligands are completely superposable with the exception of the C2-substituents. Thus, bound 2-methylfumarate maintains the same interactions with the protein as displayed by malate. These include an electrostatic interaction between the C1-carboxylate group and the positively-charged sidechains of Arg544 and His504 which serve to polarise and activate the double bond for hydride attack by FAD. The C4-carboxylate end of 2-methylfumarate is hydrogen bonded to several residues including His365 and Thr377. The interactions of 2-methylfumarate at the active site of FR are shown in Fig. 2C. The mechanism of 2-methylfumarate reduction is assumed to be the same as that shown for fumarate in Fig. 1, and is proposed to involve proton delivery via a pathway comprised of Arg381, Glu378, and Arg402. In the 2-methylfumarate-bound protein all proton transfer distances are identical to those observed in the malate-bound structure, as is the hydride transfer distance from FAD to substrate.

The physiological reaction of FR results in the formation of the achiral product succinate. In contrast to this, reduction

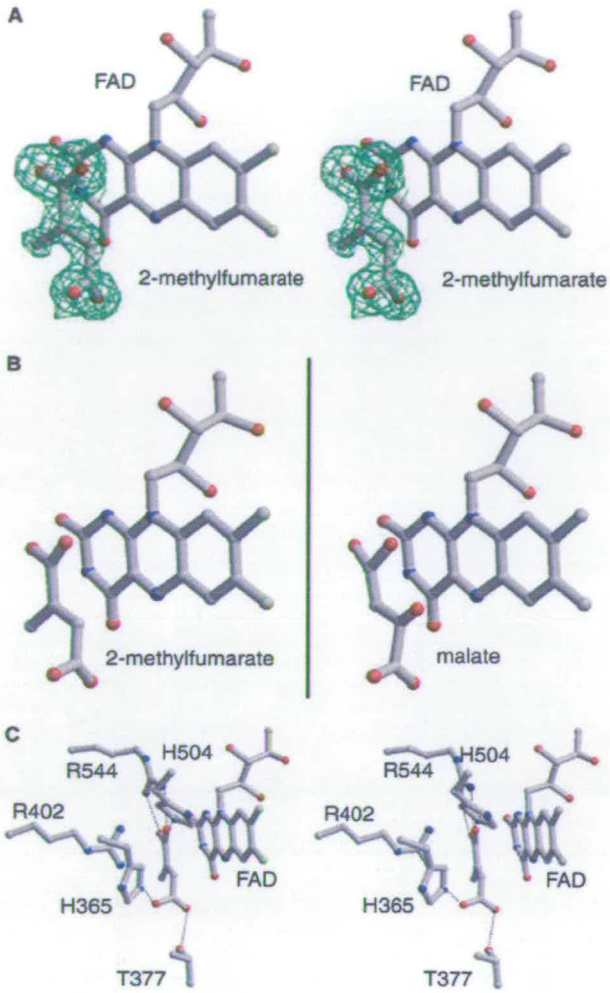

Fig. 2. (A) Stereoview of the region surrounding the FAD and bound 2-methylfumarate in FR. The electron density shown is a simulated annealing omit map calculated using Fourier coefficients F_o–F_c, where F_o and F_c are the observed and calculated structure factors, respectively, the latter based on the final model. The contour level is 3σ, where σ is the RMS electron density. (B) The left panel shows 2-methylfumarate at the active site of the enzyme while the right panel shows malate in the active site (from PDB IDB 1QJD [3]). (C) Stereoview of the active site of FR with 2-methylfumarate bound. Residues important for substrate binding and catalysis are shown. The figure was made using BOBSCRIPT [13] and RASTER 3D [14].

of the double bond in 2-methylfumarate will lead to formation of either (*R*)- or (*S*)-methylsuccinate, depending upon the mode of binding of 2-methylfumarate during catalysis. This is shown schematically in Fig. 3. Specifically, when 2-methylfumarate is bound as observed in the structure reported here then the product will be (*S*)-methylsuccinate (see Fig. 3A). If 2-methylfumarate had bound in a mode analogous to that seen for malate (see Fig. 2B), i.e., with the methyl group in the same position as the malate 2-hydroxyl group, then the product would be (*R*)-methylsuccinate (see Fig. 3B). In this way, the crystal structure of the enzyme/substrate complex enables the prediction of the hydride and proton trajectories and hence the stereochemistry of the chiral product.

3.2. Steady-state kinetics

The ability of FR to catalyse 2-methylfumarate reduction was assayed at a range of pH values between 6.0 and 10.0. At pH 7.2, the FR-catalysed reduction of 2-methylfumarate gave a k_{cat} value of $9.0 \pm 0.4\ s^{-1}$ and a K_M of $32 \pm 8\ \mu M$. At the same pH, fumarate gives rise to a k_{cat} value of $509 \pm 15\ s^{-1}$ and a K_M of $43 \pm 10\ \mu M$. Thus although both substrates exhibit similar K_M values, the k_{cat} value seen for fumarate is some 50-fold larger than that seen with 2-methylfumarate. The structural data would suggest that there is no problem with the binding and orientation of 2-methylfumarate and so it is unlikely that the fall in k_{cat} is due to steric reasons. The more likely reason is the positive inductive affect of the methyl group. It has been proposed that the transition state for the reaction involves the build up of negative charge on the substrate [3]. This suggestion is consistent with our results, since the methyl group would disfavour the build up of negative charge, raising the energy of the transition state and consequently lowering the k_{cat} value.

3.3. Characterisation of electrocatalytically produced 2-methylsuccinate using CD spectroscopy

The ability to use an electrode to drive fumarate reduction by FR has been previously demonstrated [12], and electrochemistry has become a valuable technique in the study of the enzyme. Thus, in order to produce enough product for analysis by CD spectroscopy, we carried out an electrocatalytically driven bulk enzymatic reduction of 2-methylfumarate. The CD spectrum of the 2-methylsuccinate produced was compared with those of pure (*R*)- and (*S*)-methylsuccinate, and these are shown overlaid in Fig. 4. It can be seen from this figure that the product spectrum is identical to that of pure (*S*)-methylsuccinate, indicating that reduction of 2-methylfumarate by FR results in the production of (*S*)-methylsuccinate.

3.4. Conclusions

We have shown that FR can catalyse the reduction of 2-methylfumarate, a molecule previously thought to be only

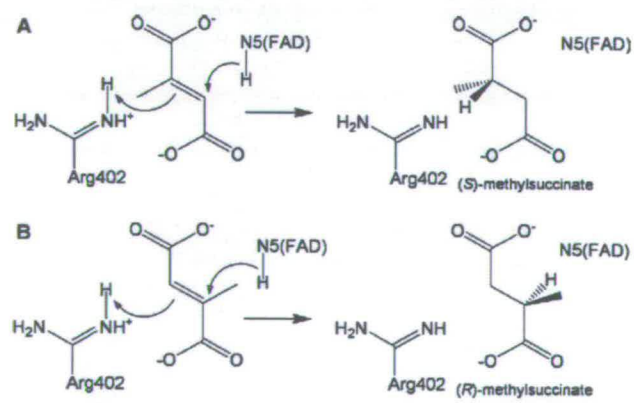

Fig. 3. Schematic representation of 2-methylsuccinate generation by FR. Panel (A) illustrates the situation as observed in the crystal structure resulting in (*S*)-methylsuccinate. Panel (B) shows the production of (*R*)-methylsuccinate if 2-methylfumarate were bound in the same way as malate in the original crystal structure.

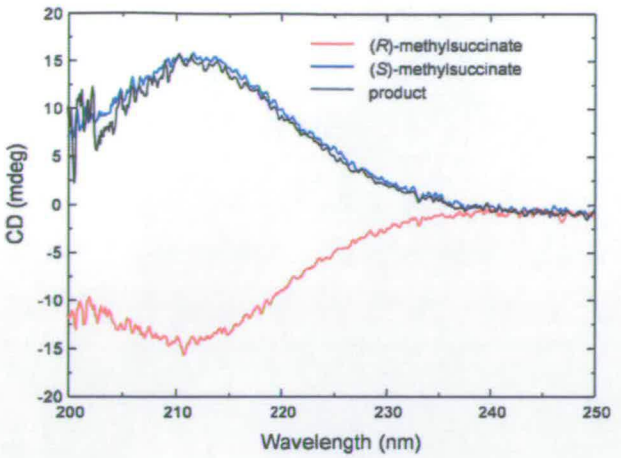

Fig. 4. CD spectra of product 2-methylsuccinate (black), (*R*)-2-methylsuccinate (red), and (*S*)-2-methylsuccinate (blue). All the compounds were at the same concentration of 5 mM. Spectra represent an average of 5 scans at 10 nm per minute.

an inhibitor of the enzyme. Crystallography of the FR:2-methylfumarate complex has allowed us to visualise the binding of this substrate at the active site of the enzyme. This structure, in combination with the previously proposed mechanism for catalysis by FR [3], has enabled us to predict the trajectories for hydride and proton transfer to 2-methylfumarate. This suggested that the resulting product should be (*S*)-methylsuccinate and this has been confirmed by CD spectroscopy adding strong support to the validity of the proposed mechanism.

We note that the ability of FR to produce chiral compounds from achiral precursors at millimolar concentrations may have future applications. The mild reaction conditions and use of an electrode as a reductant could provide an efficient and inexpensive route to further compounds. Clearly the scope of the method is determined by the ability of the enzyme to accommodate and catalyse the reduction of further compounds. Current efforts are centred upon determining which precursor compounds are viable substrates for wild-type FR, and a programme of site-directed mutagenesis is under way in an effort to alter the substrate specificity of the enzyme and therefore maximise the applicability of the method.

Acknowledgements: This work was supported by the UK Biotechnology and Biological Sciences Research Council (BBSRC) and by the Wellcome Trust funded Edinburgh Protein Interaction Centre (EPIC). The authors thank SRS Daresbury for access to synchrotron facilities.

References

[1] Iverson, T.M., Luna-Chavez, C., Cecchini, G. and Rees, D.C. (1999) Structure of the *Escherichia coli* fumarate reductase respiratory complex. Science 284, 1961–1966.
[2] Lancaster, C.R.D., Kröger, A., Auer, M. and Michel, H. (1999) Structure of fumarate reductase from Wolinella succinogenes at 2.2 Å resolution. Nature 402, 377–385.
[3] Taylor, P., Pealing, S.L., Reid, G.A., Chapman, S.K. and Walkinshaw, M.D. (1999) Structural and mechanistic mapping of a unique fumarate reductase. Nat. Struct. Biol. 6, 1108–1112.
[4] Bamford, V., Dobbin, P.S., Richardson, D.J. and Hemmings, A.M. (1999) Open conformation of a flavocytochrome c_3 fumarate reductase. Nat. Struct. Biol. 6, 1104–1107.
[5] Leys, D., Tsapin, A.S., Nealson, K.H., Meyer, T.E., Cusanovich, M.A. and Van Beeumen, J.J. (1999) Structure and mechanism of the flavocytochrome *c* fumarate reductase of *Shewanella putrefaciens* MR-1. Nat. Struct. Biol. 6, 1113–1117.
[6] Mowat, C.G., Moysey, R., Miles, C.S., Leys, D., Doherty, M.K., Taylor, P., Walkinshaw, M.D., Reid, G.A. and Chapman, S.K. (2001) Kinetic and crystallographic analysis of the key active site acid/base arginine in a soluble fumarate reductase. Biochemistry 40, 12292–12298.
[7] Pealing, S.L., Cheesman, M.R., Reid, G.A., Thomson, A.J., Ward, F.B. and Chapman, S.K. (1995) Spectroscopic and kinetic studies of the tetraheme flavocytochrome c_3 from *Shewanella putrefaciens* NCIMB400. Biochemistry 34, 6153–6158.
[8] Macheroux, P. (1999) (Chapman, S.K. and Reid, G.A., Eds.), Flavoprotein Protocols: Methods in Molecular Biology, vol. 131, pp. 1–7, Humana Press, Totowa, NJ.
[9] Otwinowski, Z. and Minor, W. (1997) Processing of X-ray diffraction data collected in oscillation mode. Methods Enzymol. 276, 307–326.
[10] Roussel, A. and Cambillau, C. (1991) TURBO-FRODO, in Silicon Graphics Geometry Partners Directory 86, Silicon Graphics, Mountain View, CA.
[11] Murshudov, G.N., Vagin, A.A. and Dodson, E.J. (1997) Refinement of macromolecular structures by the maximum-likelihood method. Acta Crystallogr. D53, 240–255.
[12] Turner, K.L., Doherty, M.K., Heering, H.A., Armstrong, F.A., Reid, G.A. and Chapman, S.K. (1999) Redox properties of flavocytochrome c_3 from *Shewanella frigidimarina* NCIMB400. Biochemistry 38, 3302–3309.
[13] Esnouf, R.M. (1997) An extensively modified version of MolScript that includes greatly enhanced coloring capabilities. J. Mol. Graph. 15, 132–134.
[14] Merritt, E.A. and Murphy, M.E.P. (1994) *Raster*3D version 2.0: a program for photorealistic molecular graphics. Acta Crystallogr. D50, 869–873.